Miner Deposita (2013) 48:1–56
DOI 10.1007/s00126-012-0436-1

ARTICLE

The Bushveld Complex, South Africa: formation of platinum–palladium, chrome- and vanadium-rich layers via hydrodynamic sorting of a mobilized cumulate slurry in a large, relatively slowly cooling, subsiding magma chamber

W. D. Maier · S.-J. Barnes · D. I. Groves

Received: 25 November 2011 / Accepted: 30 July 2012 / Published online: 19 October 2012

Abstract Platinum-group element (PGE) deposits in the Bushveld Complex and other layered intrusions form when large, incompletely solidified magma chambers undergo central subsidence in response to crustal loading, resulting in slumping of semi-consolidated cumulate slurries to the centres of the intrusions and hydrodynamic unmixing of the slurries to form dense layers enriched in sulfides, oxides, olivine and pyroxene and less dense layers enriched in plagioclase. The most economic PGE, Cr and V reefs form in large, multiple-replenished intrusions because these cool relatively slowly and their central portions subside prior to termination of magmatism and complete cumulate solidification. The depth of emplacement has to be relatively shallow as, otherwise, ductile crust would not be able to flex and collapse. In smaller intrusions, cooling rates are faster, subsidence is less pronounced and, where it occurs, the cumulate may be largely solidified, resulting in insignificant mush mobility and mineral sorting. Layering is thus less pronounced and less regular and continuous and the grades of the reefs are lower, but the reefs can be relatively thicker. An additional factor controlling the PGE, Cr and V prospectivity of intrusions is their location within cratons. Intracratonic environments offer more stable emplacement conditions that are more amenable to the formation of large, layered igneous bodies. Furthermore, intrusions sited within cratons are more readily preserved because cratons are underlain by thick, buoyant keels of harzburgite that prevent plate tectonic recycling and destruction of crust.

Editorial handling: C.M. Lesher

Electronic supplementary material The online version of this article (doi:10.1007/s00126-012-0436-1) contains supplementary material, which is available to authorized users.

W. D. Maier (✉)
Department of Geosciences, University of Oulu,
Oulu, Finland
e-mail: wolfgang.maier@oulu.fi

S.-J. Barnes
Sciences de la Terre, Université du Québec à Chicoutimi,
Chicoutimi, Quebec, Canada
e-mail: sarah-jane_barnes@uqac.ca

D. I. Groves
Centre for Exploration Targeting, University of Western Australia,
Crawley, Perth, Australia
e-mail: di_groves@hotmail.com

Introduction

The ~2.05-Ga Bushveld Complex contains by far the world's largest layered mafic–ultramafic intrusion, measuring approximately 60,000 km^2 in sub-surface outcrop (Fig. 1). In addition, the Bushveld Complex contains one of the world's largest A-type granites and important volumes of rhyolite. The complex also constitutes the world's most valuable mineral province (Naldrett 2009), hosting the bulk of global resources in PGE, Cr and V, with significant Cu, Ni, Au, Sn, fluorite, Fe and dimension stone (Wilson and Anhaeusser 1998), and, in the contact metamorphic aureole of the intrusion, the world's largest andalusite resources (Oosterhuis 1998). Clearly, a unique combination of petrogenetic processes has occurred, but an internally consistent petrogenetic model for the formation of the layered sequence hosting the PGE-, Cr- and V-rich layers has remained elusive, in part because a comprehensive compositional study covering the entire sequence has not yet been conducted. As a result, our understanding of the composition of the complex is still fragmentary.

The interpretation of cumulate rocks has remained as one of the key challenges in petrology (Campbell 1978;

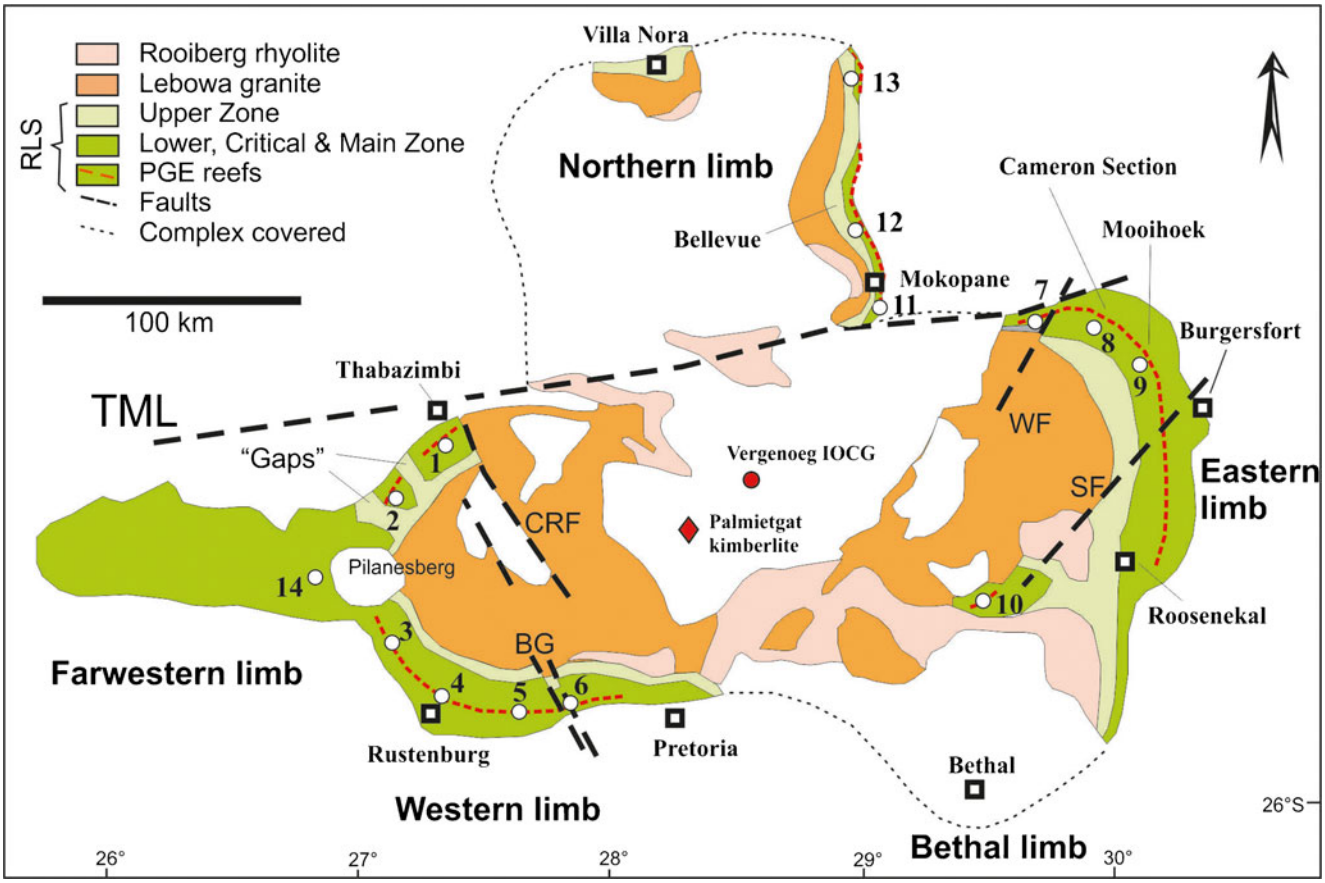

Fig. 1 Simplified geological map of the Bushveld Complex, showing the localities mentioned in the text. *TML* Thabazimbi–Murchison lineament, *CRF* Crocodile River fault, *BG* Brits graben, *SF* Steelpoort fault, *WF* Wonderkop fault, *1* Amandelbult section with Tumela, Dishaba and Northam platinum mines, *2* Union platinum mine, *3* Impala platinum mines, *4* Rustenburg platinum mine, *5* Western platinum and Karee mines, *6* Crocodile River mine, *7* Messina platinum mine, *8* Atok platinum mine, *9* Maandagshoek section with Modikwa platinum mine, *10* Mineral Range and Sheba's Ridge deposit, *11* Rooipoort, Moorddrift, and Grasvally farms, *12* Turfspruit, *13* Nonnenwerth

McBirney and Hunter 1995; Naslund and McBirney 1996; Irvine et al. 1998). In the present paper, it is argued that cumulate rocks within the Bushveld Complex and other large layered intrusions, many of which were regarded as textbook examples of classical fractional crystallization processes, are reconstituted rocks generated by crystal sorting of slurries deposited on the sloping floor of subsiding magma chambers. An overview of some geochemical studies that shaped current ideas on the formation of the layered suite of the complex is followed by examination of some of the more important geological aspects that remain unresolved, including the tectonic setting, the nature and origin of the layering and the petrogenesis of the Bushveld mineralized layers, including their remarkable lateral continuity. New whole-rock compositional data are then used to build a comprehensive modal and chemical profile through the complex. These results constrain the mode of emplacement of the layered rocks, which is of particular importance in understanding the formation of the PGE reefs. Based on these data, a holistic model for the formation of the complex and its economically important PGE, chromite and magnetite mineralization is presented. Finally, some implications that are relevant for defining the PGE–Ni–Cu–Cr–V prospectivity of layered intrusions in general are discussed.

Review of previous work

Large-scale chemostratigraphic studies on the Bushveld layered rocks began in the late 1960s by von Gruenewaldt (1971, 1973) and Molyneux (1970, 1974). Their investigations focused on the Main and Upper Zones in the relatively well exposed eastern Bushveld Complex between Steelpoort and Roossenekal (Fig. 1) and also provided detailed information on the composition of the magnetite seams, subsequently complemented by, e.g., the work of Reynolds (1985, 1986), Klemm et al. (1985) and Cawthorn and Molyneux (1986). The first mineral compositional studies across significant portions of the Bushveld layered sequence were also conducted in the eastern Bushveld, on the Jagdlust farm and adjoining areas, where Cameron (1978, 1980, 1982) analysed olivine, pyroxenes, plagioclase, chromite and other

minerals in a profile through the Lower and Critical Zones, at what is now usually referred to as the "Cameron Section" (Fig. 1). One of the key results of these studies was the documentation of small-scale cyclicity and numerous compositional reversals within the sequence, interpreted to result from multiple magma replenishment.

The first in-depth whole-rock chemical studies of the Lower and Critical Zones were conducted in the northern limb of the Bushveld Complex by Hulbert and von Gruenewaldt (1982) and Hulbert (1983) on the Grasvally farm. At this locality, exposure was provided by drill cores that intersected the entire Critical and part of the Lower Zone, following exploration for economically important chromitite seams in the Lower Zone. In the eastern and western lobes of the complex, the Lower Zone lacks chromitite seams. Hence, no commercial drilling was available and detailed studies were delayed until the Geological Survey of South Africa collared a series of boreholes (NG1–NG3) at Union Section, northwestern Bushveld, in the mid-1980s. The resulting drill cores, and others intersecting the Critical and Main Zones at Union Section, provided by Anglo Platinum, were studied by Eales and students. Of particular interest are the comprehensive studies of Mitchell (1986) on the Main Zone, of Teigler and Eales (1996) on the Lower and Lower Critical Zones and of de Klerk (1992) on the Upper Critical Zone. More recently, Ashwal et al. (2005) conducted a detailed compositional study on the 3,000-m Bellevue drill core through the Main and Upper Zones in the northern lobe (Fig. 1), including comprehensive magnetic susceptibility and rock density data. The first lithogeochemical studies on the contact rocks of the northern lobe (the Platreef) were conducted in the 1980s (Buchanan et al. 1981; Cawthorn et al. 1985; Barton et al. 1986). The iron-rich ultramafic pegmatite (IRUP) pipes of the eastern Bushveld Complex, discovery sites of platinum in 1924 (Wagner 1929; Cawthorn 1999a, b), have been examined by Stumpfl and Rucklidge (1982), Schiffries (1982) and Scoon and Mitchell (2004, 2009).

A landmark study was the characterization of the suite of fine-grained marginal rocks and sills in the floor of the eastern Bushveld Complex, interpreted to represent the parental magmas to the Bushveld Complex (Sharpe 1978, 1981). At about the same time, Davies et al. (1980) and Cawthorn et al. (1981) studied the sill suite in the western Bushveld Complex. Two types of magma suites were identified, Mg-rich basaltic andesite (B1 or Bushveld 1 magma) and tholeiitic basalt (B2 and 3). The rocks were analysed for Ir, Ru, Rh, Pt, Pd and Au by Davies and Tredoux (1985) and a full range of trace element and PGE data by Barnes et al. (2010).

Comprehensive isotopic studies on the Bushveld Complex began with the Sr isotopic work of Hamilton (1977). Subsequently, Sharpe (1985) analysed a Sr isotope profile across the entire layered sequence in the eastern Bushveld Complex, and Kruger (1994) compiled a similar profile for the western Bushveld Complex. The data showed that all Bushveld cumulates contain a pronounced crustal component ($^{87}Sr/^{86}Sr_i$ 0.704–0.709) and that there are several isotopically distinct intervals that can be correlated across the entire complex, a feature that profoundly influenced Bushveld petrogenetic models for the following decades. For example, the distinct Sr isotopic change associated with the Merensky unit has been identified in both the eastern lobe (Lee and Butcher 1990) and the western lobe (Kruger 1992). Several subsequent studies on other isotopic systems essentially confirmed these results: Maier et al. (2000) provided Nd isotopic data on the Lower, Critical and Main Zones at Union Section, and Prevec et al. (2005) added Nd isotopic data on the Merensky Reef at Impala mine. Comprehensive Pb isotope studies were conducted by Mathez and Waight (2003) and Harmer et al. (1995), and O–H isotopic studies were conducted by Schiffries and Rye (1989), Harris and Chaumba (2001) and Harris et al. (2004). Osmium isotopic studies by Hart and Kinloch (1989), Schönberg et al. (1999), McCandless and Ruiz (1991) and Reisberg et al. (2011) identified mantle-like ratios in Lower Critical Zone silicates and chromitites and more radiogenic ratios in the Upper Critical Zone, indicating the addition of an enriched component. Curl (2001) determined Os isotopes in chromite mineral separates from the B-1 marginal rocks defining γOs −0.07±0.5. On the other hand, the Nd isotope data for the B1 samples indicate εNd −5 to −6, suggesting a crustal component.

The first S isotopic studies on the Bushveld Complex were conducted by Liebenberg (1970) who showed that most of the internal PGE reefs have a mantle-like S isotopic signature. Recent work by Penniston-Dorland et al. (2011) indicates slightly positive $\Delta^{33}S$ values of 0.3±0.05 ‰ in Critical Zone and Main Zone rocks, suggesting that less than 4 % of S is derived from the crust, unless there was additional input of S from unfractionated sources. In contrast, S isotopic studies of the Platreef (e.g. Holwell et al. 2007; Penniston-Dorland et al. 2007) showed that the contact-style reefs tend to contain a variable, and commonly significant, component of crustal sulfur.

Studies on the PGE distribution in the rocks have been at the centre of geological research on the Bushveld Complex since the reports on the discovery of the reefs by Merensky (1926) and the seminal work of Wagner (1929). Subsequent contributions that characterized extended vertical and lateral portions of the layered sequence include the work of Scoon and Teigler (1994), Lee and Parry (1988) and Naldrett et al. (2009a, 2012) on the PGE contents in the Bushveld chromitites, the papers by Kinloch (1982) and Maier et al. (1999) on PGM and the kilometre-scale PGE profiles by Lee and Tredoux (1986: Lower and Lower Critical Zones in the eastern Bushveld), Maier and Barnes (1999: Lower,

Critical and Main Zones at Union Section) and Barnes et al. (2004: Upper Zone in the northern lobe). Key results of these studies include the realization that the entire lower portion of the complex contains elevated PGE contents, yet it is mostly exceedingly poor in sulfide (Barnes et al. 2009). The first detailed PGE profiles through individual reefs were provided by Lee (1983: Merensky Reef, Rustenburg Platinum Mine), Hiemstra (1986: UG2 at Western Platinum mine), Barnes and Maier (2002a: Merensky Reef at Impala mine), Wilson and Chunnett (2006: Merensky Reef in western Bushveld) and Maier and Barnes (2008: UG1, UG2 and Bastard reefs at Impala). A comprehensive regional PGE study on the Merensky Reef was published by Naldrett et al. (2009b). Godel et al. (2007) were the first to use X-ray tomography in studying the Merensky Reef. The distribution of PGE in the Platreef was documented by, e.g., Gain and Mostert (1982), White (1994), Armitage et al. (2002), Manyeruke et al. (2005), Kinnaird et al. (2005) and McDonald et al. (2005). Compilations of PGE distribution patterns along strike were provided by Maier et al. (2008a) and McDonald and Holwell (2011).

Age

From the late 1970s onwards, the emplacement age of the mafic–ultramafic layered rocks of the Bushveld Complex (the Rustenburg Layered Suite, RLS) (SACS, 1980) has been known to be around 2,050 Ma (Hamilton 1977; Von Gruenewaldt et al. 1985). The first high-precision age determination of the Merensky Reef (2.054.4 ±1.3 Ma, U–Pb on zircons, Rustenburg Platinum Mine) was published by Scoates and Friedman (2008). The age was subsequently revised to 2,056.1±0.7 Ma and a further sample from the Driekop farm in the eastern Bushveld yielded 2,055.3 ±0.6 Ma (Scoates et al. 2011), confirming that the reef formed contemporaneously in the different lobes of the complex. The new age is also consistent with the age of the Platreef (2,056.2 ±4.4 Ma; Yudovskaya et al. 2010) and the Marble Hall diorite (2,055.6 ±3.1 Ma; de Waal and Armstrong 2000), which the latter authors consider to be part of the early alkaline phase of the complex. Recent work by Scoates et al. (2012) indicates that the UG2 footwall pyroxenite is ca. 5 my older than the Merensky Reef, with two samples yielding ages of 2,060.5±1.4 and 2,059.8±1.2 Ma (U–Pb on zircons). A broadly similar U–Pb age of 2,058.9± 0.8 Ma was determined for titanite in a retrogressed xenolith in the Upper Zone by Buick et al. (2001). According to Scoates and Friedman (2008), this may reflect titanite crystallization during the emplacement of the early felsic volcanic phase of the Bushveld event (Rooiberg rhyolites, 2,061±2 Ma; Walraven 1997).

The B1 and B2/B3 marginal rocks have been dated by U–Pb on zircons by Curl (2001) who obtained ages of 2,050± 4 Ma for a B1 sample and 2,052±6 Ma for a B2 sample. These data place the marginal rocks within error of most cumulate rocks of the RLS.

The Bushveld granites and granophyres show cross-cutting field relationships relative to the layered mafic–ultramafic rocks and were originally thought to be significantly younger than the RLS (Coertze et al. 1978; Retief 1985 in Vermaak and Von Gruenewaldt 1986). However, the rocks are now known to be broadly coeval to the RLS (2,054.4± 1.8 Ma; Walraven and Hattingh 1993). The key implication of the available age data is that the entire giant Bushveld event was of relatively short duration, on the order of 5–10 my. This is broadly analogous to many continental flood basalt provinces (e.g. Columbia River, North Atlantic, Deccan, Emeishan; Mahoney and Coffin 1997; He et al. 2007), lending credence to the suggestion of the involvement of a mantle plume in the origin of Bushveld magmatism (Hatton and Schweitzer 1995; Olsson et al. 2011).

Layered intrusions containing PGE reefs occur predominantly in the late Archean and early Proterozoic (Groves et al. 1987; Naldrett 2010; Maier and Groves 2011; Bushveld, Great Dyke, Stillwater, Penikat, Lac des Iles). Only one potentially economic PGE-bearing intrusion is younger than 1.8 Ga—Skaergaard at 55.7±0.3 Ma (^{40}Ar–^{39}Ar; Hirschmann et al. 1997), and only one is older than 2.9 Ga—Stella at 3.033.5±0.3 Ma (Schmitz et al. 2004). The age of PGE deposits generally shows a good correlation with the formation of a new crust (Hatton and Von Gruenewaldt 1990; Groves et al. 2005; Maier and Groves 2011), which, in turn, represents supercontinent amalgamation and breakup, notably at ca 2.75–2.60 Ga during Kenorland amalgamation (Stillwater, Great Dyke) and at 2.05–1.8 Ga during Columbia amalgamation (Bushveld, Mirabela, Panton). The 2.45 Ga intrusions of the Baltic Shield and the Superior craton herald the breakup of Kenorland in Baltica and Superia. Deposits tend to be rare in periods of supercontinent stability during which little juvenile crust formed. Notably, apart from the Bushveld province and its satellites (Molopo Farms, Uitkomst), the 2,050 Ma event does not seem to represent a major crust-forming episode; broadly coeval mafic events elsewhere are confined to the Phalaborwa (ca. 2,060.6±0.5 Ma; Reischmann 1995) and Schiel (2,059±36 Ma; Walraven et al. 1992) alkaline complexes in South Africa that may represent the early alkaline phase of the Bushveld event, and the Otanmäki and Kevitsa ultramafic–mafic layered intrusions within the Karelian craton of north-central Finland (2,058±4 Ma; Mutanen and Huhma 2001). Thus, compared to, e.g., the global 2.7-Ga komatiite event, the Bushveld magmatic episode (0.7–1 million km^3; Harmer and Armstrong 2000) appears to have been a relatively local event.

Tectonic setting and magma emplacement

The bulk of the Bushveld Complex and most of the world's other significant PGE- mineralized intrusions are associated with stabilized cratons (Groves et al. 1987; Maier and Groves 2011). Most deposits occur within the central portions of the cratons, notably the super-large deposits that host the bulk of world PGE reserves: the Bushveld Complex in the Kaapvaal craton, the Great Dyke in the Zimbabwe craton and the Stillwater Complex in the Wyoming craton. Other notable deposits that are located more than ~50 km inboard from the craton margin include Panski Tundra, Fedorova Tundra, Koillismaa, Portimo and Penikat within the Karelia and Kola cratons, Big Trout Lake within the Superior craton, Munni Munni in the Pilbara craton and Panton in the North Australian craton. The central disposition of the intrusions within cratons is counter-intuitive because magma ascent through up to 250-km-thick SCLM should be more difficult than through relatively thin-rifted craton margins, unless the SCLM delaminated (Olsson et al. 2011). It is likely that the magmas used pathways represented by trans-lithospheric suture zones along which protocratonic nucleii were assembled. This allows dense primitive magmas to ascend rapidly through relatively light upper crust (Naldrett 2010), thereby limiting differentiation and loss of PGE to segregating sulfide. In the case of Bushveld, the Thabazimbi–Murchison lineament is believed to be particularly important, as discussed in the suceeding text. In several other intrusions, there is good evidence for structural control on emplacement expressed by, e.g., the elongated shapes of the Great Dyke (Prendergast and Wilson 1989) and the Monts de Cristal intrusion of Gabon (Edou-Minko et al. 2002) and by the vicinity of major lineaments and suture zones.

Importantly, in none of the major deposits is there compelling evidence for significant rifting. For example, in the case of the 2.45-Ga PGE-mineralized intrusions of the Fennoscandian Shield, craton extension is suggested by the occurrence of broadly coeval craton-wide dyke suites (Vuollo and Huhma 2005), but flood basalts are lacking. The same applies to the Bushveld Complex. It is conceivable that significant amounts of lavas have been eroded (Cawthorn and Walraven 1998; Arndt 2005), but alternatively, extension could have been relatively localized, caused by transpression within far-field compressional regimes (e.g., Holzer et al. 1999; Silver et al. 2004). Maier and Groves (2011) argued that the lack of protracted extension is a key factor in the formation of PGE deposits because magmas can pond and differentiate in the upper crust, allowing the formation of large intrusions with regular and laterally continuous layering, characteristic of the richest PGE deposits.

Holzer et al. (1999) proposed that the Kaapvaal craton was under a NW–SE compressional tectonic regime during Bushveld magmatism, in response to collision with the Zimbabwe craton, and that the Bushveld magmas were emplaced due to localized transpressional extension along reactivated major crustal lineaments, for example, the Thabazimbi–Murchison lineament (TML: Silver et al. 2004) or the Crocodile River and Steelpoort faults (Cawthorn et al. 2002). There is evidence that the TML and the Crocodile River fault were active already during Bushveld emplacement; the Upper Critical Zone is markedly thinned in the Brits graben compared to the adjacent domains (Maier and Eales 1997), and iron mineralization at Thabazimbi along the northern extension of the Crocodile River fault (Fig. 1) was upgraded during or shortly after Bushveld emplacement (van Deventer et al. 1986). Alternatively, the Bushveld magmas may have been emplaced in response to backarc extension (e.g. at the TML; Clarke et al. 2009), but a subduction-related model would seem less consistent with the relatively short duration of the Bushveld event.

Distribution and connectivity of Bushveld lobes

The layered mafic–ultramafic sequence of the Bushveld Complex crops out in four distinct lobes: the western, eastern, northern and far western lobes (Fig. 1). An additional lobe, termed the Bethal or southern lobe, is covered by >100 m of Karoo sedimentary rocks (Buchanan 1975). The individual lobes were originally considered to be connected at depth, largely based on similarities in igneous stratigraphy (Hall 1932). The recognition of a gravity low in the centre of the complex (Cousins 1959) temporarily dispelled this model, but Cawthorn et al. (1998) and Webb et al. (2003) reinterpreted the gravity data, lending support to the original model of connectivity of the limbs. The existence of hidden mafic–ultramafic layered rocks below the centre of the complex is consistent with the identification of pyroxenite xenoliths, interpreted to be of Bushveld lineage, in the Palmietgat kimberlite (Webb et al. 2011; Fig. 1). Other evidence for extension of the layered sequence towards the centre of the complex includes 2D seismic reflection surveys that indicate down-dip extension of the Merensky Reef package for >50 km to the east of the Pilanesberg Complex (Campbell 1990; in Viljoen 1999) and exposure of Critical Zone rocks in the dome-like Mineral Range, located several tens of kilometres to the west of the eastern Bushveld limb (Fig. 1) (Iljina and Lee 2005).

Stratigraphy and petrography of the layered suite

The RLS is sub-divided into five stratigraphic zones (Fig. 2), including the Marginal Zone (not shown), Lower Zone (LZ), Critical Zone (CZ), Main Zone (MZ) and Upper Zone (UZ) (Hall 1932).

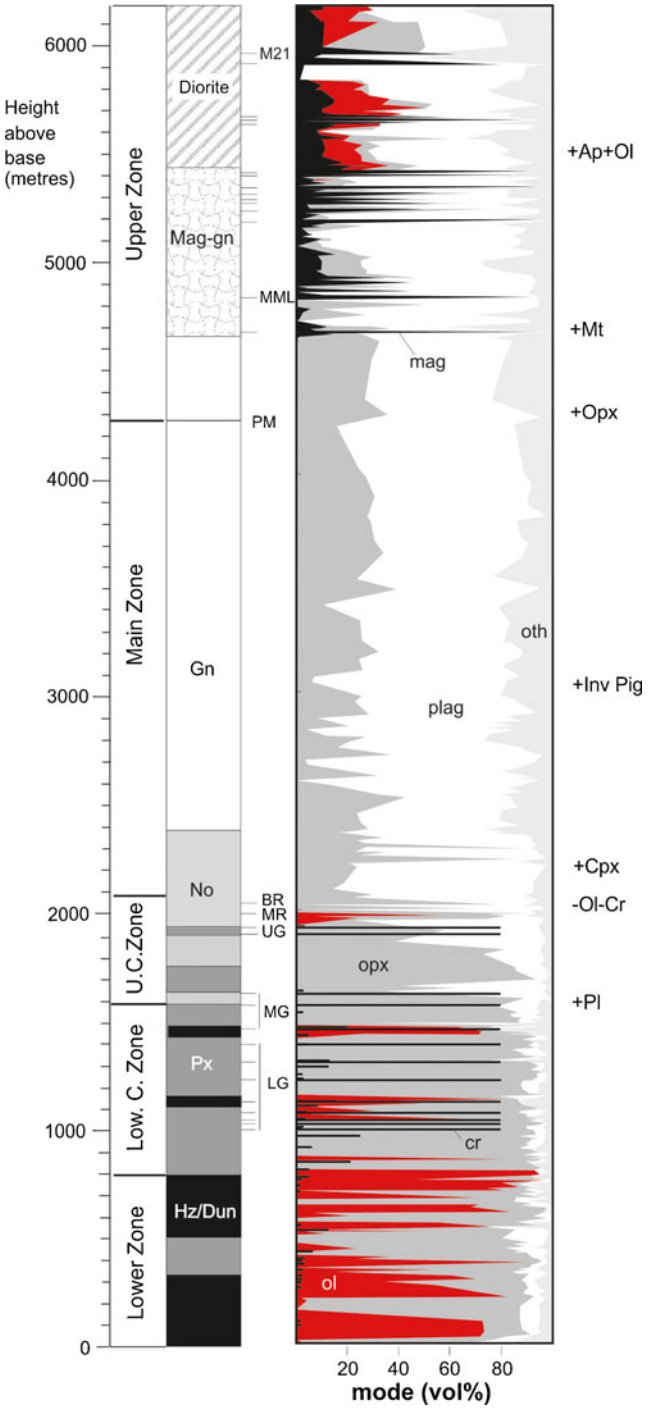

Fig. 2 Modal proportions of minerals in the Rustenburg layered suite. Data compiled from Mitchell (1986), Teigler (1990a), de Klerk (1992), Maier and Barnes (1999) and Ashwal et al. (2005). Marker horizons: *LG* lower group chromitites, *MG* middle group chromitites, *UG* upper group chromitites, *MR* Merensky Reef, *BR* Bastard Reef, *PM* Pyroxenite Marker, *MML* main magnetite layer, *M21* magnetite layer 21. *Abbreviations* to the right of the column indicate first appearance (+) and disappearance (−) of cumulus phases: *Pl* plagioclase, *Ol* olivine, *Cr* chromite, *Cpx* clinopyroxene, *Inv Pig* inverted pigeonite, *Opx* orthopyroxene, *Mt* magnetite, *Ap* apatite

The *Marginal Zone* is of variable thickness (0 to several hundreds of metres) and consists largely of quenched to fine-grained norites in contact with the LZ (B-1 suite) or very fine-grained to fine-grained gabbronorite in contact with CZ (the B-2 suite) and MZ (B-3 suite) (Sharpe 1981). Xenoliths of quartzite (e.g. on the Clapham farm) and dolomite (e.g. on Hendriksplaas) locally attest to interaction with the floor rocks. Less common are anorthosite xenoliths (Bristow et al. 1993, p. 46). The latter could suggest that some Marginal Zone rocks crystallized from residual liquids derived from within the chamber (Sharpe 1981; Eales and Cawthorn 1996). A model of relatively late injection of the Marginal Zone is consistent with some of the field evidence, notably intrusive relationships of Marginal Zone rocks relative to CZ rocks (e.g. along the Tweefontein–Lydenburg road, 25.2 km stone: Bristow et al. 1993).

The *Lower Zone* (LZ) on the western limb of the complex consists predominantly of harzburgite and dunite (60 vol.% at Union Section; Teigler and Eales 1996) as well as orthopyroxenite (approximately 40 vol.%). Plagioclase is not present as a cumulate phase, with the exception of a ~90-cm norite layer midway up the sequence that has been delineated in both the western and eastern limbs of the complex (Teigler 1990a; Lee and Tredoux 1986). The modal data compiled in Fig. 2 highlight the intricate interlayering of olivine- and orthopyroxene-rich rocks in the LZ that, analogous to similar rocks, e.g. in the Rum and Muskox intrusions, inspired early workers to develop the concept of multiple magma replenishment in layered intrusions (Brown 1956; Irvine 1970). In places, the layering may be prominently exposed in the field, for example, on the Jagdlust farm where relatively resistant

Fig. 3 Photographs of lithologies in the Lower and Lower Critical Zones. **a** A profile from the floor rocks to the top of the Upper Critical Zone in the Olifants River Trough (the so-called Cameron Section), eastern Bushveld Complex. View towards NW. The quartzitic floor rocks of the Complex form the gently sloped hills 2–3 km to the right of the road. The Bushveld Complex dips at about 20° to the left (to the SW). The Lower Zone contains the pyramid-shaped hills to the immediate right of the road in the distance. The hill tops and the SW-dipping dip slopes are formed by relatively resistant orthopyroxenites, while depressions between the pyramids are formed by weathered-out olivine-rich rocks. The boundary between the Lower Zone and Lower Critical Zone is located near the road. The gently sloped hill to the left of the road represents the Critical Zone, with the base of the Upper Critical Zone located approximately 300 m from the foot of the hill. The dip slope at the top of the hill is formed by the UG1 chromitite and associated rocks, with the steep cliff beneath being formed by leuconorite and anorthosite. **b** Interlayered harzburgite–orthopyroxenite layers of the C1 unit, Lower Critical Zone, exposed in Winterveld mine adit, eastern Bushveld. **c** The LG6 chromitite near the adit to the Jagdlust mine, eastern Bushveld. C = densely packed chromite, M = disseminated chromite. **d** The MG3 chromitite exposed on the farm Jagdlust, containing abundant autoliths of pyroxenite and anorthosite. **e** The MG2–3 sequence and the contact between the Lower Critical Zone and Upper Critical Zone on the farm Tweefontein, eastern Bushveld; see *truck* for scale. **f** The anorthosite layer at the base of the Upper Critical Zone, exposed on Jagdlust. Note the undulating chromite stringer of variable thickness and overlying narrow zone of anorthosite adcumulate (reproduced with permission of J Scoates)

orthopyroxenite forms pyramid-shaped ridges within a plain of weathered olivine-rich rocks (Fig. 3a). The highest modal olivine contents occur in a dunitic–harzburgitic interval near the top of the LZ that is also characterized by the most primitive mineral and whole-rock compositions of the analysed sequence (Cameron 1978; Teigler 1990a; Teigler and Eales 1996). Amongst LZ rocks, the dunites are closest to monomineralic compositions, forming olivine adcumulates with only minor orthopyroxene oikocrysts (Fig. 4a). Plagioclase, clinopyroxene and other minor minerals comprise up to ~10 % of most other LZ samples, apart from the basal 50 m of the intrusion where these components reach approximately 30

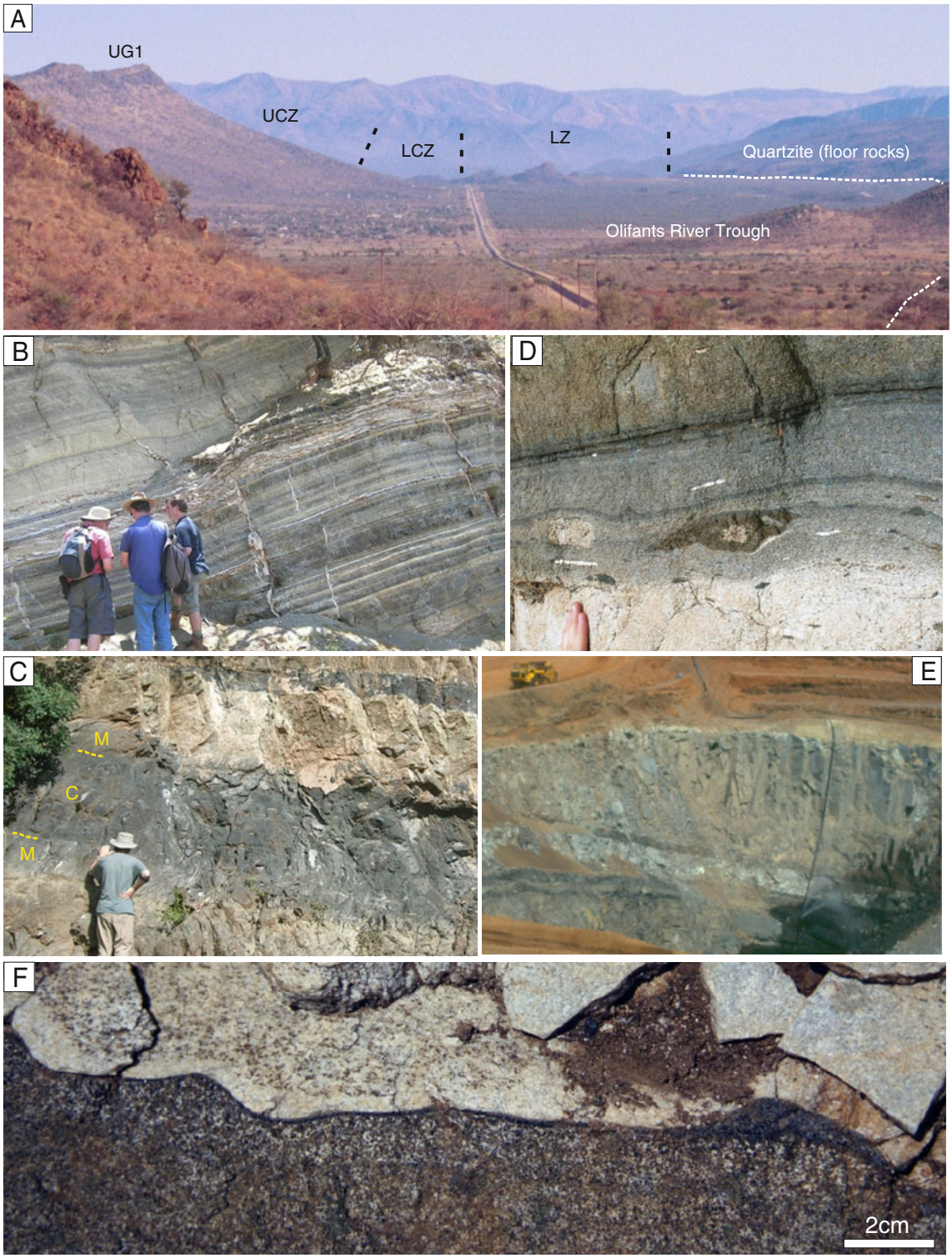

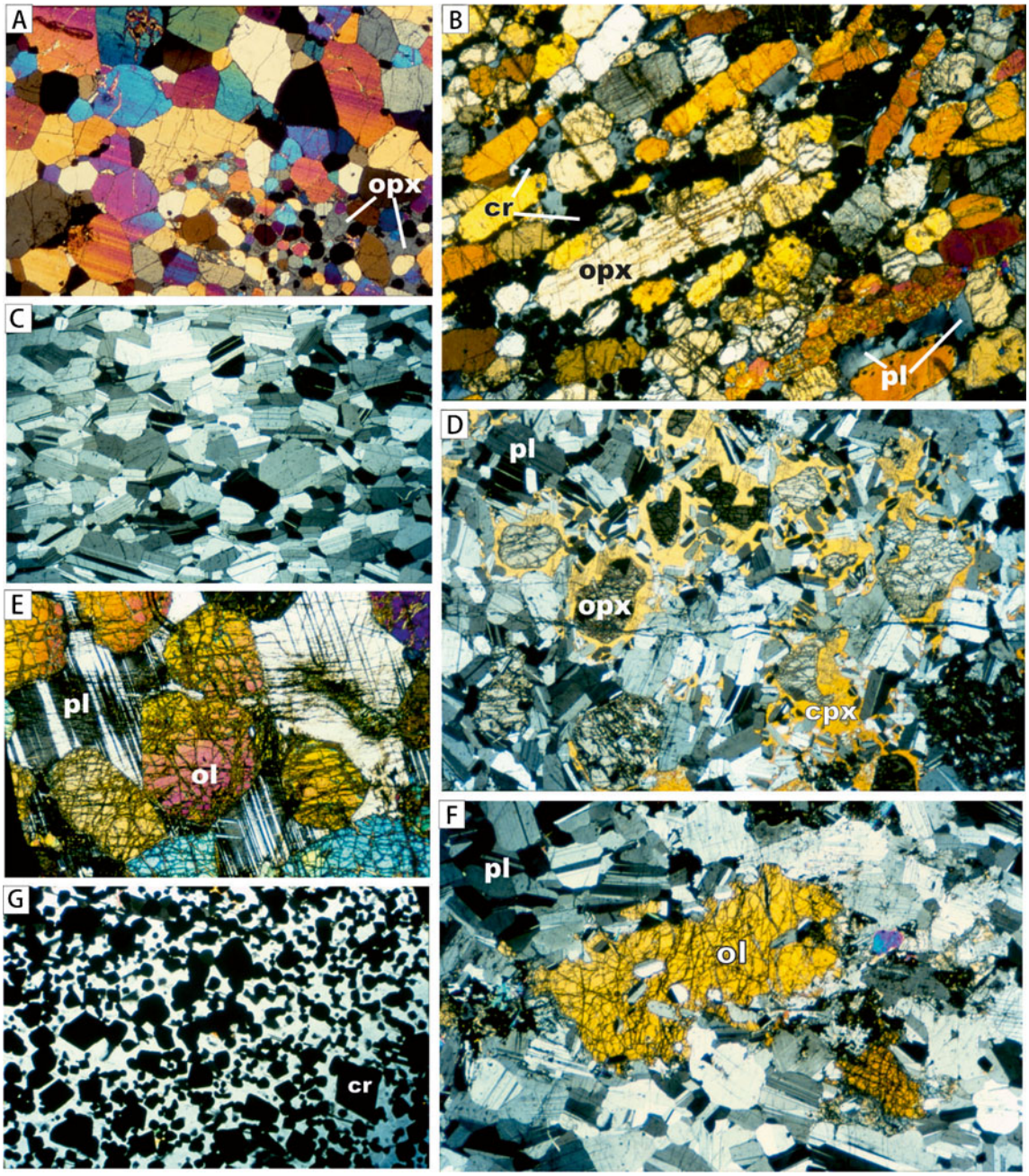

Fig. 4 Representative rock types from the Lower and Critical Zones. **a** Olivine adcumulate, with orthopyroxene oikocrysts, Lower Zone, Union Section. Field width 4 mm. **b** Laminated orthopyroxene–chromite mesocumulate, UG2 unit, Impala section. Field width 4 mm. **c** Anorthosite adcumulate, 40 m below Merensky Reef, to the southwest of Brits. Field width 8.7 mm. **d** Gabbronorite orthocumulate, Merensky footwall, to the southwest of Brits. Field width 8 mm. **e** Olivine orthocumulate with large grains of intercumulus plagioclase, Pseudoreef, Upper Critical Zone, Amandelbult section. Field width 8.7 mm. **f** Troctolite, FW8, Impala Wildebeestfontein North mine. Note the anhedral nature of olivine and rounded inclusions of plagioclase in olivine. **g** UG2 chromitite to the southwest of Brits. Gangue consists of orthopyroxene and makes up about 50 % of rock. Field width 4 mm

modal% (Fig. 2). Chromite makes up <1 modal% in most LZ rocks, irrespective of lithology. Notably, the LZ shows more pronounced lateral variation in thickness and lithology than the overlying stratigraphic intervals. In some trough structures, it reaches a thickness of >1 km, for example, in the Olifants River trough at Cameron Section (Fig. 3a) or near Burgersfort in the eastern lobe (Button 1976; Wilson and Chunnett 2010), but it is thinner or absent above swells between the troughs. Facies changes of the LZ across the swells indicate that compartmentalization was effective during crystallization (Scoon and Teigler 1994). This is also expressed in the lithological and compositional variation of

the LZ between limbs. In the western Bushveld Complex, olivine-rich rocks occur throughout the LZ, whereas in much of the eastern Bushveld olivine-rich rocks are relatively less prevalent and confined to the upper portion of the LZ (Teigler 1990a, b; Cameron 1978) and along its base (to the NE of Burgersfort; Wilson and Chunnett 2010; Wilson 2012). The latter rocks appear to be somewhat more primitive than LZ rocks from elsewhere in the Bushveld Complex (maximum Fo_{92}, as opposed to the normal maximum values of $Fo_{89–90}$), except for the northern limb, where high Fo contents (91) correlate with relatively high Cr/Fe of chromite (Hulbert and Von Gruenewaldt 1982; Hulbert 1983). Based on Th and REE whole-rock concentrations, Maier and Barnes (1998) concluded that the LZ rocks contain 10–20 % trapped liquid component. Godel et al. (2011) combined textural studies with laser ablation analysis of minerals to show that the LZ and LCZ rocks crystallized from magma of B-1 composition and that the calculated percentage of trapped liquid component is consistent with the petrographic observations.

Next in the stratigraphy is the *Lower Critical Zone* (LCZ), which is ~700–800 m in thickness and consists predominantly of orthopyroxenite (89 %: Teigler and Eales, 1996). Harzburgitic rocks occur within two intervals (Fig. 2), including the C1 unit of Cameron (1982) where harzburgite is finely interlayered with orthopyroxenite (Fig. 3b). There are nine major chromitite seams (Lower Group or LG seams 1–7 and Middle Group or MG seams 1–2), of which LG6 (the sixth from the base; Fig. 3c) hosts the largest chromite reserve on Earth (Crowson 2001). The seams have been correlated, albeit at variable thickness, across much of the complex (Cousins and Feringa 1964; Teigler et al. 1992; Teigler and Eales 1996), highlighting that the LCZ shows less pronounced lateral variation than the LZ. The base of the LCZ has been defined as the level where there is a significant increase in intercumulus plagioclase (from 2 to 6 %: Cameron 1978). In contrast, Teigler (1990a) preferred to place the boundary ~200 m lower, at the top of the main olivine-rich interval (Fig. 2).

In the western and eastern lobes of the complex, the base of the *Upper Critical Zone* (UCZ) is defined by a laterally continuous, 1–3-m-thick anorthosite layer (Fig. 3d–f). It overlies orthopyroxenite with a sharp but undulating contact marked by a 1–2-mm chromitite stringer and, in places, an overlying 1–2 cm selvage of anorthosite adcumulate (Fig. 3f). In the northern limb, fine-grained UCZ rocks overlie thick harzburgites of what is believed to be the LZ, implying that the LCZ could be absent (Hulbert 1983; Maier et al. 2008a). In addition, the contact sequence between the LZ and the UCZ locally contains large xenoliths or rafts of quartzite and dolomite (Hulbert 1983; Maier et al. 2008a; Yudovskaya et al. 2012). These field relationships suggest that, along the northern limb, the LZ and UCZ may form distinct sill-like intrusive bodies.

The UCZ is up to ~500 m in thickness (Fig. 2). The main lithologies are orthopyroxenites (~70 %; Fig. 4b), norites (~25 %; Fig. 4d) and anorthosites (~5 %; Fig. 4c) (Teigler and Eales 1996; authors' unpublished data). The pyroxenites may form adcumulates or laminated ortho- or mesocumulates. The norites typically are mesocumulates, containing several percent of intercumulus clinopyroxene, forming in many cases large oikocrysts (Fig. 4d). Anorthosites mostly occur as mesocumulates in which large mottles of intercumulus orthopyroxene and clinopyroxene constitute up to 20 % of the rock. However, anorthosite may also form adcumulates, for example, as centimetre- to decimetre-thick selvages at the base of the UCZ (Fig. 3f) and below the Merensky Reef (Fig. 5d). Olivine-bearing rocks (harzburgite and troctolite) make up <1 % of the UCZ (Fig. 2; Fig. 4e, f) and are essentially confined to the northwestern Bushveld (Viljoen et al. 1986a, b; Eales et al. 1988; Maier and Eales 1997) where they form part of the Merensky and Pseudo Reefs. In most of the remainder of Bushveld, the predominant mafic mineral of the Merensky Reef is orthopyroxene, and the Pseudo Reefs are absent. The Merensky and Pseudo Reefs are decimetre- to metre-wide coarse-grained to pegmatoidal orthocumulate layers locally characterized by up to 40 % of intercumulus material (Fig. 4e). Chromite is a trace component in most UCZ rocks, but the mineral may be locally concentrated to form bedding-parallel schlieren (Fig. 4b). In addition to disseminated chromite, the UCZ contains four to five major chromitite seams, including Middle Group (MG) seams 3–4 (Fig. 3d, e) and Upper Group (UG) seams 1–2 (Fig. 5a, b; 1–3 in the eastern lobe) as well as dozens of minor seams and stringers, including those below the UG1 chromitite (Fig. 5a), above the UG2 (Fig. 5b) and bracketing the Merensky Reef pegmatoid (Fig. 5d). The Bushveld chromitites contain variable gangue contents that progressively increase with height (de Waal 1975; Maier and Barnes 1999), with the UG seams having up to 40 % gangue component (Fig. 4g).

A feature that is particularly characteristic of the UCZ is the occurrence of cyclic units (Cameron 1982; Eales et al. 1986, 1988, 1990). The base of the units typically consists of ultramafic rocks (i.e. chromitite and/or harzburgite and/or pyroxenite) that are overlain by progressively more feldspathic rocks (i.e. first norite and then anorthosite; Fig. 5b). The units have thicknesses between a few millimetres (Fig. 6a) to several tens of metres, exceptionally reaching several hundreds of metres (in the cyclic unit overlying the MG4 chromitite; Eales et al. 1990). Platinum-group element mineralization tends to be concentrated in the basal ultramafic portions of the larger units, particularly in the case of the economically important Merensky Reef (Fig. 5c, d) and UG2 chromitite (Fig. 5b), as well as the sub-economic Pseudo Reef harzburgite and Bastard Reef pyroxenite.

Most authors place the base of the 2–3-km-thick *Main Zone* (MZ) at the top of the Bastard cyclic unit, defined by

Fig. 5 Photographs of Upper Critical Zone rocks. **a** The UG1 footwall chromitite stringers at Dwars River. Note the autolith of anorthosite within chromitite band at the lower left and the warping of chromite around the autolith indicating the flow of chromite crystal slurry. **b** The UG2 chromitite at Karee mine, western Bushveld. The main chromitite has an undulating basal contact with footwall anorthosite. Also note the presence of several leader seams and the sharp contact between the UG2 pyroxenite and the hanging wall anorthosite. **c** The Merensky pyroxenite on Hackney, eastern Bushveld, showing a sharply transgressive bottom contact of pyroxenite, cutting the banding in noritic footwall. **d** Merensky Reef at Impala Platinum mine, western Bushveld. Note the chromitite stringers at the base and 10 cm above the base of pyroxenite and the anorthosite zone immediately below the reef. **e** Hanging wall contact of Merensky pyroxenite on Driekop, eastern Bushveld, showing Merensky pegmatoid invading the hanging wall norite

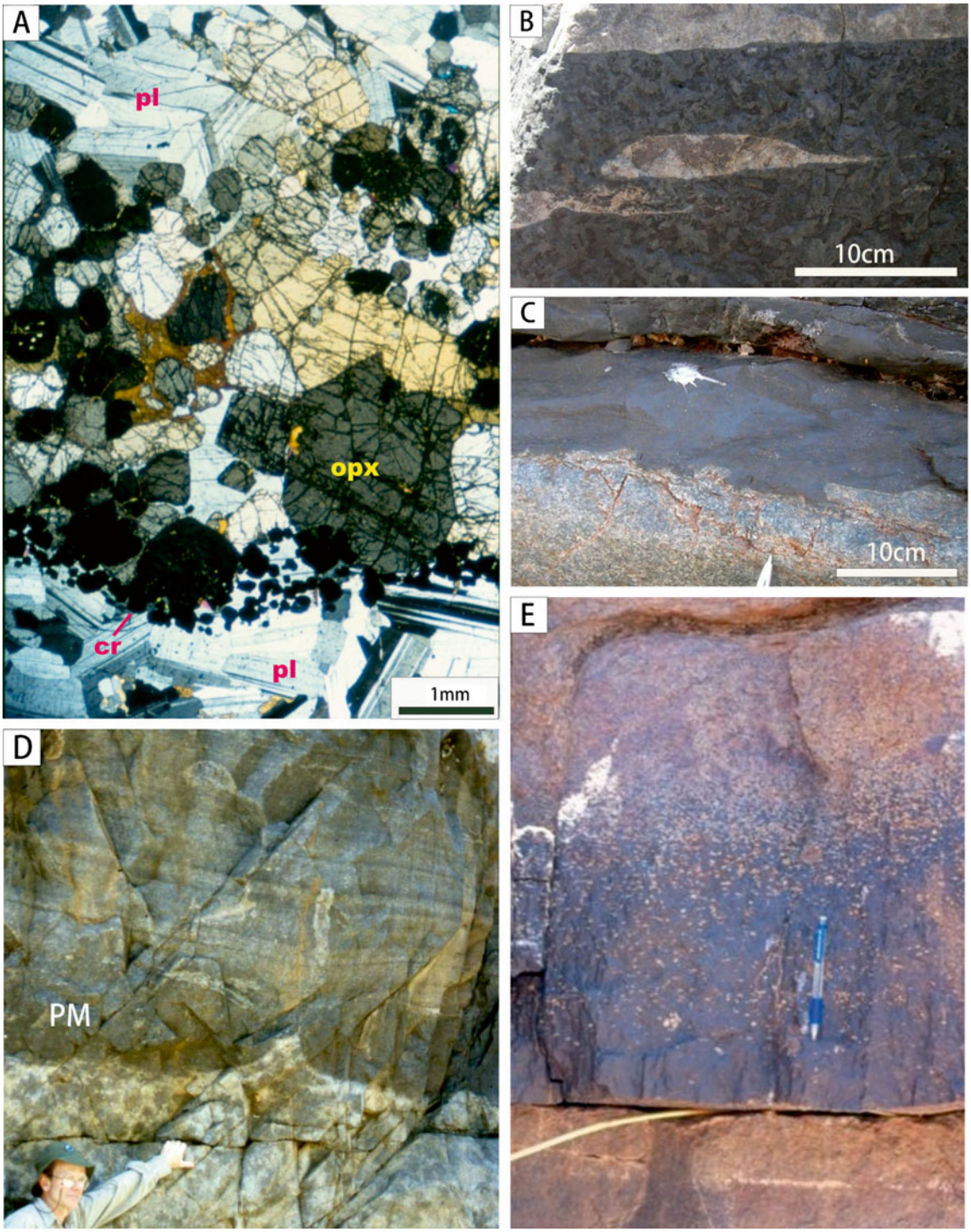

Fig. 6 Photographs of **a** miniature cyclic unit in Pseudoreef interval, Amandelbult section, western Bushveld, with anorthosite at the base overlain by a chromitite stringer, orthopyroxenite and then norite. **b** Anorthosite autoliths with wispy tails in UG1 chromitite, Dwars River. The preservation of these delicate tails is inconsistent with autolith entrainment in magma and is instead interpreted to reflect the residual origin of anorthosite invaded by chromitite slurry. **c** Undulating basal contact of Main Magnetite Layer, Magnet Heights, eastern Bushveld. **d** The pyroxenite marker (*PM*) on the farm Mooimeisjesfontein, eastern Bushveld (from Maier et al. (2001)). Note the undulating contact between melagabbro and anorthosite footwall reminiscent of load cast structure. The anorthosite forms flame-like injections into the overlying melagabbro. **e** Magnetite layer 1 at Magnet Heights. Note the sharp lower contact with anorthosite and the progressive increase in plagioclase content with height

the upper contact of the Giant Mottled Anorthosite (e.g. de Klerk 1992), whereas Kruger (1990) prefers to place the contact at the level of the Merensky Reef, based on a significant change in Sr isotope ratio within the Merensky unit (Kruger 1992). Towards the top of the MZ, there is a prominent melanocratic layer (pyroxenite or melanorite), termed the Pyroxenite Marker (Fig. 6d). This marks a significant compositional reversal and contains some PGE mineralization (Maier et al. 2001; Maier and Barnes 2010). Based on changes in $^{87}Sr/^{86}Sr_i$, Kruger (1990) placed the base of the Upper Zone at this horizon, whereas most other authors (e.g. SACS 1980) take the base of the UZ as the stratigraphic level where cumulate magnetite appears, several hundreds of metres further up in the stratigraphy. Based on the evidence presented in the following sections, Kruger's sub-division has been adopted in this paper (Fig. 2). The bulk of the MZ consists of mostly relatively massive norite and gabbronorite with typically 10–30 % orthopyroxene, 10–20 % clinopyroxene and about 50 % plagioclase (Fig. 2). Intervals that show distinct centimetre- to metre-scale layering are largely confined to the Pyroxenite Marker interval and underlying rocks (Quadling and Cawthorn 1994). A few relatively thin (decimetres to a few metres in thickness) pyroxenite layers may also occur in the lower MZ (Mitchell 1986, 1996), but it remains unknown whether these are enriched in sulfide and PGE.

The approximately 1–2-km-thick *Upper Zone* (UZ) has traditionally been sub-divided into three subzones based on cumulate mineralogy. Sub-zone A contains cumulus plagioclase, low-Ca pyroxene and magnetite. In sub-zone B, olivine becomes an additional cumulus phase. Sub-zone C is defined by the appearance of apatite and is also characterized by the occurrence of numerous large country rock xenoliths. Subzones A and B consist of cyclic units of magnetitite, gabbronorite and anorthosite. In sub-zone C, granular ilmenite is present in the oxide layers, and the cyclic units consist of Fe oxide layers overlain by ferrodiorites (Molyneux 1970; von Gruenewaldt 1971). If Kruger's proposal is accepted, i.e. to place the base of the UZ at the level of the Pyroxenite Marker, the nomenclature for the subzones has to be revised, with the interval above the Pyroxenite Marker constituting sub-zone A and the overlying rocks forming subzones B to D.

The number of magnetite layers varies between localities. In the northern limb of the complex, 16 layers have been recorded (Barnes et al. 2004), whereas up to 26 layers are known from the eastern and western limbs (Cawthorn and Molyneux 1986; Tegner et al. 2006). The oxide layers are between a few centimetres to >10 m in thickness (magnetite layer 21) and many contain abundant anorthosite xenoliths. Most layers have sharp lower contacts, but the upper contacts may be gradational (Fig. 6e). The fourth layer from the bottom (in the eastern limb) is the 1–2-m-thick Main Magnetite Layer from which >50 % of the world's V production is derived (Crowson 2001). It is mined in both the western and eastern Bushveld. The uppermost magnetite layer 21 can reach a thickness of 60 m (www.petmin.co.za 2010) but is more usually on the order of 10 m in thickness. It is characterized by a particularly large amount of anorthosite xenoliths and a reversal in plagioclase composition towards more calcic values (Von Gruenewaldt 1971).

Nature and origin of layering

Review of main concepts

The remarkable diversity in the style of layering within ultramafic–mafic intrusions implies that the formation of the layers is unlikely to be related to a single mechanism (Naslund and McBirney 1996). Processes such as crystal settling (Wager 1963), magma replenishment (Brown 1956), in situ crystallization at the bottom of the magma chamber (Campbell 1978), percolation of interstitial melts and fluids through semi-consolidated cumulates (Irvine 1980), density currents sweeping down along the sidewall of intrusions (Irvine et al. 1998) and emplacement and mobilization of crystal slurries (Emeleus 1986; Eales 2002) could all have contributed to the formation of the layers, particularly in the largest, most slowly cooling intrusions. Some pegmatoidal layers have been explained through sub-solidus textural maturation (McBirney and Hunter 1995) and this model may be applicable to some portions of the laterally extensive pegmatoids at the base of the Merensky Reef and the Pseudo Reefs and below the UG2 chromitite (Barnes and Maier 2002a; Cawthorn and Boerst 2006), although some of these pegmatoids clarly have a replacement origin (Reid and Basson 2002). A model of flux melting and recrystallization of noritic protocumulates was envisaged for the anorthosite selvages underlying the Merensky pegmatoid (Nicholson and Mathez 1991; Boudreau 2008). In addition, some examples of layering have been explained by intrusion of sills into semi-consolidated cumulates (Bédard et al. 1988).

The remarkable lateral extent of many layers in the Bushveld Complex has remained particularly difficult to explain. For example, the Merensky Reef, the UG2 and LG6 chromitites and the Main Magnetite Layer can be correlated for >100 km of strike and several kilometres of dip in both eastern and western lobes (e.g. Cousins and Feringa 1964; Cawthorn and Molyneux 1986). The Pseudo Reef and Boulder Bed horizons occur over a >30-km strike length in the western lobe (Maier and Eales 1997). Perhaps most notably, the UG1 chromitite and its characteristic footwall stringers can be correlated across the entire western and eastern lobes, although the detailed nature of the package may vary considerably (e.g. anorthosite may be

confined to the footwall of the main chromitite or host the entire chromitite package, as seen in parts of Impala mine; Maier and Barnes 2008). In stark contrast to the relative lateral continuity of many of the ultramafic layers of the Critical Zone, the thickness of their leucocratic host intervals may show considerable lateral variation (Eales et al. 1988). For example, the thickness of the feldspathic rocks in the UG2–Merensky interval increases from 20 m in the northwestern Bushveld to 250 m in the southwestern Bushveld (Maier and Eales 1997). The interval between the UG1 and UG2 chromitites lacks feldspathic rocks at Union Section but contains up to 100 m of norite elsewhere in the Western lobe (Cousins and Feringa 1964). The contrasting lateral continuity of the ultramafic and mafic layers of the Critical Zone has been explained by the thermal erosion of feldspathic cumulates by primitive replenishing magmas in the proximity of magma feeder zones (Eales et al. 1988), but we will argue subsequently for a different mechanism.

Amongst students of layered intrusions, the model of gravity-driven fractionation via crystal settling in combination with replenishment and mixing of magmas remains perhaps the most popular explanation for the origin of the layering (e.g. Naldrett et al. 2012). Some features of the Bushveld Complex remain difficult to reconcile with this model, including the fine-scale rhythmic banding, for example, in the C1 unit of the LCZ (Fig. 3b) or in the hanging wall of the Pseudo Reefs at Union Section (Viljoen et al. 1986a) where it is referred to as "inch-scale" layering. However, such layers are relatively rare and could potentially have formed through crystal ageing (Boudreau 1994). Another feature that is difficult to reconcile with crystal settling is the interlayering of adcumulates and orthocumulates, for example, in the Jimberlana intrusion of Western Australia (Campbell 1978). The latter author argued that the adcumulates reached textural equilibrium during in situ crystal growth at the surface of the cumulate pile, particularly where low degrees of supercooling prevailed, i.e. in the central portions of the intrusion. Phase layering would have formed due to fluctuating supersaturation: orthocumulates would form at greater degrees of supercooling and thus be relatively concentrated at the margins and in the upper portions of the intrusion. This model has also been applied to the formation of the PGE reefs (Barnes and Naldrett 1986). However, the sulfide content of many PGE reefs is higher than the cotectic ratio, proposed to be ~0.6 % by Barnes et al. (2009), and thus some preferential concentration of sulfides is required. Furthermore, the high metal tenors of the reef sulfides requires equilibration of the sulfides with large volumes of silicate magma (see Campbell and Naldrett (1979)), which would be difficult to achieve in a narrow crystallization front. Another reason why the Campbell model remains controversial is that it cannot be readily applied to the Bushveld Complex. Adcumulates are rare and largely confined to dunites at the top of the LZ and some anorthosites. Most LZ and LCZ rocks contain ~10 % intercumulus material (Fig. 2), and incompatible trace element contents are 5–30 % of those of the B1 parental magmas (see table in the "Electronic supplementary material"), indicating that the rocks are mesocumulates. The estimation of the trapped liquid component in the feldspathic rocks is more difficult as these rocks may have crystallized from mixtures of several distinct magma types, but the incompatible element abundances allow a rough estimate of about 20–40 % liquid component for the Main Zone cumulates (Barnes et al. 2010).

Formation of magnetite and chromitite layers

Of particular interest are the massive chromitites and magnetitites, in part because of their economic value, but also because of their particularly prominent layering. Looking at the chromitites first, up to 14 major seams are normally distinguished (LG1–7, MG1–4, UG1–3), with thicknesses between ~1 dm and 2 m (Fig. 3c–e). They mostly show good continuity along strike, but thicknesses may vary between lobes and between segments within lobes. In addition to the main seams, there are dozens of thin layers that show less lateral continuity, i.e. they may bifurcate, terminate or merge with thicker seams on a scale of centimetres to hundreds of metres (Fig. 5a). However, the combined thickness of individual chromitite packages (e.g. the UG1 seam and its footwall chromitite stringers, Fig. 5a) is broadly constant along strike (Maier and Teigler 1995). The host rocks to the chromitite seams are mostly orthopyroxenite (LG1–3–5–6–7, MG2–4) or harzburgite (LG2 and 4; Teigler and Eales 1996), but in the UCZ, the chromitite seams normally overlie anorthosite (Fig. 5a, b). In most cases, the contacts of the seams with their silicate host rocks are knife-sharp. Textural and compositional variation across seams has been documented by Hiemstra (1986), Maier and Barnes (2008), Voordouw et al. (2009a, b) and Von Gruenewaldt and Worst (1986). Many, but not all, seams show denser packing of chromite in the centre (Voordouw et al. 2009a; Von Gruenewaldt et al. 1986). In the case of the LG6, a central densely packed domain is bracketed by decimetre-thick zones of more diffuse chromite (Fig. 3c). Platinum-group elements tend to be concentrated at the margins, at least in the case of the well-studied UG1 and UG2 (von Gruenewaldt et al. 1986; Hiemstra 1986; Maier and Barnes 2008). Our observations indicate that many chromitites are relatively enriched in xenoliths compared to their host rocks, e.g. the LG6, the MG3 (Fig. 3d), the UG1 (Fig. 5a, 6b) and the UG2 and UG3. Xenoliths are commonly elongated, have narrow tails (Fig. 6b) and may show extreme length-to-width ratios (Fig. 3d). In some cases, xenoliths are concentrated at specific levels of the seam, for example, mid-level within the UG2. In places, chromitites may drape around xenoliths (e.g. in the

UG1 or MG3; Fig. 3d, 5a), but in most cases the top and bottom contacts of the thicker seams do not bulge around xenoliths, even where the latter constitute a significant portion of the seams (Fig. 3d).

Many of the textural characteristics of the chromitite seams are shared by the magnetite seams. The most economic seam is the Main Magnetite Layer as this combines considerable thickness (up to ~3 m) with some of the highest V contents amongst Bushveld magnetitites (1.5–2 % V_2O_3; Klemm et al. 1985). In this seam, the sharp and undulating basal and top contacts are well exposed (e.g. at Magnet Heights), showing pothole-like depressions at the base (Fig. 6c). Elongated autoliths and xenoliths are abundant and are concentrated near the base and mid-level within the seam. The latter horizon can be traced for tens of kilometres along strike (Cawthorn and Molyneux 1986).

The petrogenesis of the oxide seams remains poorly understood. Magmatic differentiation may drive the magma to cotectics along which chromite and magnetite crystallize together with other minerals. To accumulate the oxide layers, either the minerals must separate effectively from the magma or the magma needs to be pushed into the stability field of the oxides by a sudden change in composition, temperature or pressure. The crystal fractionation model (Toplis and Carroll 1996; Cawthorn and Molyneux 1986; Tollari et al. 2008a, b; Naldrett et al. 2009a, b) requires that after the oxides crystallize, they are preferentially accumulated on the chamber floor because the cotectic porportions of oxides and silicates are ~1 % for chromite (Barnes 1998b) and in the 5–30 % range for magnetite (Toplis and Carroll 1996). Cawthorn and McCarthy (1980) argue that the variation in Cr content across magnetite layers is consistent with the in situ crystallization of magnetite, and Naldrett et al. (2012) interpreted the V contents across the UG2 chromitite to result from crystal fractionation. However, one of the main criticisms of crystal fractionation models has been that the high yield strength of basaltic magmas prevents the effective segregation of small (originally <0.2 mm; e.g. Jackson 1961) magnetite or chromite crystals to form laterally extensive massive oxide layers with knife-sharp bottom and top contacts (McBirney and Noyes 1979). Irvine et al. (1998) proposed that cumulate layers in the Skaergaard intrusion precipitated from density currents of crystal slurries that sweep down the chamber walls, and this model could potentially be applied to the Bushveld oxide layers. However, while it is conceivable that the currents erode the mushy unconsolidated top layer of the previously deposited cumulate, thereby causing the knife-sharp boundaries between layers, density currents cannot readily explain the abundant, highly elongated, sub-horizontally orientated anorthosite autoliths within Bushveld chromitite and magnetitite layers (Fig. 3d). These fragments, or at least their wispy tails, should have been dismembered during flow and/or unmixed from the oxide slurries due to negative buoyancy.

A number of alternative models have been proposed for the formation of the oxide seams, none of which is entirely satisfactory. For example, mixing of resident with replenishing magmas (Irvine 1975; Sharpe and Irvine 1983) may cause supersaturation in oxides due to the curvature of phase boundaries. However, in order to form the laterally extremely extensive Bushveld layers, the proportions and compositions of the mixing end-members would have to be broadly constant across the entire 400-km-wide intrusion, which seems difficult to accept. In what constitutes a variant of the magma mixing model, O'Driscoll et al. (2010) proposed that addition of a plagioclase component to the intruding magma, for example, by assimilation of plagioclase-rich floor rocks, may trigger Cr–Al spinel saturation, leading to the formation of thin chromitite stringers in the Rum intrusion.

Phase stability fields of oxides can be shifted by changes in pressure (Cameron 1980; Lipin 1993). This is a particularly elegant mechanism to explain the massive oxide layers as pressure changes would affect the entire magma chamber simultaneously. Mondal and Mathez (2007) and Naldrett et al. (2012) have argued that the shifts in chromite stability fields resulting from pressure change would be negligible, but relevant experiments remain to be done.

Temporary super-saturation in magnetite or chromite could also be achieved by an increase in the oxygen fugacity of the magma, for example, via contamination (Ulmer 1969). With regard to the magnetitites, the model was rejected by Toplis and Corgne (2002) and Balane et al. (2006) who showed that the relatively high V contents of the Bushveld seams (up to 2.2 % V_2O_5) require the fO_2 of the magma to have been in a narrow range of NNO to NNO-1, inconsistent with significant oxidation peaks. For chromitite layers, the contamination model was recently re-evaluated by Naldrett et al. (2012). By means of thermodynamic modeling, the authors concluded that contamination with the country rocks is unlikely to drive Bushveld magmas into the stability field of chromite. However, whether the combination of magma mixing, P-change and oxidation in response to magma replenishment could trigger oxide supersaturation is an open question.

Nicholson and Mathez (1991) and Boudreau (2008) suggested that the thin chromitite stringers that border the Merensky pegmatoid formed through volatile fluxing that caused reduction of the pyroxene stability field and enlargement of the olivine, spinel and plagioclase stability fields. The chromitite stringers would thus represent hydration fronts. However, the model cannot be easily applied to explain thicker chromitites because of mass balance considerations, that is, there are no complementary zones of Cr depletion associated with the massive chromitite seams.

Furthermore, Barnes and Maier (2002a) have shown that the microstructures and textures of plagioclase grains in the anorthosite footwall are not consistent with the notion that these minerals represent residual material as the grains are elongate parallel to the horizontal, show normal zonation and exhibit high-temperature deformation and micro structures consistent with compaction (Figs. 4c and 5d).

One of the most popular models for the formation of massive magnetite layers is saturation of the magma in Fe oxide liquid (Philpotts 1967; McBirney 1975; Naslund 1983; Zhou et al. 2005). Several experimental studies have produced immiscible Fe oxide liquids from silicate liquids (Roedder 1978; Freestone 1978; Naslund 1983). However, the experiments that produced Fe oxide liquids started with silicate liquids with compositions that are very different to natural rocks. Toplis and Carrol (1995, 1996) and Tollari et al. (2006, 2008) showed that using compositions close to natural basalts and diorites, magnetite or ilmenite crystallize before the magmas become saturated with Fe oxide liquid. Therefore, the weight of experimental evidence does not support the immicibility model. Textural arguments have also been made in support of immiscibility, with a number of workers reporting the presence of Fe-rich and Fe-poor melt inclusions in apatites from layered intrusions (e.g. Jakobsen et al. 2005; Charlier et al. 2011). However, London (2008) argued that melt inclusions in general are not reliable indicators of overall melt composition due to boundary layer effects. Eales and Cawthorn (1996) rejected the liquid immiscibility model for the Bushveld magnetite layers on the grounds that the Fe oxide liquid would not have formed sharp planar contacts with the underlying cumulates. Instead the dense liquid would have percolated into the interstitial spaces in the cumulate.

Formation of anorthosites

The origin of anorthosite layers also remains unresolved. Some authors have proposed flux melting of noritic protocumulates (Nicholson and Mathez 1991; Boudreau 2008) to form the footwall anorthosite to the Merensky Reef (Fig. 3f). However, some anorthosites clearly are intrusive (see below) and thus it is difficult to apply the concept in a general sense. The most widely accepted mechanism remains one of gravitational crystal fractionation (Cawthorn and Ashwal (2009) and references therein). This has been successful in explaining the petrogenesis of massive-type anorthosite complexes (Ashwal (1990) and references therein) where negatively buoyant plagioclase crystals may accumulate at the roof of magma chambers from where they may rise diapirically through the crust. The model is more difficult to apply to the formation of stratiform, laterally extensive and often delicate plagioclase layers within layered intrusions. However, some anorthosite complexes are clearly layered (Michikamau: Emslie 1965; Laramie: Scoates 2000; Kunene: Maier et al. 2008b), suggesting that there are some similarities in the genesis of layered anorthosite massifs and anorthosite layers in layered intrusions.

A particularly enigmatic occurrence of anorthosite has been observed at Smokey Hills mine, on Maandagshoek farm in the eastern Bushveld. Here, anorthosite forms a pothole locally injecting and brecciating pyroxenitic and chromititic host rocks of the UG3 unit in a sill-like manner (J Mungall, T Oberthür, written communication; Fig. 7). Such a process would be consistent with the knife-sharp contacts of many anorthosite layers and with the similarity in the composition of footwall and hanging wall rocks to the layers, but it would require effective downward draining of dense residual liquid after emplacement of plagioclase-rich slurries, analogous to the mechanism proposed by Scoates et al. (2010) for the formation of the Poe Mountain anorthosite. The model implies that some layered intrusions may represent sill complexes and that cumulate piles may not necessarily be emplaced in a bottom-to-top sequence. However, in most Bushveld layers, the An content of the plagioclase is broadly similar to the noritic host rocks, suggesting that if the anorthosites formed from injecting slurries, these must have been derived relatively locally.

Patterns of down-dip compositional variation

The extent of down-dip variation in the Bushveld Complex is not well documented, in part because: (1) the centre of the intrusion is not exposed, (2) the dip of layering is mostly so steep (15–70°) that the mining operations expose only a few kilometres of down-dip exposure and (3) lithological and compositional information is largely confined to the reef intervals. It also remains unclear whether the available exposure comprises predominantly a lateral (along strike) component or whether post-emplacement tilting of the intrusion additionally introduced a significant down-dip component to the exposure.

One of the main areas where there is good down-dip exposure is the northern part of the western lobe where mining occurs over some 10 km in down-dip direction. Along the Union and Amandelbult sections (Fig. 1), Anglo Platinum exploits the UG2 and Merensky Reefs at a relatively shallow depth (down to ~1,500 m), whereas the Northam platinum mine exploits the reefs down-dip from Amandelbult at average depths of 1,750 m and a maximum depth of 2,063 m (Smith 2007). Notably, Northam mine shows the highest grades of the UG2 and the Merensky Reef in the Bushveld (Cawthorn 1999b; Viljoen and Schürmann 1998) and the proportion of feldspar-rich rocks within the UG2–Merensky Reef interval appears to be somewhat lower than at Union and Amandelbult sections (Viring and Cowell 1999). An analogous pattern of down-dip compositional variation, together with an increase in the size and depth of

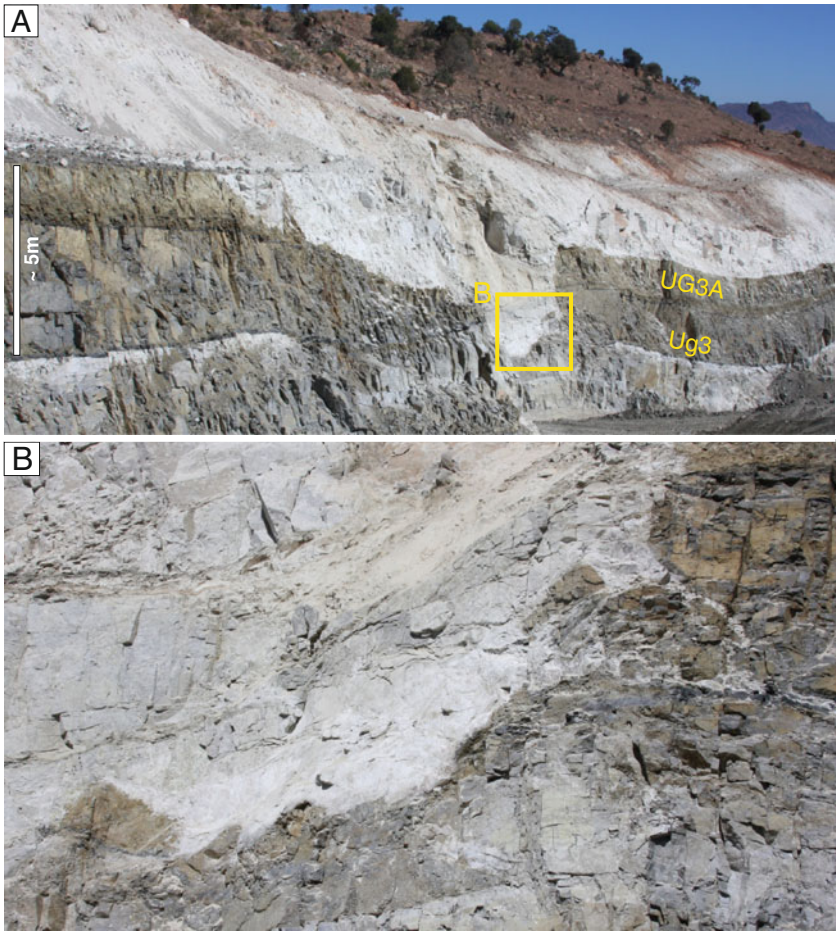

Fig. 7 Photographs showing **a** transgressive anorthosite at Smokey Hills platinum mine, eastern Bushveld. Anorthosite forms a depression structure in UG3 unit, interpreted as a pothole. **b** Close-up image showing the intrusion of anorthosite below UG3 chromitite (*right central*), locally causing fragmentation of UG3 and its hanging wall pyroxenite (*lower left*). This exposure suggests that the stratiform anorthosite layer below UG3, formed through the intrusion of plagioclase-rich magma. Photographs reproduced with the permission of J Mungall and T Oberthür

potholes, has also been recorded on a smaller scale within Union and Amandelbult sections (Eales et al. 1988; Viljoen 1999; Viring and Cowell 1999). In addition, down-dip lithological variation is well exposed in the northern lobe of the Bushveld Complex, on the Rooipoort and Moorddrift farms, where the internal reefs (Merensky, UG2) transform to a more disseminated, low-grade style of mineralization as the margin of the intrusion is approached (Maier et al. 2008a). In the central sector of the Platreef, Yudovskaya and Kinnaird (2010) have shown that the abundance of xenoliths decreases, and the proportion of ultramafic and chromite-enriched rocks increases down-dip. Furthermore, the grade of mineralization may increase significantly down-dip, for example, on Zwartfontein (Akanani project), where mineralized intervals of up to 44 m with up to 4.4 ppm PGE have been intersected. In summary, it appears that wherever there is exposure, the down-dip lithological and compositional variation is more pronounced than along-strike variation.

In contrast to the Bushveld Complex, the preserved portions of the Great Dyke represent only its central and lower segments, with the upper and peripheral segments having been eroded (Prendergast 1988, 1991). Complex patterns of down-dip variation in chromitite composition and lithology have been documented by Prendergast and Wilson (1989). In some layers (e.g. CID), disseminated chromite first transforms into massive seams in a down-dip direction, which then pinch out to be replaced by thick layers of disseminated streaky chromitite in the centre of the intrusion. Of note is the fact that bulk sulfide contents in the Great Dyke appear to be significantly higher than in the (internal) Bushveld reefs. Both the Main and Lower Sulfide Zones can have significantly more than 1 % sulfides over several tens of metres (Prendergast and Wilson 1989). Furthermore, Wilson and Tredoux (1990) showed that bulk sulfide and PGE contents are higher in the axis of the intrusion than at the margins.

A transition from marginal thin chromitite stringers to centrally located seams, reaching up to 90 m in thickness, has been described from the Kemi intrusion, Finland (Alapieti et al. 1989). Below the thickened central segment of the intrusion, there is a dyke of massive chromitite, interpreted to be a feeder zone to the complex (Alapieti et al. 1989). Anderssen et al. (1998) documented a progressive increase in thickness and Au grade of the Platinova reefs towards the centre of the Skaergaard intrusion. Another example of well-characterized down-dip lithological variation is the Jimberlana intrusion (Campbell 1986a), where layering becomes more pronounced, ultramafic layers thicken and orthocumulates transform to adcumulates towards the centre of the intrusion.

Based on evidence from the Bushveld and other layered intrusions summarized earlier, the variations in stratigraphy between the western and eastern lobes of the Bushveld Complex can be placed into a new context. In the eastern lobe, there are three instead of two UG chromitite seams, the UG chromitite package contains more plagioclase-bearing interlayers, potholes are smaller and less abundant, without showing undercuts and having less steep edges than those in the northwestern part of the Bushveld, and PGE grades of the reefs are slightly lower than in the west (Gain 1985; Mossom 1986; Cawthorn 1999b; Naldrett et al. 2009b). Of further note is the contrast in the stratigraphic setting of the Merensky Reef and UG2 within their pyroxenitic host rocks. In the west, both layers occur at the base of pyroxenites (Viljoen et al. 1986a,b; Leeb-du Toit 1986), whereas in the eastern lobe they occur towards the top of pyroxenite layers (Gain 1985; Mossom 1986; Mathez and Mey 2005). These lithological differences are interpreted here to result from a relatively more up-dip location of the exposed eastern lobe (Fig. 8), as discussed in more detail in a later section.

Modification, disturbance and discordance of layering

The remarkable lateral continuity of many Bushveld layers on a regional scale has led to an under-appreciation of locally developed disturbances and irregularities in layering that are particularly evident in the well-exposed UCZ. Irregularity is expressed by transgressive contacts of the reefs relative to their footwalls (in the form of so-called potholes), by regional-scale transgressions of the UZ through the entire underlying cumulate package (the so-called "gaps" in the northwestern Bushveld), by pipe-like transgressive bodies of magnetite, Fe-rich ultramafic pegmatite, or sulfide and by numerous structures reflecting ductile and brittle deformation on various scales. Although some of the latter are clearly of post-magmatic origin, syn-magmatic deformation

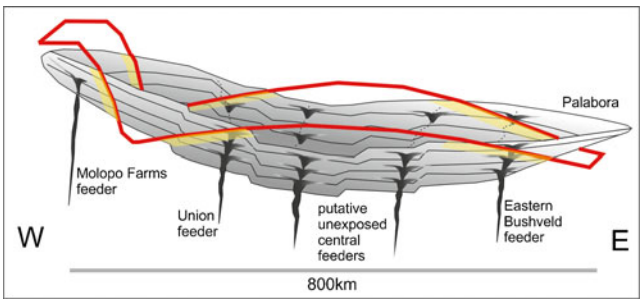

Fig. 8 Schematic diagram, showing how tilting of a complex during tectonism can lead to exposure of reef sections in the west that formed in a relatively down-dip disposition and those in the east at a relatively up-dip disposition (view from south). *Red line* shows the present land surface and the exposed segments of the complex are shown in *yellow shade*. Several proposed and putative feeder zones are shown schematically (see text for explanation)

is expressed in the form of high-temperature shear zones in the reef interval (Carr et al. 1994), and many irregular, in places chaotically oriented small-scale folds. It is becoming increasingly clear that such structures also occur, albeit probably relatively less commonly, in other intervals of the Bushveld Complex, other PGE-bearing layered intrusions (e.g. Stillwater, Penikat, Rum, Mochegorsk) and in layered anorthosite complexes (Scoates et al. 2010). In the following section, these features are described in some detail because it is argued that they are relevant to the formation of the PGE reefs.

Syn-magmatic and late magmatic deformation

Due to relatively pronounced colour contrast, centimetre to decimetre-scale folds and schlieren are particularly evident in interlayered mafic–ultramafic rocks, including pyroxenite–norite and chromitite-anorthosite (Figs. 9 and 10; Cameron 1963; Lee 1981; Viljoen et al. 1986a). In the Bushveld Complex, a particularly well-exposed example of syn-magmatic deformation occurs along the Tweefontein–Lydenburg road, eastern Bushveld, where portions of the Marginal Zone and the overlying LCZ have been irregularly folded (Fig. 9a; Bristow et al. 1993, field locality 5.2). Other examples occur in the UG1 footwall sequence (Figs. 9b, c), as well as the Merensky and the Bastard units (Figs. 10) where chromitite, pyroxenite and melanorite may form sub-angular fragments and irregularly folded schlieren in leuconorite and anorthosite. Decimetre-scale updomings of melanorite into overlying leuconorite that resemble inverted load cast structures occur in the UG2 footwall on Driekop (Fig. 9d). Other structures that may be explained by density contrasts include anorthosite diapirs intruding into overlying chromitite, described from Northam (Viring and Cowell 1999) and Dwars River (Nex 2004), and flames of anorthosite intruding upwards into melanorite of the Pyroxenite Marker on Mooimeisjesfontein, eastern Bushveld (Fig. 6a; Maier et al. 2001). Vertical feldspar stringers and dykelets, particularly common within and above massive chromitite seams (Viljoen et al. 1986a, Fig. 10; Nex 2004), but also recorded within the Merensky Reef, may be interpreted as a result of compaction and filter pressing of feldspar-rich intercumulus liquid (e.g. Barnes and Maier 2002a; Godel et al. 2006; Bédard et al. 2007). Carr et al. (1994) documented the presence of "hot shears" in the Merensky Reef, and similar structures were described in the Poe Mountain Anorthosite (Scoates et al. 2010). Indirect evidence for syn-magmatic deformation of cumulates includes elongated orthopyroxene oikocrysts in the hanging wall of Merensky Reef potholes, interpreted to have crystallized from moving crystal slurries (Carr et al. 1994). Analogous features have been described in the LG6 chromitite (Ireland 1986). Good examples of syn-magmatic

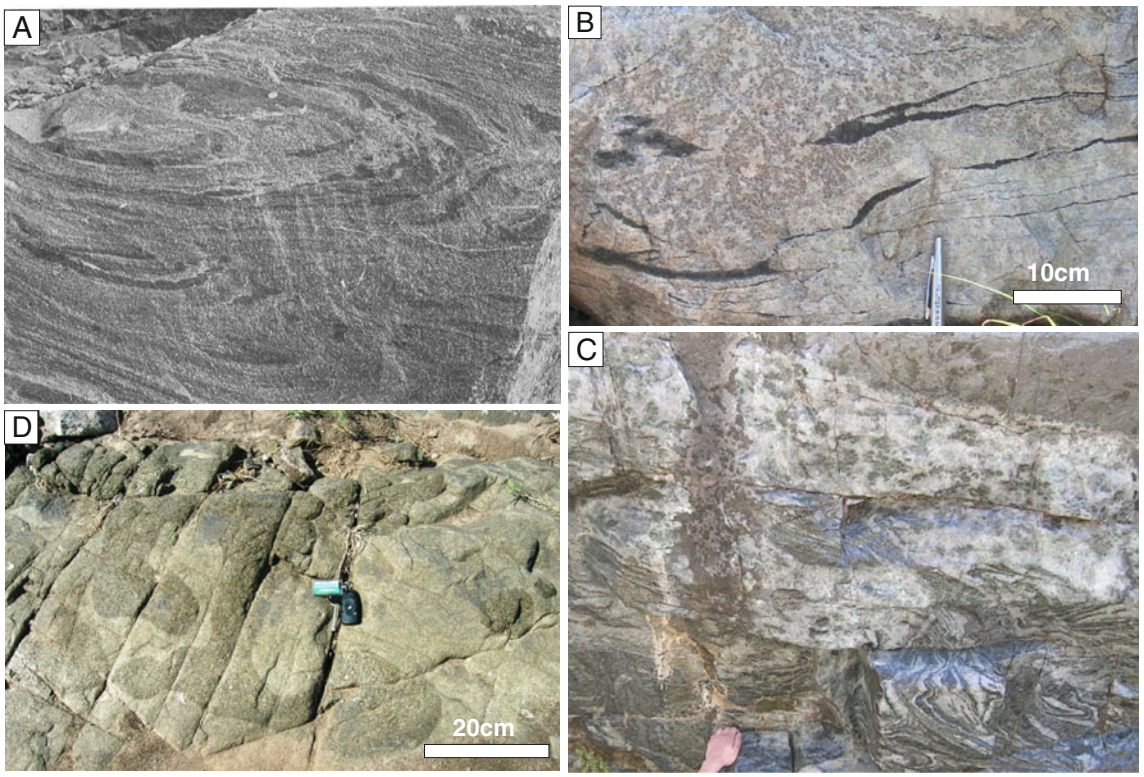

Fig. 9 Ductile deformation in the Upper Critical Zone. **a** Fold of pyroxenite and norite in Marginal Zone, Tweefontein–Lydenburg road, 25.2 km stone (reproduced with permission of RG Cawthorn). Field width ~1m. **b** Footwall of UG1 chromitite (50 cm below main seam), Dwars River, showing folding of chromite stringers. **c** UG1 footwall (10 m below main seam), Dwars River, illustrating the complex deformation of banded norite–anorthosite sequence at the ductile–brittle transition in response to intrusion of mottled anorthosite. Photographed *hand* provides scale. **d** Plan view of updoming of melanorite into leuconorite, UG2 hanging wall, Driekop farm, eastern Bushveld

cumulate slumping also occur in other layered intrusions, notably Rum (O'Driscoll et al. 2010), Stillwater (Czamanske and Zientek 1985), Lille Kufjord (Robins 1982), Fongen Hyllingen (Wilson and Sorensen 1996), Kap Edvard Holm (Tegner et al. 1993), Duke Island (Irvine 1986) and the Poe Mountain anorthosite (Scoates et al. 2010). In the Bushveld, as at Rum and Fongen Hyllingen, deformation may be concentrated in specific layers (e.g. Viljoen et al. 1986a; Fig. 8) that contain fragments of the footwall and hanging wall. These observations indicate that trapped liquid was heterogeneously distributed in the cumulate rocks, locally triggering slumping below the top of the crystal pile.

Transgressive layers and potholes

Some prominent and well-exposed ultramafic layers of the UCZ and UZ, notably the UG chromitites, the Merensky, Pseudo and Bastard reefs, and the Main Magnetite Layer, show transgressive contacts to their leucocratic footwall rocks (Figs. 5 and 6), resulting in depressions with variable depth and width. The larger examples are usually referred to as potholes (Fig. 11), but in the present paper the term is applied in a broader sense to depressions of every scale. The ultramafic rocks thicken in the potholes (e.g. Hahn and Ovendale 1994) as do the overlying mafic layers (Fig. 11b), although to a progressively lesser degree with height above the pothole. Potholes have widths and depths between a few millimetres and >1 km (Viljoen and Hieber 1986, Fig. 30; Viljoen 1999; Van der Merwe and Cawthorn 2005). In some cases, several successive ultramafic layers can be affected by a pothole at the same locality (Viljoen et al. 1986a, Fig. 13), but elsewhere potholes only affect one layer, leaving the under- and overlying ultramafic layers undisturbed. The detailed cross-sectional shapes of potholes can be very complex (Fig. 11d; Viljoen et al. 1986a,b; Viljoen and Hieber 1986; Leeb-du Toit 1986; Viljoen 1999). One of the most important observations is that up-dip contacts of potholes tend to be steeper than down-dip contacts (Fig. 11c; Carr et al. 1994), suggesting that potholes formed on an inclined magma chamber floor. In plan view, potholes tend to be roughly circular or ovoid (Fig. 11a), but examples that are elongated in the down-dip direction have also been described (Viljoen and Hieber 1986). The latter are particularly common in the UG3 chromitite layer at Maandagshoek, where most potholes form channel-like structures. Most of the initial descriptions of potholes were from the Merensky Reef, but this is at least partly due to the excellent exposure resulting from a long history of mining. In addition, potholes are now known to occur in the Bastard pyroxenite

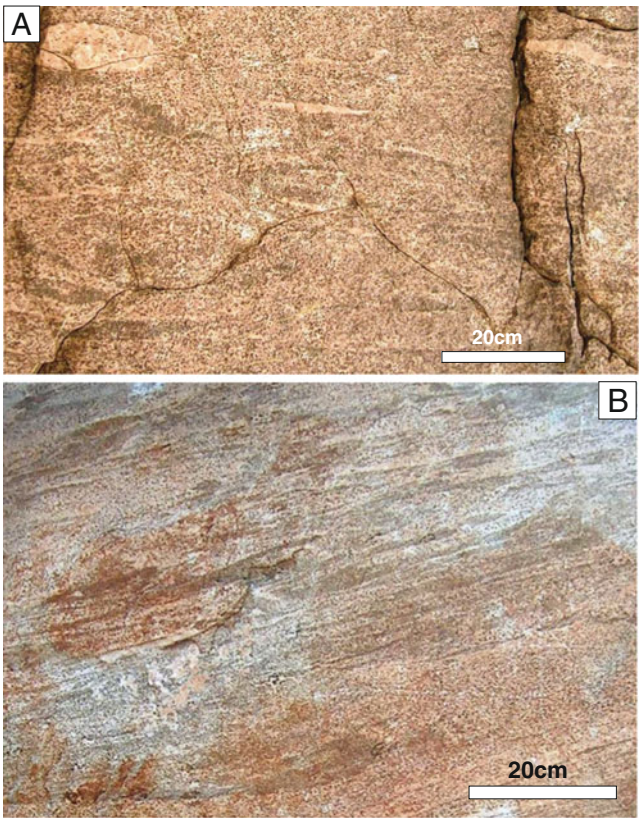

Fig. 10 **a** Anorthosite and melanorite schlieren in leuconorite, MG4 hanging wall, Cameron Section, Jagdlust. Note that in several instances anorthosite schlieren are underlain by pyroxenite or rim pyroxenite. The anorthosite–pyroxenite pairs are interpreted to have resulted from the unmixing of noritic proto cumulates. **b** Ductile deformation in Merensky footwall unit, Hackney. Note the rimming of pyroxenitic schlieren by anorthosite as well as the transgressive anorthositic veins at the *lower left*, interpreted to represent liquid escape structures

(Viljoen and Hieber 1986), the UG3 chromitite (e.g. on Maandagshoek, van der Merwe and Cawthorn 2005), UG2 chromitite (Fig. 11b, d), UG1 chromitite (Fig. 11e; Leeb-du Toit 1986, Fig. 12), LG6 chromitite (e.g. at Cameron Section; Coertze 1958) and in the Main Magnetite Layer (Fig. 6c). It remains unknown whether potholes also occur in the Lower and Main Zones. One of the best outcrops of potholes was temporarily exposed at Karee mine (Fig. 11a; Van der Merwe and Cawthorn 2005). At this locality, UG2 potholes show variable width (1 cm–10 m) and depth (millimetres to 3 m). Egg box-like features reminiscent of the contact between the LZ and UCZ (Fig. 3f) are common, but particularly enigmatic are sporadic star-shaped (Fig. 11f) and dendritic patterns (Fig. 11g), reminiscent of textures related to supercooling.

Outside the Bushveld Complex, pothole-like structures have been described in the J-M reef of the Stillwater Complex, where they are referred to as "ballrooms" (Raedeke and Vian 1986; Harper 2004), from the Penikat intrusion of Finland where they are called "channels" or "depression structures" (Halkoaho 1990a, b; Alapieti and Lahtinen 2002) and from the Poe Mountain anorthosite (Scoates et al. 2010). Transgressive channel-like features extending in a direction normal to the strike also occur at Mimosa mine in the Great Dyke (Prendergast 1988), and structures referred to as potholes were recently described in the Fedorova–Pansky intrusion (Kazanov and Kalinin 2008).

Bushveld potholes have been interpreted as a result of thermo-mechanical–chemical erosion of cumulates by hot magma replenishing the magma chamber (Schmidt 1952; Irvine et al. 1983; Campbell 1986b; Eales et al. 1988; Viljoen 1999) or by cumulate resorption and/or non-deposition in response to volatile fluxing of the compacting cumulate pile (Barry 1964; Von Gruenewaldt 1979; Kinloch 1982; Buntin et al. 1985; Ballhaus 1988), consistent with the occurrence of pegmatoidal domains in the centre of some potholes (Fig. 11c). One of the earliest interpretations was that potholes represent slump structures in semi-consolidated cumulate slurries (Barry 1964; Cousins 1964; Viljoen and Hieber 1986), based on analogies with similar structures in sandstones (Stewart 1966). The model has been revived by Carr et al. (1994) who conducted a detailed survey of pothole distribution at Western Platinum Mine. The authors argue that potholes are preferentially distributed in strike-parallel zones, which they interpreted to represent pull-apart structures that formed due to sagging of semi-consolidated cumulate slurries during subsidence of the centre of the Bushveld Complex.

Transgressive ultramafic bodies

The Bushveld Complex hosts a large number of transgressive iron-rich ultramafic bodies (IRUPs), commonly in the form of pipes (Fig. 12). The pipes predominantly consist of medium- to coarse-grained or pegmatoidal Fe-rich clinopyroxenite and wehrlite. Harzburgite and magnesian dunite also occur but subordinate in abundance. The mineralogy of the IRUPs is complex, comprising olivine (forsterite and hortonolite), ortho- and clinopyroxene, chromite, Ti-magnetite, ilmenite, amphibole, phlogopite, sulfides (pyrrhotite, pentlandite, chalcopyrite), PGM (sperrylite, Pt-Fe alloy) and rare graphite (Schiffries 1982, Stumpfl and Rucklidge 1982; Viljoen and Scoon 1985; Scoon and Mitchell 1994, 2009). Some pipes are concentrically zoned, consisting of outer shells of Fe-rich pegmatoidal pyroxenite and an inner zone of harzburgite and magnesian dunite. Four pipes (Mooihoek: Fig. 1, Driekop, Onverwacht, Twyfelaar) contain high-grade PGE mineralization (Wagner 1929).

Transgressive magnetite pipes

The MZ and UZ of the Bushveld Complex contain abundant transgressive, broadly carrot-shaped magnetite pipes, with depths and widths of up to >100 m (Willemse 1969). In a detailed field mapping project, Von Gruenewaldt (1971)

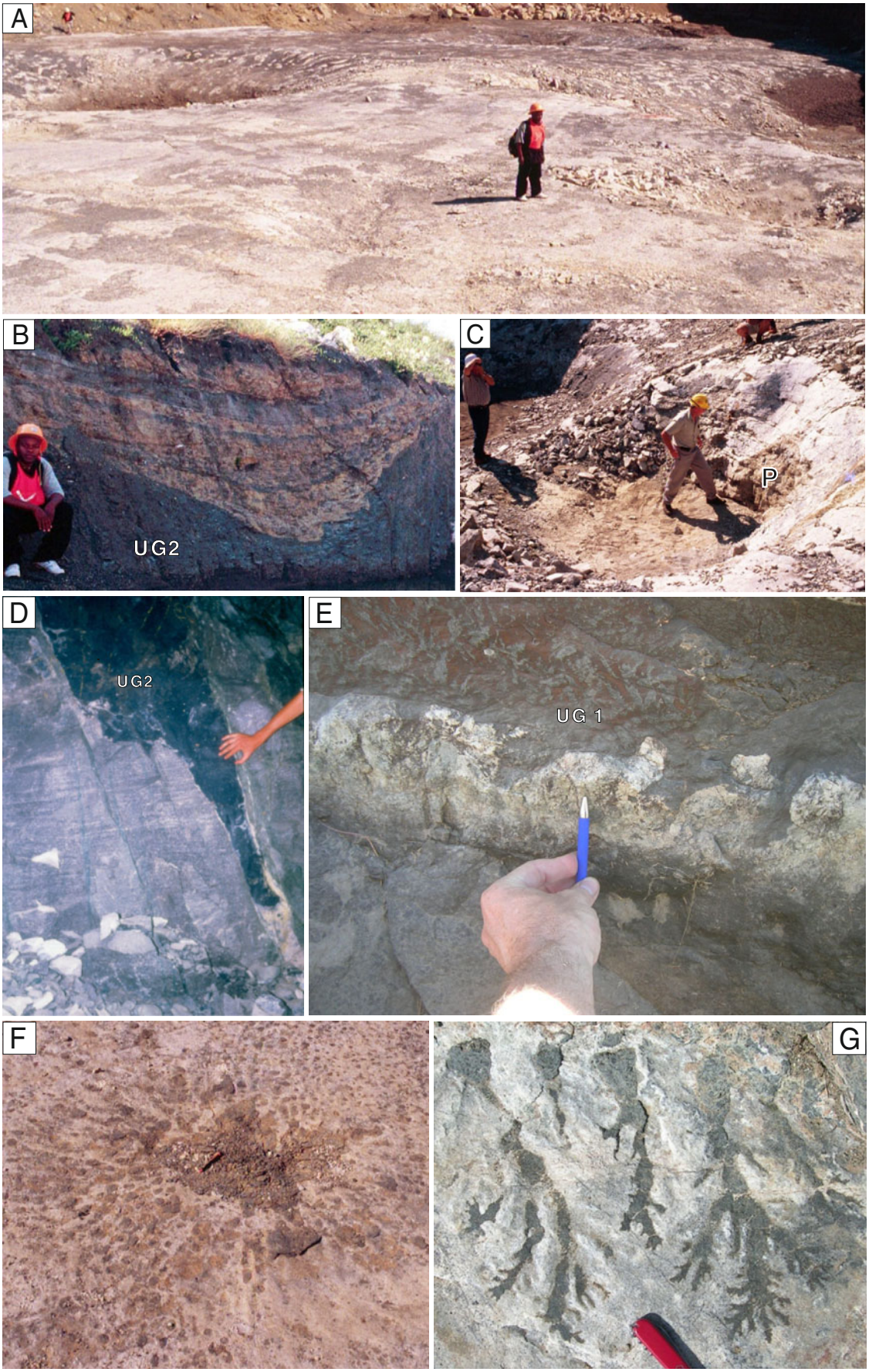
A
B
UG2
C
P
D
UG2
E
UG 1
F
G

◀ **Fig. 11** Photographs of potholes: **a** The anorthositic floor rock of the UG2 chromitite exposed at Karee mine. The overlying UG2 chromitite has been scraped off and mined. Potholes occur on the scale of several metres to centimetres and have variable depths (millimetres to 3 m). **b** Potholed UG2 at Karee mine. Note that the layers located at about 2 m above the pothole have resumed a sub-parallel orientation, indicating that potholes formed at a syn-magmatic stage. Also note the flame-like protrusions of chromitite into the pyroxenitic hanging wall. **c** Dome-like pegmatoid in the centre of pothole at Karee mine. **d** Sharply transgressive UG2 pothole at Crocodile River Mine, western Bushveld, cutting the sub-horizontal layering in norite. Note the feldspathic phase associated with pothole. **e** Small potholes along the base of the UG1 main seam, Dwars River. **f** Star-shaped arrangement of small potholes, Karee mine (note the *marker pen* for scale). **g** Dendritic chromitite forming small potholes at the base of UG3, Maandagshoek

described more than 100 pipes in the Roossenekal area, which suggests that they are extremely common throughout the complex. The pipes appear to be concentrated at certain stratigraphic levels, particularly in the uppermost MZ and in the vicinity of magnetite layer 8, mid-level within the UZ. Amongst the largest magnetite pipes is Kennedy's Vale pipe, which was mined until 2003. Willemse (1969) showed that the composition of the pipes correlates with that of adjacent magnetite seams. This feature would be consistent with the model of Scoon and Mitchell (1994), who suggested that the seams and the pipes formed from Fe-rich (immiscible) melts that locally infiltrated downwards, and with the model of Nabil (2003) for the discordant oxide-bearing ultramafic intrusions of the Duluth Complex, MN, USA, which were interpreted as collapsed magnetite layers plunging into the underlying semi-consolidated cumulates. Both models could explain why no magnetite pipes occur above the uppermost magnetite seam (Willemse 1969). Some of the Bushveld pipes contain sulfides (e.g. Kennedy's Vale), but PGE contents have not been determined. Bearing in mind

Fig. 12 Satellite phases of the Mooihoek iron-rich ultramafic pipe, eastern Bushveld. Note that the Fe-rich ultramafic phase forms bleb- and drop-like masses as well as veins extending downwards, suggesting the downward percolation of magma

that there is a laterally persistent zone of PGE enrichment in the footwall of the Main Magnetite Layer (Liebenberg 1970; von Gruenewaldt 1976) and above the lowermost magnetite layers of the northern limb (Barnes et al. 2004), it is conceivable that some magnetite pipes have elevated PGE contents.

Sulfide pipes

In the far western lobe of the Bushveld Complex, in an area of about 25×6 km immediately to the west of the Pilanesberg alkaline complex, there are numerous transgressive Ni-sulfide bearing pipe-like bodies, referred to as the Vlakfontein Ni pipes (Fig. 1; Liebenberg 1970; Vermaak 1976a). The nature and origin of these pipes remain incompletely understood because the published descriptions focus on the mineralogy and regional geology of the pipes. The bodies occur mostly within interlayered pyroxenite, harzburgite and, to a lesser extent, norite, located about 200–500 m above the base of the Bushveld Complex (Liebenberg 1970). The sulfides in the pipes consist of pyrrhotite, pentlandite and cubanite with less abundant mackinawite and chalcopyrite, with the latter concentrated in the periphery and the upper levels of the pipes. The ore contains inclusions of brecciated chromite and rounded norite. Noble metal contents remain poorly known. Page et al. (1982) reported metal grades of ~1 ppm Pd, ~0.8 ppm Pt, 0.1–0.2 ppm Rh, 0.2 ppm Ru and 1 ppm Ir in the ore, whereas Liebenberg (1970) cited PGE values up to 15 dwts (approx. 30 g/t) in a sulfide pegmatoid with 6.5 % Ni, and Wagner (1929) reported up to 11 ppm Au and 6 ppm Ag. These data suggest significantly lower PGE tenors of sulfides (i.e. PGE in 100 % sulfide) than in the Merensky and UG2 reefs.

Early petrogenetic models related the pipes to putative sulfide pools at the base of the Complex (Schwellnus 1935), which led to extensive geophysical surveys and the drilling of a 1,000-m borehole in the 1930s. No sulfides were encountered. Liebenberg (1970) proposed that the emplacement of the pipes was structurally controlled, and he argued that the sulfides were emplaced syngenetically from above. He drew comparisons to IRUPs, based on field observations such as the pinching-out of the bodies at depth, and compositional data indicating relative Fe enrichment of the silicate minerals (Fo_{65}, En_{74}). However, a syngenetic, magmatic origin of the ores, perhaps via draining of sulfides from the reef horizons, would seem to be inconsistent with the relatively low PGE tenors of the sulfides in the pipes. Moreover, the S in the Ni pipes is isotopically light ($\delta^{34}S = -5$; Liebenberg 1970), implying some introduction of floor-derived sulfur. Vermaak (Vermaak 1976a) suggested that the pipe sulfides were injected from below into structures of Pilanesberg age (1,310±60 Ma; Emerman 1991), which would imply an epigenetic origin.

Large-scale transgressive features

In the so-called Gap areas to the southwest and northeast of Amandelbult Section in the northwestern Bushveld Complex (Fig. 1), the UZ transgressively cuts through the entire MZ, CZ and LZ sequence to rest directly on the floor rocks of the complex (Wilson et al. 1994). In the vicinity of the "Gaps," the dip of the Merensky Reef and other cumulate layers steepens to approximately 30° and the strike swings to a direction normal to the basal contact of the intrusion (Viljoen et al. 1986a). The "Gaps" are thus unlikely to be graben structures. Instead the available data have been interpreted to be consistent with a model whereby the "Gaps" represent magmatic transgressions that formed prior to complete solidification of the cumulate pile (Wilson et al. 1994), perhaps representing giant potholes. Similar structures have been described from the Liloise intrusion in Greenland (Chambers and Brown 1995), implying that cumulates may remain unconsolidated to considerable depth below the top of the cumulate pile. However, the field evidence seems difficult to reconcile with the recent geochronological data by Scoates et al. (2012), indicating a ~5-Ma age span for the Bushveld cumulates, and with most numerical studies that proposed that the mush zone at the top of cumulate piles is relatively thin (up to a few metres: Morse 1988; Holness et al. 2011; Tegner et al. 2009), although Sparks et al. (1985) modeled a mush zone with a thickness on the order of hundreds of metres.

Occurrence of PGE mineralization in the Bushveld and other layered intrusions

Classification schemes for the different styles of PGE mineralization in layered intrusions have been proposed by a number of authors. For example, Naldrett (2004, 2009) subdivided the deposits based on the type of parental magma from which the rocks crystallized. In the present paper, we use the classification of Maier (2005) which is based on host rock type and stratigraphic setting within the intrusions, partly because it is relatively easy to apply in the field: In this classification, there are seven types of deposits: (1) contact reefs, (2) PGE reefs in the peridotitic and pyroxenitic lower portions of layered intrusions, (3) PGE-enriched chromitite layers, (4) silicate-hosted PGE reefs in interlayered mafic–ultramafic rocks, commonly within the central portions of layered intrusions, (5) PGE reefs in the magnetite-enriched upper portions of layered intrusions, (6) PGE-mineralized transgressive Fe-rich ultramafic pipes and (7) vein-hosted PGE deposits in the roof of the intrusions:

1. *Contact reefs* occur along the sidewalls and the base of layered intrusions (Fig. 13). The type locality is the Platreef on the Sandsloot farm and surrounding areas in the northern lobe of the Bushveld Complex (Fig. 1), where the Anglo Platinum Mogalakwena mine is presently the world's only platinum mine exploiting contact-style PGE mineralization. Contact reefs are characterized by thick (tens to hundreds of metres) sequences of mafic–ultramafic rocks, including pyroxenite and gabbronorite, with subordinate peridotite and anorthosite. Sulfides occur mostly in disseminated form, making up between <1 and ~5 % of the rocks. In places, sulfides have been injected into the floor rocks of the intrusions (e.g. Kilvenjärvi, Finland: Andersen and Thalhammer 2006; Platreef: Holwell and McDonald 2006). The reef rocks are commonly vari-textured (or taxitic) and contain abundant autoliths and/or fragments of country rock, the latter interpreted as xenoliths or remnants of the host rocks into which the Platreef has injected as sills (Maier 2002; Manyeruke et al. 2005; Kinnaird et al. 2005). Other evidence for crustal contamination includes highly variable $^{87}Sr/^{86}Sr_i$ (Barton et al. 1986), low $_{\varepsilon}Nd$ (Pronost et al. 2008), high $^{187}Os/^{188}Os_i$ (Reisberg et al. 2011) and enrichment in LILE and other incompatible trace elements (Maier et al. 2008a; McDonald and Holwell 2011). Values of $\delta^{34}S$ that differ from mantle values (Holwell et al. 2007) suggest that at least some of the sulfur in the ores are derived from the country rocks. However, Iljina and Lee (2005) have proposed that the contact mineralization in the Portimo intrusion of Finland represents the abuttal of the internal reefs against the margin of the intrusion and that in situ contamination was not critical to the formation of PGE mineralization but merely overprinted the magmatic sulfides. Lee (1996), Holwell et al. (2007), Penniston-Dorland (2007) and Maier et al. (2008a) have presented evidence from the Platreef consistent with this model.
2. *Silicate-hosted PGE reefs in the peridotitic–pyroxenitic lower portions of layered intrusions* tend to be relatively thick and most have relatively low PGE grades (<1–2 ppm PGE over several metres). The main exception is the Main Sulfide Zone of the Great Dyke where PGE grades reach several parts per million over up to 5 m (Prendergast and Wilson 1989; Oberthür 2002). Other potentially economic examples include the Munni Munni intrusion of Australia (2–5 ppm over 2–5 m; Barnes 1993) and the Mirabela intrusion of Brazil where the PGE and sulfide mineralized interval is several tens of metres thick but contains <1 ppm PGE (Barnes et al. 2011). The Main Sulfide Zone of the Great Dyke shows no evidence for a crustal S or Os component (Li et al. 2008; Schönberg et al. 2003), possibly consistent with sulfide saturation having been reached by magma differentiation. As the amount of sulfides in the reefs does

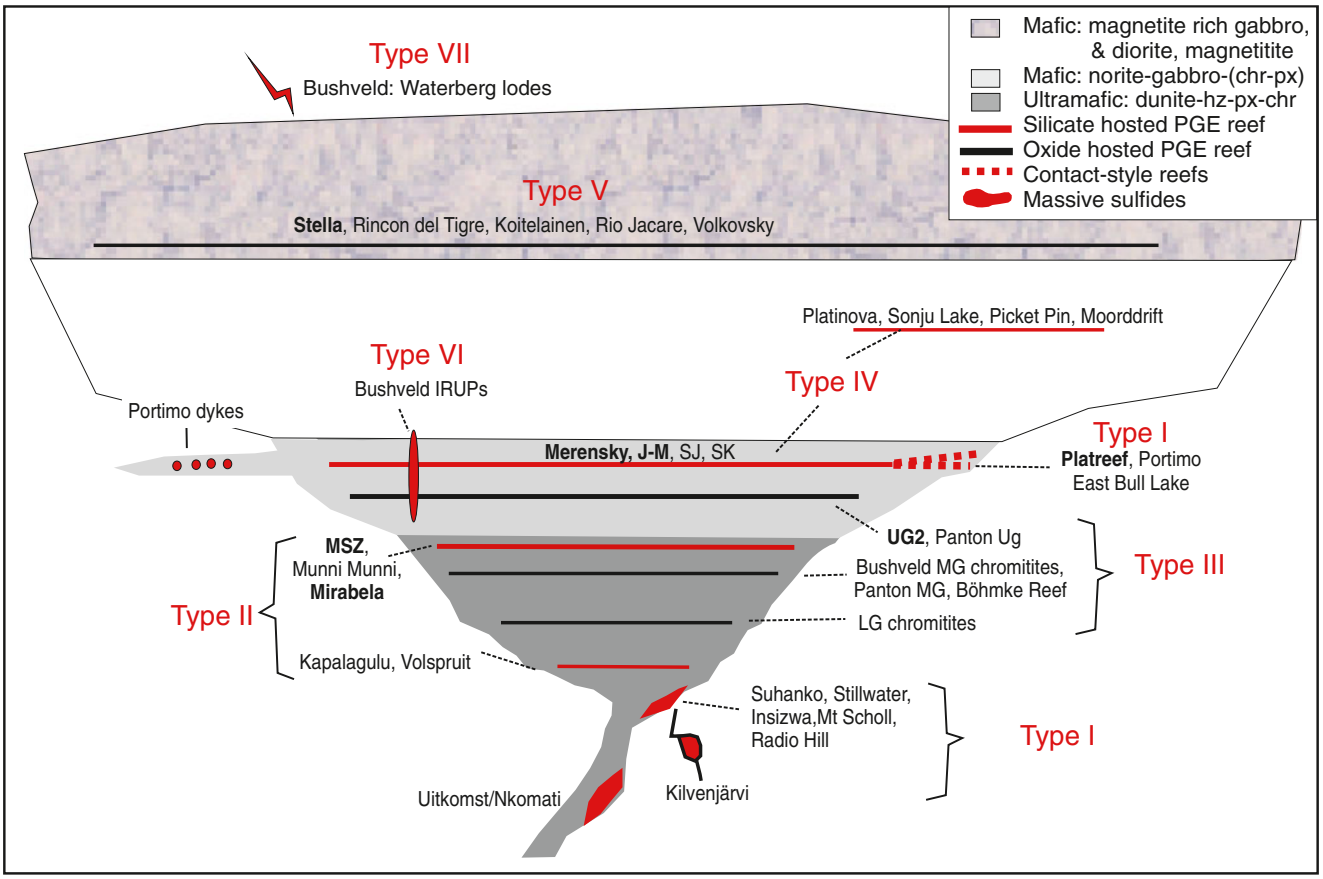

Fig. 13 Schematic diagram showing the occurrence of PGE mineralization in mafic–ultramafic intrusions and their feeder conduits. *J-M* J-M reef of Stillwater Complex, *SJ* Sompujärvi reef of Penikat intrusion, *SK* Siika Kämä reef of Portimo intrusion, *LG–MG–UG* lower–middle–upper group chromitites of Bushveld. *Bold typeface* indicates that reef is economic (modified from Maier (2005))

not significantly exceed the cotectic ratio of ~0.6 % (Barnes et al. 2009), the reefs could have formed through relatively minor concentration of sulfides, in response to preferential settling of sulfide through the silicate magma, or via percolation of sulfide melt through semi-consolidated cumulates. Alternatively, sulfide saturation of the magma could have been triggered by magma mixing. This model is consistent with the fact that several examples of such reefs occur near the transition from the ultramafic to the mafic portions of the intrusions (e.g. Great Dyke, Mirabela, Munni Munni). Furthermore, in most of the ultramafic rocks, the dominant pyroxene is orthopyroxene, whereas at the level of the reefs it is clinopyroxene, possibly suggesting influx of a distinct magma. The Volspruit PGE-mineralized zone in the ultramafic portion of the Bushveld Complex (up to 3 ppm PGE over up to 30 m; Hulbert 1983; Harmer 2004) contains a crustal S isotopic signature consistent with sulfide saturation having been triggered by contamination.

3. *PGE-enriched chromitite layers* occur in the lower to central portions of many layered intrusions, notably in those examples where orthopyroxene crystallized before clinopyroxene (Bushveld, Scoon and Teigler 1994; Stillwater, Zientek et al. 2002; Great Dyke, Oberthür 2002). In most of these cases, the PGE-rich chromitites occur within the lower peridotitic or pyroxenitic portions of the intrusions, but in some cases massive chromitites may also occur within interlayered ultramafic–mafic cumulates situated up to 2 km above the base of the intrusion (Bushveld: Cousins and Feringa 1964; Teigler and Eales 1996; Akanvaara and Koitelainen: Mutanen 1997). The thickness of the mineralized seams varies from a few millimetres to ~1.5 m, i.e. the reefs are much thinner than the ultramafic-hosted silicate reefs described earlier, but grades are normally much higher in the chromitites, reaching ~6 ppm in the UG2 and several tens of parts per million in the Merensky Reef chromitites. In the Bushveld Complex, the correlation between chromitite and PGE is exceptionally good such that even the thinnest chromitite stringers tend to contain elevated PGE grades. However, this is not necessarily the case in all layered intrusions. For example, the thick chromitites at the base of the Kemi intrusion

appear to be barren of PGE, yet a (low-grade) PGE reef occurs in pyroxenite within the upper portion of the intrusion (T Halkoaho, personal communication). The origin of the PGE enrichment in chromitite layers remains controversial partly because many of the most PGE-enriched seams tend to be very S-poor (commonly <100 ppm S; Scoon and Teigler 1994) and the PGE are predominantly hosted by PGM (e.g. Hiemstra 1986). Von Gruenewaldt et al. (1986) and Naldrett and Lehmann (1988) have proposed that the PGE were originally hosted by PGE-rich magmatic sulfides, segregated in response to magma mixing, but that these sulfides were subsequently removed by late magmatic fluids and/or by reaction of sulfide with chromite. The Bushveld seams show a progressive increase with height in PPGE (Rh, Pt, Pd) at broadly constant IPGE (Os, Ir, Ru) contents (Naldrett and von Gruenewaldt 1989; Scoon and Teigler 1994). This trend coincides with decreasing Cr/Fe of the chromitites and has been interpreted to result from the combined effects of differentiation and progressively more vigorous magma mixing (Campbell et al. 1983). A problem with the magma mixing model for the PGE is that, by implication, the chromitites would have to also be related to magma mixing, as proposed by, e.g., Sharpe and Irvine (1983), but there is rarely any evidence for compositional reversals in terms of major or trace elements or Sr isotope ratios above chromitite seams. Schönberg et al. (1999) showed that the Sr of gangue material in chromitite seams is systematically more radiogenic than in the host rocks to the chromitites and argued that this reflects selective roof contamination of those magma pulses from which the chromitites formed. However, it is difficult to comprehend how roof contamination would leave no chemical trace in the host rocks to the chromitites.

4. *Silicate-hosted PGE reefs within the interlayered mafic–ultramafic portions of layered intrusions* include the type example Merensky Reef (Vermaak 1976b; Ballhaus and Stumpfl 1986; Viljoen et al. 1986a,b; Viljoen and Hieber 1986; Mossom 1986; Ballhaus and Sylvester 2000; Barnes and Maier 2002a; Arndt et al. 2005; Wilson and Chunnett 2006; Godel et al. 2006, 2007; Mitchell and Scoon 2007; Naldrett et al. 2009b), the J-M reef of the Stillwater Complex (Barnes and Naldrett 1985; Boudreau, 1988; Zientek et al. 2002; Harper 2004; Godel et al. 2007) and the SJ, AP and PV reefs of the Penikat intrusion in Finland (Halkoaho et al. 1990a, b; Alapieti and Lahtinen 2002). In the case of the Merensky Reef of the western Bushveld Complex, ~1–3 % disseminated sulfides occur in predominantly ultramafic rocks (harzburgite, orthopyroxenite and chromitite) or melanorites at the base of a cyclic unit, overlying anorthosite or leuconorite. In places, notably at Impala and Rustenburg mines, PGE also occur in the feldspathic footwall to the ultramafic rocks (Leeb-du Toit 1986; Barnes and Maier 2002a). In many cases, the main mineralized zone consists of pegmatoid, bracketed by two thin chromitite stringers that contain the peak grades. In the eastern Bushveld, the mineralized interval is located towards the top of an approximately 2–4-m pyroxenite layer. As at most localities in the west, a thin chromitite stringer located at the top of the mineralized zone marks the peak grades. Pegmatoids may also be present, but they tend to overlie the peak reef (Mossom 1986; Mitchell and Scoon 2007; Naldrett et al. 2009b). The SJ reef of the Penikat intrusion also occurs predominantly in ultramafic rocks at the base of a cyclic unit, but as is the case in the Merensky Reef, the feldspathic rocks in the immediate footwall to the ultramafic rocks may also be strongly mineralized. The JM reef of the Stillwater Complex occurs in the first olivine-bearing unit within the mafic part of the intrusion. The rock types hosting the JM reef range from harzburgite, through troctolite and gabbronorite to anorthosite. Chromitite is absent, but PGE grade correlates well with the abundance of sulfides (Zientek et al. 2002). The PV and AP reefs of the Penikat intrusion are somewhat distinct from the other examples discussed as they occur in predominantly plagioclase-rich rocks. However, an ultramafic layer is present in the immediate hanging wall of the PV reef (Halkoaho et al. 1990a, b).

Several models have been proposed to explain the formation of Merensky-type reefs. The most widely accepted model is one whereby sulfide saturation of the silicate magma and segregation of an immiscible sulfide liquid was triggered by mixing between different magmas, either comprising differentiated and primitive members of the same lineage (Irvine 1975) or magmas of different lineage (Campbell et al. 1983; Naldrett and Von Gruenewaldt 1989), consistent with the interlayering of ultramafic and mafic cumulates in the reef intervals and with the fact that some of the reefs occur near the transition between distinct magma types (Merensky Reef: Naldrett et al. 1986; Penikat: Alapieti and Lahtinen 2002). It has been argued that magma mixing was facilitated by the relatively large density contrasts between primitive replenishing and differentiated resident magmas (Campbell et al. 1983), resulting in magma fountaining, high R factors and thus high metal tenors of any immiscible sulfide liquid. We can think of several criticisms of the magma mixing model. First, it has recently been shown that Bushveld parental magmas were strongly undersaturated in sulfide melt (Barnes et al. 2010), yet magma mixing can only result in sulfide supersaturation if the mixing end members are close to sulfide saturation

(Cawthorn 2002; Li and Ripley 2005). Second, in the case of PGE reefs in magnetite-bearing gabbros or magnetitites, discussed in more detail subsequently, there is mostly no chemical evidence for magma mixing, so the process does not seem to be required to form PGE reefs. Third, it remains an open question whether magmas with different viscosities can effectively mix and homogenize across a 400-km-wide intrusion. Fourth, sulfide saturation in response to magma mixing would have to be followed by preferential settling of the sulfide liquid to the top of the cumulate pile, yet whether sulfide droplets can settle through a strongly convecting large magma chamber remains unproven.

Some authors have proposed that the Merensky Reef sulfides formed through contamination of the magma in staging chambers at depth, followed by entrainment of the sulfides (Lee and Butcher 1990; Arndt et al. 2005). However, strong evidence for this model is lacking; whereas initial Sr isotope ratios do show a significant increase in the Merensky Reef interval, this forms part of a broader 100-m interval throughout which $^{87}Sr/^{86}Sr_i$ increases (Eales et al. 1990; Kruger 1994), and thus no clear correlation between the PGE mineralization and crustal component exists. Furthermore, the trace element ratios of the Merensky Reef pyroxenite are not substantially different from those of other UCZ pyroxenites, which can mostly be modeled as a mixture between B1 and B2/B3 magma (Barnes and Maier 2002a). Finally, mass-independent S isotope data (Penniston-Dorland et al. 2011) indicate that the sulfur in the Bushveld layered rocks is isotopically broadly similar to mantle. This does not rule out contamination, as Lesher and Burnham (2001) have demonstrated, but casts further doubt on the role of contamination in the formation of the Merensky sulfides.

Naldrett et al. (2009a, b) proposed that the Merensky Reef sulfides segregated from a sulfide undersaturated magma pulse that contained several 100 ppb PGE. The PGE enrichment would reduce the required thickness of the magma column from which the PGE in the reef are extracted to a few tens of metres, as opposed to hundreds of metres if the magma had the PGE levels of B1 marginal rocks (30–40 ppb Pt + Pd). A thin magma column would facilitate efficient concentration of sulfides at the base of the chamber to produce the decimetre-wide reef. Naldrett et al. suggested that the postulated high PGE contents were acquired when the magmas cannibalized and resorbed previously deposited PGE-rich magmatic sulfides lodged in a feeder conduit or a staging chamber. However, all Bushveld sills analysed so far have Pd contents in the range of other terrestrial basalts and show only minor relative Pt enrichment (Fig. 14). There are only limited PGE data available for potential parental magmas to other layered intrusions. The chilled margin of the Penikat intrusion has 13 ppb Pd (Halkoaho 1994). For the Great Dyke, Prendergast and Keays (1989) give a value of 0.6 ppb Pt and 4 ppb Pd. For Stillwater, the USGS database for dykes with <1,000 ppm S (n=22) gives 1–30 ppb for both Pt and Pd (Zientek et al. 1986). Thus, there is presently no evidence that exceptionally PGE-rich magmas, such as those proposed by Naldrett et al. (2009a, b) for the Bushveld Complex and by Keays et al. (2010) for the Stillwater Complex, exist. Furthermore, the model is also inconsistent with the low solubility of Pt in basic magmas as determined by experiments and thermodynamic calculations. Borisov and Palme (2000) have shown that the solubility of Pt in basic magmas is in the 5–30 ppb range depending on fO_2. Higher Pt contents would thus have to be carried in the form of PGM.

A particularly elegant model for triggering sulfide saturation and PGE reef formation involves changes in pressure (Cawthorn 2005) as this would affect the entire intrusion simultaneously and thus could explain the lateral continuity of the reefs. The model is difficult to test by analysis of the rocks as the subtle pressure changes envisioned would not result in significant compositional

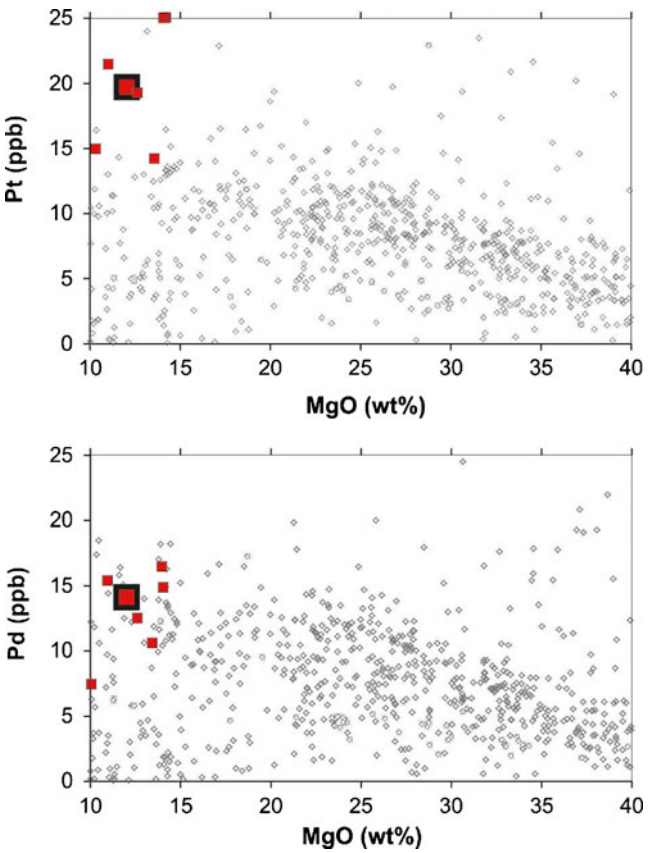

Fig. 14 Platinum and Pd contents of basic and ultrabasic magmas, Bushveld sills are indicated as *red squares* (with the *large square* indicating average composition). Data compiled from Barnes and Fiorentini (2008) and Maier et al. (2009)

changes, but experiments at controlled pressure variations may offer added insight. In particular, it needs to be determined whether small pressure changes <0.1 kbar could trigger sulfide supersaturation. The MZ is approximately 2 km in thickness, and if this was emplaced as a single pulse, pressure may have to be increased by up to 0.6 kbar. However, whether such large influxes are realistic remains controversial. Furthermore, the MZ magma was likely strongly sulfide undersaturated (Barnes et al. 2010). Another problem with the model is that sulfides formed due to pressure change would still have to settle through the magma, facing similar problems to those outlined for the magma mixing model.

5. *PGE reefs in the upper portions of layered intrusions* tend to be relatively wide (up to tens of metres) and have variable tenors. Examples include the Bushveld Complex (Von Gruenewaldt 1979), the Stella intrusion (Maier et al. 2003), Skaergaard (Andersen et al. 1998), Koitelainen (Mutanen 1997), Sonju Lake (Miller et al. 2002), Rincon del Tigre (Prendergast et al. 1998) and Rio Jacaré (Sá et al. 2005). Mineralization is hosted by magnetitites, magnetite gabbros and gabbronorites. In the UZ of the Bushveld Complex, there is only one PGE-enriched horizon of note, forming a laterally persistent, decimetre-wide zone of disseminated sulfides, with 0.7 ppm Pt, 0.9 ppm Pd and 0.5 ppm Au, in the immediate footwall of the Main Magnetite Layer (von Gruenewaldt 1979). The relatively low PGE contents of the Bushveld UZ could be explained by the fact that the intrusion lost much of its PGE budget in the LZ and CZ. At Stella and Skaergaard, the reefs are richer, suggesting that these intrusions remained sulfide-undersaturated throughout more of their crystallization history. This model is consistent with a low crustal component in these intrusions (Stewart and DePaolo 1990; Maier et al. 2003). At Stella, it has been proposed that sulfide saturation was triggered by abundant magnetite crystallization which led to a decrease in fO_2, reduction of sulfate to sulfide, and hence falling S solubility (Maier et al. 2003). A similar model may apply to Koitelainen and Rincon del Tigre. However, at Skaergaard and Sonju Lake, there is no strong positive correlation between sulfur and magnetite contents.
6. *Transgressive iron-rich ultramafic pipes* can host some of the highest PGE grades in the Bushveld Complex, with up to hundreds of parts per million PGE in some samples (Wagner 1929). However, mineralization is highly heterogenous and the bodies tend to be small, giving these deposits a subordinate economic importance. Scoon and Mitchell (2009) proposed that the IRUPs formed from both upsurging and downward percolating melts that may have triggered melting and downward percolation of reef sulfides as outlined in a later section.
7. A rare type of *PGE deposit hosted by quartz-monazite veins* occurs at Naboomspruit in volcanic and sedimentary rocks overlying the RLS (the Waterberg deposit; McDonald et al. 1999). The veins may contain hundreds of parts per million PGE, particularly Pt, with lesser amounts of Pd and Au. The metals are postulated to have precipitated from oxidized, low-T, low-salinity fluids, possibly due to increase in pH in response to replacement of feldspar in the wall rocks (McDonald et al. 1999). Although hydrothermal PGE deposits appear to be rare in the Bushveld Complex, an increasing number are described from elsewhere in the world (e.g. Bursztyn and Olivo 2010), testifying to the fact that PGE can be mobile under certain conditions.

Formation of PGE reefs via late magmatic fluids?

In a series of papers, Boudreau and co-workers (e.g., Boudreau and McCallum 1992; Boudreau and Meurer 1999a, b; Willmore et al. 2000) suggested that the PGE in the reefs of the Stillwater and Bushveld Complexes and other layered intrusions precipitated from late magmatic fluids that ascended through the compacting crystal pile. The authors argue that a high-T fluid percolating through the semi-consolidated cumulates dissolved the sulfides and soluble metals (Pd, Cu and Pt). The fluid moved up into the fluid-undersaturated melt above the cumulate pile and re-dissolved into the melt. At the re-dissolution front, the magma became saturated in sulfide and a sulfide liquid formed to collect the PGE and processes would proceed as normal. In this model, none of the alteration or structural complexity that is so typical of hydrothermal deposits would be expected.

The main evidence presented includes the presence of (1) fluid inclusions and hydrous melt inclusions in silicates and oxides from the reefs, (2) pegmatoids and pegmatites associated with many reefs, (3) desulfidation in and around potholed reef and (4) high Cl/F ratios of apatites below the reef horizons. Evidence for localized, potentially fluid-driven recrystallization is abundant in the Bushveld as expressed by plagioclase halos around chromitite rafts and xenoliths (Viljoen et al. 1986a; Maier and Barnes 2003), replacement of layered rocks by felsic rocks adjacent to potholes (Carr et al. 1994) and potentially non-magmatic Pt/Pd ratios (UG1: Maier and Barnes 2008; IRUPs: Stumpfl and Rucklidge 1982). The model is feasible for the generation of some Pd-rich horizons, but given the low solubility of Pt in silicate magma, it is unclear how the magma can become sufficiently Pt-rich at the mineralization front, unless the Pt moves directly from fluid into sulfides. Another problem with the model concerns the whereabouts of the PGE-depleted material beneath the reefs. In order to form two 1-m reefs containing 10 ppm PGE each via leaching of PGE from footwall rocks containing 100 ppb PGE, 200 m of

completely depleted material beneath the reefs is required, for which there is no evidence in the field or in boreholes. Furthermore, the fluids must also dissolve the insoluble metals Ir, Ru and Rh in order to produce PGE patterns in the Merensky Reef that are broadly consistent with those of the B1 magmas.

Constraints from S contents of Bushveld magmas

In order to constrain the formation of the PGE reefs, it is necessary to know the S solubility and the S content of the parental magmas to an intrusion. For the Bushveld Complex, this can be deduced from the suite of fine-grained marginal rocks and sills emplaced along and below the basal contact of the complex (Sharpe 1978, 1981; Davies et al. 1980; Cawthorn et al. 1981). Barnes et al. (2009) report average S concentrations of approximately 450 ppm for B1 magma, 275 ppm for B2 magma and 100 ppm for B3 magma. The trace sulfides in the sills have magmatic textures and mantle-like S/Se ratios, consistent with a primary magmatic origin (Barnes et al. 2010). The measured S values are significantly lower than those previously reported by Davies and Tredoux (1985). Barnes et al. (2009) propose that the difference is due to the improvement in analytical methods.

The low S contents of the Bushveld magmas have profound implications for the formation of the reefs in that none of the magmas would have been saturated in sulfides at the time of their emplacement in the magma chamber. Barnes et al. (2010) showed that average B1 magma (11.9 % MgO) reaches sulfide saturation after 16 % crystallization (Fig. 15) during the crystallization of orthopyroxene. More primitive B1 compositions with, e.g., 14.5 % MgO would reach sulfide saturation after as much as 40 % crystallization. These results indicate that the Merensky and other Bushveld reefs cannot have formed through mixing of replenishing and residual magmas as proposed originally by Campbell et al. (1983) and subsequently by many other authors. This remains valid even if the resident magma was sulfide-saturated. For example, modeling with the PELE programme of Boudreau (1999) indicates that 9:1 mixtures of fractionated, sulfide-saturated B1 magma with primitive B2 magma are sulfide-undersaturated for the first 6 % of crystallization. A larger proportion of replenishing magma would lead to more severe S undersaturation in the hybrids. Thus, instead of triggering sulfide saturation, magma mixing would likely result in sulfide-undersaturated hybrids, inconsistent with the systematic enrichment of sulfides and PGE in the basal, ultramafic portions of cyclic units. Sulfide saturation could conceivably be achieved if not only the resident but also the replenishing magmas were already fractionated and thus sulfide-saturated. However, in that case, the replenishing magma would likely have been PGE-poor. Moreover, although there are some fractionated B1 sills in the floor of the complex (e.g. ECBV021, 8.84 % MgO; Barnes et al. 2010) that could represent differentiation products of relatively more primitive B1 magma, these sills are also sulfide-undersaturated and they occur below the LZ and LCZ, not the UCZ. The majority of sills below the UCZ formed from strongly sulfide-undersaturated B2 magmas.

Other models invoked to trigger sulfide saturation, including changes in pressure potentially associated with magma replenishment, or contamination, are also implausible in light of the low S contents of the Bushveld magmas. The available data are more consistent with a model whereby sulfide saturation was reached in response to differentiation. Because the proportions of sulfide in the reefs are supercotectic (i.e. the orthopyroxenites have >0.6 % sulfide and the gabbronorites have >0.1 %), the formation of the reefs must have involved some additional concentration of sulfides, potentially via preferential settling of sulfide liquid through the silicate magma or percolation of sulfides through semi-consolidated cumulates (Godel et al. 2007). Chung and Mungall (2009) have argued that sulfide percolation may be impeded at low sulfide contents, but there is textural and compositional evidence in support of the process in the form of PGE-rich sulfides below the Merensky Reef (Viljoen 1999; Barnes and Maier 2002a). Such sulfide percolation could have been facilitated in deforming cumulate slurries when sulfide droplets are squeezed through small pore spaces.

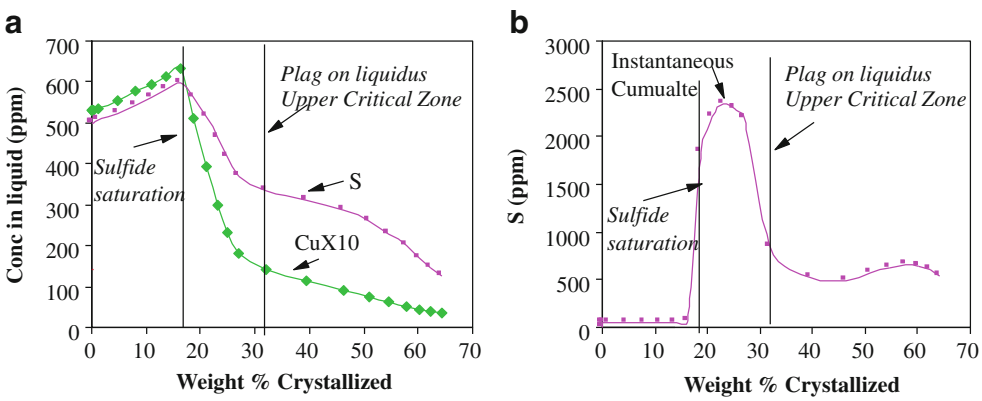

Fig. 15 Plot of wt.% crystallized versus **a** S and Cu concentrations of crystallizing B1 liquid. **b** S contents of instantaneous (cotectic) cumulates (modified from Barnes et al. (2009))

Chemical stratigraphy of the Bushveld Complex: new results

In order to re-evaluate the petrogenesis of the Bushveld PGE reefs, a lithogeochemical section has been compiled through the Bushveld Complex, based largely on analysis of samples collected by the Rhodes University group in the 1980s and 1990s (e.g., de Klerk 1992; Mitchell 1986; Teigler and Eales 1996; Maier and Eales 1997). The rocks are mostly from the NG suite of drill cores located at Union Section in the northwestern Bushveld, except for the samples from the ~400-m-thick Pyroxenite Marker interval which were collected from the drill core on the Moorddrift farm, northern Bushveld (Maier and Barnes 2010), and the UZ samples, collected from the drillcore on the Bellevue farm, 10 km to the north of Mokopane (see detailed descriptions in Barnes et al. (2004); Ashwal et al. 2005).

The major and minor elements were previously determined by WD-XRF at Rhodes University and the University of Québec at Chicoutimi (UQAC), Canada, except for P_2O_5 in the NG samples, which was determined by ICP-MS at Cardiff University, UK. The lithophile trace elements (Cr, Ni, Cu, Co, Zn, Sc, V, REE, Th, U, Nb, Ta, Y, Zr, Hf, Cs, Sr, Ba, Rb) were also determined by ICP-MS at the University of Cardiff. Sulfur was analysed by Leco® infrared spectrometry (Barnes et al. 2009), Se was analysed by thiol cotton fibre-INAA (Barnes et al. 2009) and PGE levels were analysed by ICP-MS after Ni-sulfide fire assay with Te-coprecipitation at UQAC (see Savard et al. (2010) for analytical details). Mineral modes and petrographic descriptions for the samples from the LZ and LCZ are given in Teigler and Eales (1996). The petrography of the UCZ samples is described in de Klerk (1992), that of the MZ samples in Mitchell (1986) and that of the UZ samples in Ashwal et al. (2005). All data are provided in the "Electronic supplementary material", and the most important compositional trends in the composite section are summarized in the following text.

Major and compatible lithophile elements

The major element compositional variation across the studied sequence is illustrated by plots of whole-rock MgO and Cr contents and Mg# of orthopyroxene vs. stratigraphic height (Fig. 16a). Ratios of Cr/V and Ni/Sc show broadly similar trends, due to higher bulk compatibility of Cr and Ni relative to V and Sc, and thus are also useful differentiation indexes, at least in samples free of significant amounts of sulfide and chromite. The data indicate a broad trend of progressive differentiation with height, albeit with numerous major and minor compositional reversals, notably at the base of the sequence, towards the top of the LZ, in the lower portion of the LCZ (where there is a sharp increase in Cr; Fig. 16a), at the top of the UCZ and in the Pyroxenite Marker interval. The reversal at the base of the complex is analogous to those documented in other layered intrusions (e.g. Latypov (2003) and references therein) and may reflect elevated trapped liquid contents due to an enhanced cooling rate. The LZ and CZ reversals broadly coincide with olivine- and/or chromite-rich intervals and, like the reversal in the pyroxenite marker interval, have previously been explained by magma replenishment to the Bushveld chamber (Von Gruenewaldt 1973; Cameron 1978, 1980, 1982; Eales et al. 1990; Cawthorn et al. 1991). Magma replenishment is also held responsible for causing the spectacular modal layering, namely, in the PGE- and Cr-mineralized CZ, characterized by the occurrence of cyclic units. Replenishment of the chamber probably occurred through emplacement of all three Bushveld parental magma types (Eales et al. 1990; Naldrett et al. 2009a, b, 2012; Wilson and Chunnett 2006). Replenishment with tholeiitic basalt (B2 and B3) is consistent with the progressive upward increase in Sr isotopic ratio (Fig. 16b), whereas replenishment with basaltic andestite (B1) is indicated by the lack of progressive Cr and PGE depletion in the CZ (Fig. 16c). However, other data are not entirely consistent with a model whereby the ultramafic layers formed *solely* in response to magma replenishment. Detailed studies by Eales et al. (1990) in the MG3 and MG4 units and Maier and Eales (1997) in the UG2–Merensky Units have shown that changes in lithology, Mg# and An content tend to be decoupled, with the result that the most magnesian orthopyroxenes occur in norites rather than pyroxenites (Fig. 17). This could suggest that modal variation was at least partly caused by crystal sorting, perhaps in slurries sweeping down the chamber walls (Irvine et al. 1998), or in crystal mushes that slumped down-dip along the top of the cumulate pile during chamber subsidence, as will be discussed in more detail in a later section.

Incompatible lithophile trace elements and Sr–Nd isotopes

The distribution of incompatible trace elements in the cumulates is controlled by several factors, including the nature of the parental magma, its state of differentiation, the modal proportions of the main rock-forming minerals, the composition and proportion of trapped melt and percolation of late magmatic and hydrothermal fluids. The relative importance of these factors can be difficult to unravel. For example, many rocks from the LZ and LCZ have higher incompatible trace element contents than most MZ rocks and many of the UZ rocks, possibly in part due to higher trapped melt contents in the LZ, but mainly because the basaltic andesite B1 magma is significantly enriched in incompatible trace elements relative to the tholeiitic B2 and B3 magmas (Fig. 16b; Table 1). The zirconium contents of the LZ and CZ rocks are mostly between 5 and 20 ppm (Fig. 16b), indicating trapped melt contents of about 5–30 % in the LZ and CZ (based on

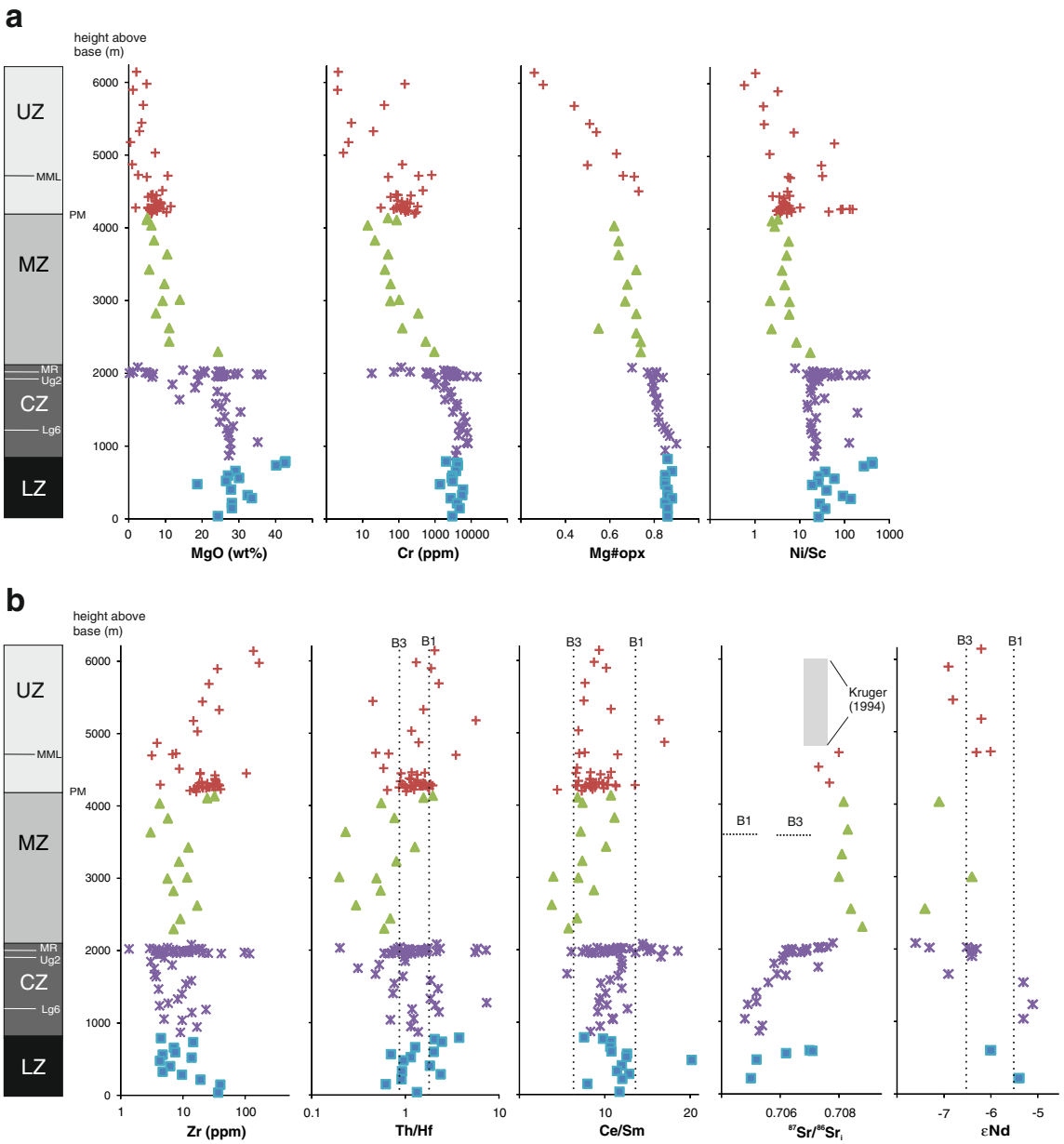

Fig. 16 Compositional profiles through Rustenburg Layered Suite. **a** MgO (whole rock), Cr (wr), Mg#opx and Ni/Sc (wr). **b** Whole rock Zr, Th/Hf, Ce/Sm, initial Sr isotope ratio and εNd. Compositions of B1 and B3 are from Curl (2001) and Barnes et al. (2010). **c** Whole rock S, Cu, Pt + Pd and Ir contents. *Red diamonds* in Critical Zone denote chromitites and PGE reefs. **d** Whole rock Cu/Zr, Cu/Pd, Pt/Pd, S/Se, Pt + Pd/Os + Ir + Ru. *Red diamonds* in Critical Zone denote chromitites and PGE reefs. Compositions of B1 and B3 are from Barnes et al. (2010) and primitive mantle (PM) is from Becker et al. (2006). *LZ* Lower Zone; *CZ* Critical Zone; *MZ* Main Zone; *UZ* Upper Zone (abbreviations of marker layers as in Fig. 2)

77 ppm Zr in B1 magma; Barnes et al. 2010; Table 1). The MZ contains approximately 10 ppm Zr, translating to 36 % trapped liquid (based on 23 ppm Zr in B3 magma; Table 1). Some, but not all, ultramafic layers in the UCZ have much higher incompatible trace element contents than associated norites and anorthosites, presumably because of relatively higher trapped liquid components in the ultramafic rocks. This applies, for example, to the Merensky Reef and UG2 pyroxenite at Amandelbult (Fig. 18) and the Bastard pyroxenite in much of the western Bushveld (De Klerk 1992). This aspect is particularly notable because the ultramafic rocks are denser than the mafic rocks and thus might be expected to compact more efficiently. Other intervals that are relatively enriched in incompatible trace elements include the basal and the relatively differentiated top portions of the complex. Of further note is that the intervals immediately below and above the MZ appear to be particularly enriched in incompatible elements (Fig. 16b).

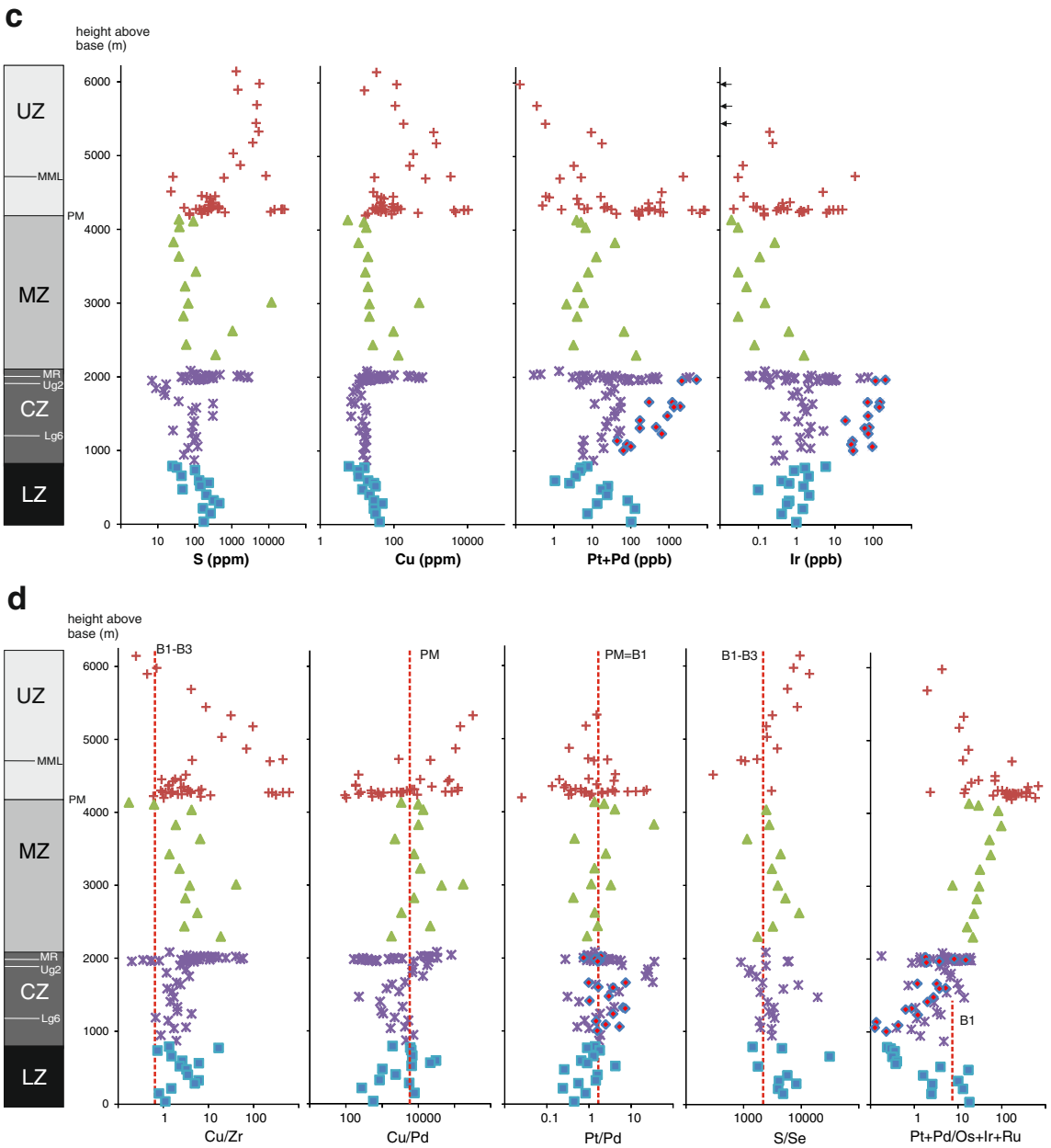

Fig. 16 (continued)

In order to see through the modal effects, it is useful to examine ratios of incompatible trace elements and isotopes. All Bushveld cumulates have a strong crustal component, as indicated by elevated Th/Hf, Ce/Sm and $^{87}Sr/^{86}Sr_i$ (Fig. 16b). Comprehensive incompatible trace element data remain unavailable for the Eastern lobe, but equivalent stratigraphic levels in the eastern and western Bushveld have essentially identical $^{87}Sr/^{86}Sr_i$ isotope ratios (Sharpe 1985; Kruger 1994), suggesting that the crustal component was acquired prior to final emplacement. Evidence for considerable in situ contamination is mainly confined to the basal portion of the northern lobe (the Platreef), whereas in the remainder of the complex the trace element and Sr isotope ratios of the basal rocks differ little from those of the remainder of the sequence (Fig. 16b), which is inconsistent with significant in situ contamination.

In terms of variation with height, the trends for incompatible trace elements and $^{87}Sr/^{86}Sr_i$ are decoupled. For example, Th/Hf and Ce/Sm ratios are highest in the UCZ and UZ, whereas initial Sr isotope ratios are highest in the MZ. The MZ stands out in terms of virtually all compositional parameters examined. Major compositional changes occur over relatively narrow intervals immediately below and above the MZ. At the lower contact of the MZ, $^{87}Sr/^{86}Sr_i$ increases sharply over an interval of about 100 m, starting from the UG1 or its immediate footwall rocks to the top of the Bastard Unit (Fig. 19). Thorium/Hf and Ce/Sm ratios also change across the CZ–MZ

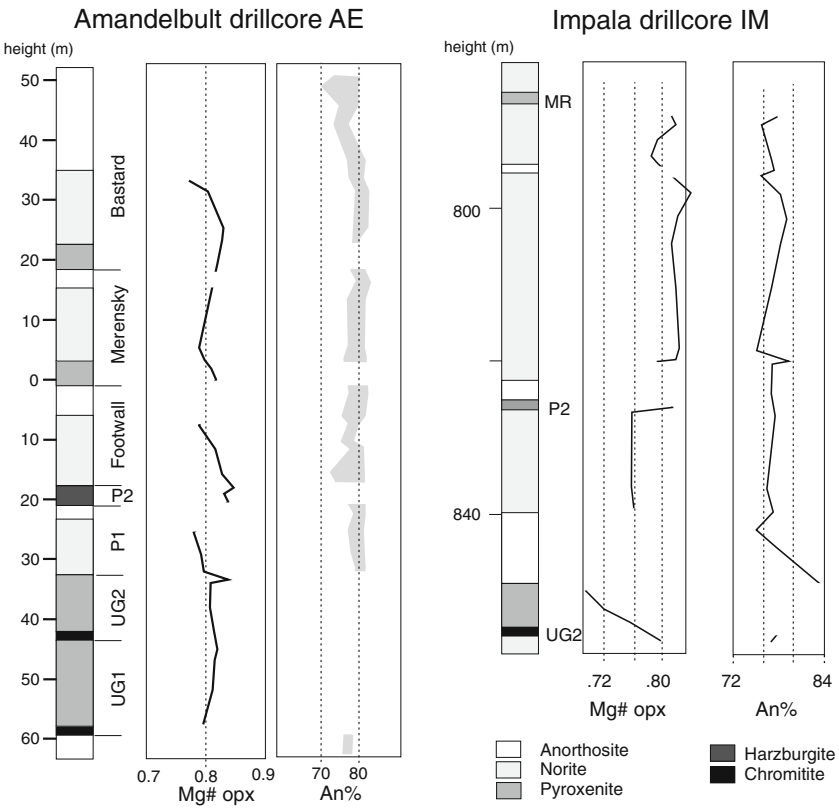

Fig. 17 Mg# of orthopyroxene and An content of plagioclase plotted vs height in Upper Critical Zone cyclic units at Amandelbult (data from Eales et al. 1990) and Impala sections (data from Maier and Eales 1997). In Amandelbult profile, height is in metres below or above Merensky Reef. Units P1 and P2 represent lower and upper Pseudoreef, respectively. In Impala profile, depth is in metres below the top of the drill core

boundary (Fig. 16b), and analogous to the Sr isotope pattern, there is a tendency that the pyroxenitic bases of cyclic units have more B1-like signatures, whereas the more plagioclase-rich upper portions have more B3-like signatures (Fig. 19). This has been explained by a model of progressive mixing of resident B1–B2 hybrid magma with replenishing B1 magma (Campbell et al. 1983; Eales et al. 1986). The basal pyroxenites precipitated mainly from the fresh magma, whereas the overlying norites accumulated from increasingly mixed B1 and B2 magma. At the top of the MZ, across the up-to-400-m-wide Pyroxenite Marker interval, $^{87}Sr/^{86}Sr_i$ falls from 0.708 to 0.707, and $_{\varepsilon}Nd$, Ce/Sm and Th/Hf increase. Notably, detailed Sr isotopic studies of minerals in mafic–ultramafic horizons near the base and the top of the MZ (Merensky Reef and

Table 1 Summary of composition of parental magmas to Bushveld

Name of marginal rock suite	B1	B2	B3
Rock type	Melanorite–pyroxenite	Gabbronorite	Gabbronorite
Magma type	SHMB	Tholeiitic basalt	Tholeiitic basalt
Crystallization sequence	ol > opx + cr > opx + pl > cpx + opx + pl	pl + ol > pl + cpx + opx	pl + ol > pl + cpx + opx
MgO (wt.%): range - avg	8–14.5 (11.85)	3.5–9.5 (6.9)	7–9 (7.7)
Mg#	0.71	0.54	0.62
Cr (ppm)	965	200	407
Ni (ppm)	284	106	132
Zr (ppm)	77	54	23
$^{87}Sr/^{86}Sr_i$	0.70471–0.70599 (0.70540)	0.70618–0.70728 (0.70681)	0.706–0.70618 (0.70611)
εNd	−4.6 to −6.1 (−5.6)	−4.9 to −6.7 (−6.1)	−6.4 to −6.6 (−6.5)
Pt + Pd (ppb)	33	12.5	16
Pt/Pd	1.5	2.5	2.9
Cu/Pd	4,200	20,000	1,100

Data from Barnes et al. (2010), Harmer and Sharpe (1985) and Curl (2001)

SHMB siliceous high-Mg basalt

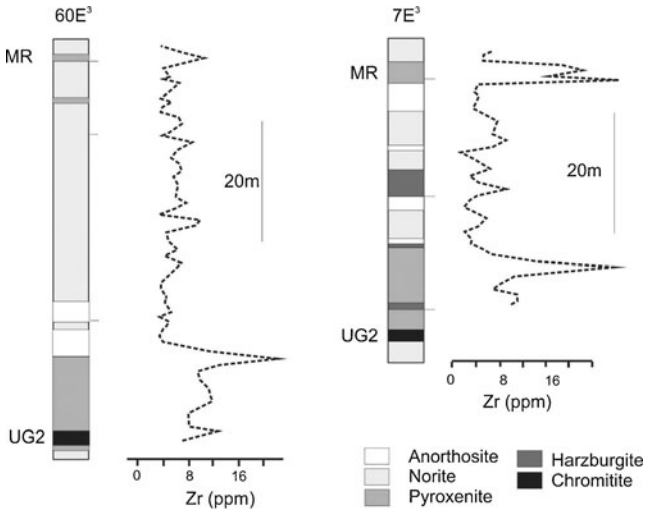

Fig. 18 Zirconium concentrations in the UG2–Merensky Reef interval at Amandelbult section. Data taken from Maier and Eales (1997). Colour coding for rock types as in Fig. 17

Pyroxenite Marker, respectively) have shown considerable isotopic disequilibrium (Eales and Cawthorn 1996; Prevec et al. 2005; Seabrook et al. 2005).

Sulfur and chalcophile elements

The majority of the rocks of the Bushveld Complex contain remarkably little sulfur, with <100 ppm measured in most samples from the LZ, CZ and MZ (Fig. 16c; Maier and Barnes 1999; Barnes et al. 2009). This could suggest that the bulk of cumulates crystallized from sulfide-undersaturated magma, consistent with the fact that the B1–B3 Bushveld magmas are strongly sulfide-undersaturated. The model can be assessed by considering the concentration of incompatible trace elements. As discussed above, the Zr contents of the rocks suggest 5–30 % trapped liquid in the LZ and CZ rocks (Fig. 16b). As B1 magma has about 450 ppmS (Barnes et al. 2010), the S contents of cumulates are broadly consistent with the crystallization of the rocks from sulfide-undersaturated magma. The S/Se ratios of most rocks are mantle-like, implying that no significant S has been lost during late magmatic or hydrothermal fluid percolation (Barnes et al. 2009).

However, the chalcophile element contents of most cumulates are inconsistent with crystallization from sulfide-undersaturated magma. The Cu/Zr ratios are above that of B1 (Fig. 16d) and the concentration of Pd in the LZ and LCZ is mostly >>5 ppb (Fig. 20), too high to be controlled by trapped melt alone. These data instead indicate the presence of cumulus sulfides. To explain the elevated PGE levels at low S contents, Barnes et al. (2009) suggest two possible solutions. Either after sulfide saturation was achieved, the sulfide liquid percolated downwards into the cumulate pile—in that case, the amount of sulfide liquid need not be at cotectic proportions—or, alternatively, the magma that was emplaced into the chamber was a crystal mush carrying a small proportion of sulfide liquid.

The basal rocks of the intrusion have up to 500 ppm S and ~50 ppm Cu. The presence of cumulus sulfides in this interval is consistent with Cu/Pd ratios that plot below the primitive mantle values (Fig. 16d). Based on the lithophile trace element data discussed above, there is little evidence that the sulfides formed in response to contamination. Sulfide percolation or sulfide saturation due to supercooling is instead more consistent with the data.

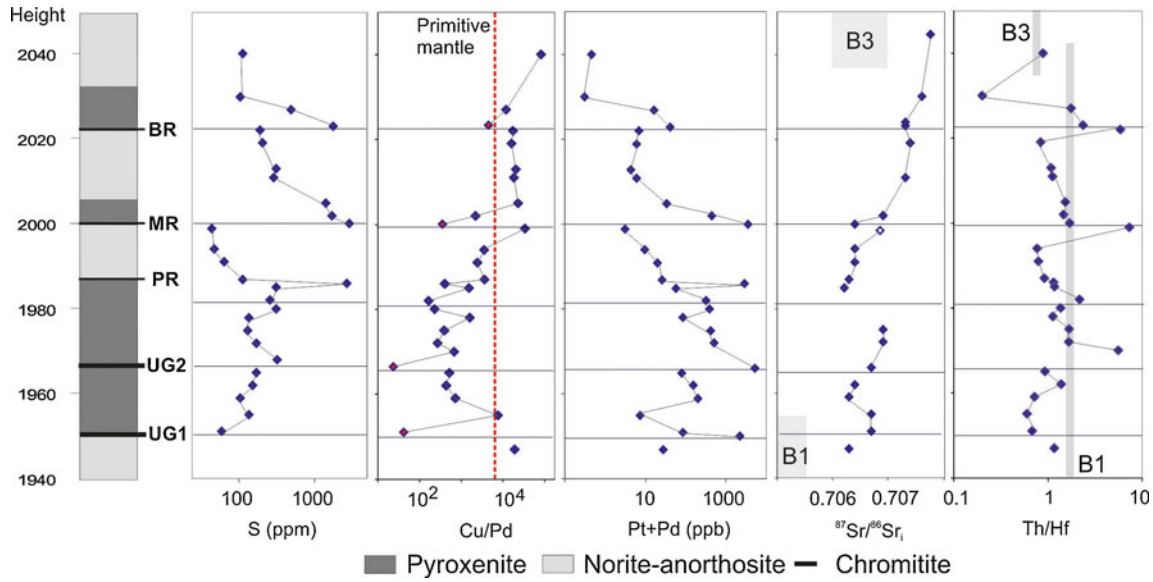

Fig. 19 Variations in S, Cu/Pd, Pt + Pd, initial Sr isotope ratios, and Th/Hf with stratigraphic height in UG1–Bastard Reef interval. Primitive mantle value is from Becker et al. (2006). *Vertical grey bands* represent the compositional range of Bushveld B1 and B3 magmas

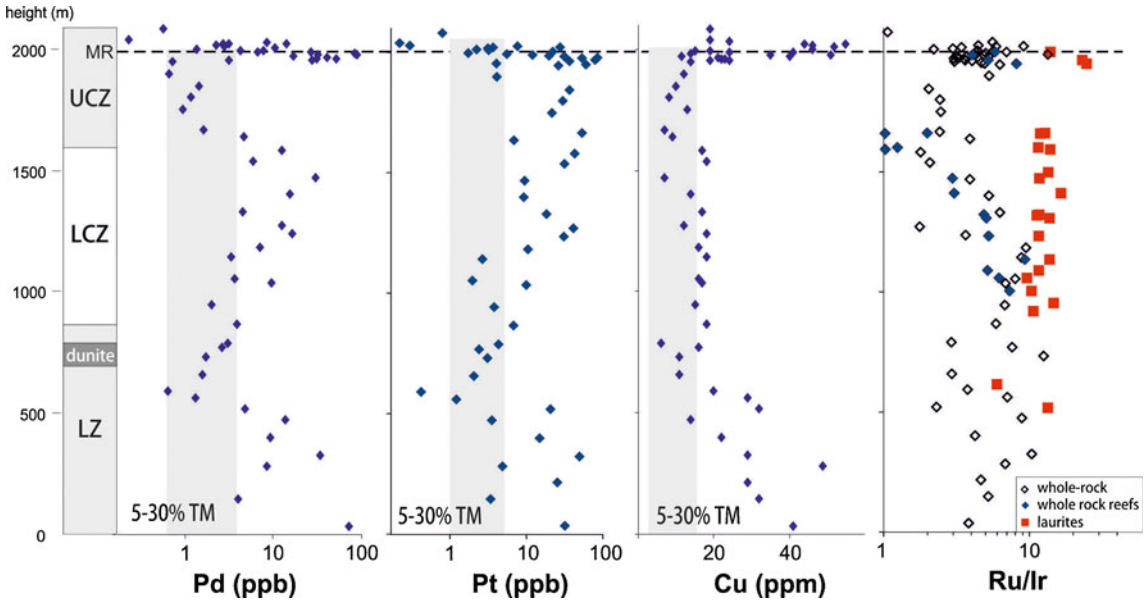

Fig. 20 Palladium, Pt, Cu, and Ru/Ir in whole rocks and laurites, plotted vs stratigraphic height in the Lower and Critical Zones, Union Section. *Grey vertical bands* indicate compositional range that may be accounted for by 5–30 % trapped liquid (*TM*)

The dunites and associated rocks at the top of the LZ are relatively depleted in all PGE and Cu (Fig. 20). Copper/Pd ratios are at mantle level and Cu/Zr is near unity (Fig. 16d), suggesting that these rocks crystallized from sulfide-undersaturated magma. This is consistent with the fact that the dunites show the highest values of whole rock Mg# and forsterite component in olivine, implying that they crystallized from the most primitive magmas in the analysed profile.

The reef interval in the uppermost CZ is characterized by relatively high S, PGE and Cu contents compared to the under- and overlying rocks (Figs. 16, 19). This has been explained by progressively more enhanced magma mixing towards the top of the CZ due to enhanced density contrasts between resident and replenishing magmas (Campbell et al. 1983) or mixing-in of relatively differentiated, nearly sulfide-saturated magma (Naldrett et al. 2012). Notably, whereas the PGE contents of the reefs progressively increase with height (Figs. 16, 19; Naldrett and Von Gruenewaldt 1989; Scoon and Teigler 1994; Barnes and Maier 2002b; Naldrett et al. 2009a), the PGE tenor, as expressed by Cu/Pd ratios, decreases (Fig. 19). This could be explained by the progressive metal depletion of the Bushveld residual magma in response to sulfide segregation or by lower R factors.

All chromitites in the CZ are PGE-enriched relative to their silicate host rocks (Scoon and Teigler 1994; Maier and Barnes 2008; Naldrett et al. 2009a). The LG chromitites contain significantly less PGE than the MG and UG seams, but a sulfide component must have been present in all cases, based on the elevated Pd contents of the seams (Scoon and Teigler 1994). This raises a perplexing question. Many of the chromite crystals contain abundant laurite inclusions (Maier et al. 1999) which would appear to require that the magma was sulfide-undersaturated at the time of chromite formation (Brenan and Andrews, 2001). Moreover, the composition of the laurites is decoupled from that of the host chromitite seams as expressed by Ru/Ir (Fig. 20).

The MZ is relatively PGE-poor, mostly at <10 ppb Pt + Pd (Fig. 16c). As the contents of lithophile trace elements, S and Cu, are also low, it is difficult to judge whether the rocks crystallized from sulfide-saturated magma: the low metal contents could reflect low trapped liquid contents. Barnes et al. (2010) found low S contents and mantle-like Cu/Pd in the B3 sills, consistent with sulfide-undersaturation of the magmas. This result is surprising in view of the high crustal component of the magmas and suggests that the contaminant must have been very S-poor. Metal ratios in the MZ cumulates are variable: in some samples, Cu/Pd and Cu/Pt ratios plot below the primitive mantle, consistent with the presence of a small sulfide component, whereas many other samples have Cu/Pd above the primitive mantle, suggesting a depleted parent magma. Copper/Zr ratios are mostly significantly above unity (Fig. 16d), also consistent with a small cumulus sulfide component in the rocks. The combined metal data for the MZ thus suggest that the B3 magma was initially sulfide-undersaturated during emplacement but reached sulfide saturation during crystallization within the Bushveld chamber.

The Pyroxenite Marker interval contains elevated S, Cu and PGE contents (Maier et al. 2001; Maier and Barnes 2010; Fig. 16c). Above the Pyroxenite Marker interval, the concentrations of the PGE drop rapidly, whereas S contents increase, particularly in the magnetite layers of the UZ (Fig. 16c; Barnes et al. 2004; Harney et al. 1990). The standard model employed to explain the lithophile and chalcophile element data of the Pyroxenite Marker and its

overlying rocks has been one of replenishment with magma of Critical Zone lineage, followed by mixing of primitive and resident magma (Harney et al. 1990; Maier et al. 2001), but Maier and Barnes (2010) proposed an alternative model of cumulate reorganization due to subsidence of the intrusion, which is discussed in more detail below.

Pd/Ir and (Pt + Pd)/(Os + Ir + Ru) ratios are commonly used as magma differentiation indexes because IPGE are compatible during the fractionation of basaltic magma (Barnes et al. 1985). The (Pt + Pd)/(Os + Ir + Ru) ratios are lowest at the top of the LZ (Fig. 16d), consistent with the lithophile element data, showing that this interval is the most primitive (Fig. 16a). Ratios then increase into the UCZ with a reversal at the level of the UG chromitites and associated rocks. The MZ and the base of the UZ have the highest (Pt + Pd)/(Os + Ir + Ru) ratios, whereas there is a gradual reversal throughout the remainder of the UZ.

The platinum/Pd ratios of the rocks are highly variable (Fig. 16d). Most samples have Pt/Pd > unity, with the exception of some Pyroxenite Marker samples and many of the basal rocks of the complex, both in the analysed Union Section profile and in the Platreef of the northern lobe (Manyeruke et al. 2005; Kinnaird et al. 2005; Maier et al. 2008a, b). As also reflected in many other element ratios, strong reversals in Pt/Pd occur at the base and top of the Main Zone. A feature that remains difficult to explain is that Pt/Pd ratios in the sulfide-bearing layered suite are broadly similar to those in the sulfide-deficient marginal suite. The sulfide melt–silicate melt partition coefficient of Pd is believed to be significantly higher than that of Pt (Stone et al. 1990; Barnes 1998a, b; Sattari et al. 2002), consistent with the observation of Barnes and Picard (1993) that Pt/Pd in the Cape Smith picrites is around unity, whereas the associated Raglan ores have Pt/Pd <0.5. The $D_{sulf/sil}$ for Pd at Raglan thus appears to have been at least twice that of Pt. By implication, the sulfide-bearing Bushveld cumulates should have significantly lower Pt/Pd than the barren marginal rocks, particularly since the former are believed to have equilibrated at high R factors. We considered whether the magmas achieved Pt saturation in the chamber, but this seems unlikely because (1) the most primitive, sulfide-undersaturated rocks at the top of the LZ are depleted in both Pt and Pd (Fig. 20) and (2) the remainder of the LZ and CZ are elevated in both Pt and Pd, indicative of the presence of cumulus sulfides. The data thus suggest that Pt saturation did not occur before sulfide saturation. Another possibility is that within the relatively slowly cooling main intrusion, Pd was relatively mobile at the late magmatic stage. Extremely high Pt/Pd ratios interpreted to result from preferential Pd mobility have been reported from the UG1 chromitite (Maier and Barnes 2008). In this model, the high Pt/Pd of the internal reefs would, in part, be a secondary feature, whereas the relatively lower Pt/Pd of many of the marginal rocks would be a primary feature.

Towards a model for the Bushveld Complex and other PGE-mineralized layered intrusions

Composition and crystallization sequence of Bushveld magmas

Past authors have recognized that many PGE-mineralized layered intrusions crystallized from two compositionally distinct suites of parental magmas (Irvine et al. 1983; Kruger and Marsh 1985; Naldrett et al. 1986; Alapieti et al. 1989; Miller and Andersen 2002), originally termed the U (ultramafic) and A (for Al_2O_3 rich) magmas (Irvine et al. 1983). For most intrusions, the nature of the parental magmas has been inferred from the crystallization sequences of the intrusions and cumulate geochemistry (e.g. Helz 1985; Lambert et al. 1994; Lambert and Simmons 1987, 1988; Bédard 1994). In the case of the Bushveld Complex, the composition of the parental magmas can be better constrained by means of the fine-grained sills and marginal rocks exposed at and below the base of the complex that have similar crystallization sequences, whole-rock and mineral trace element signatures and emplacement ages as the cumulate rocks (Sharpe 1981; Cawthorn et al. 1981; Harmer and Sharpe 1985; Scoates and Friedman 2008; Barnes et al. 2010; Godel et al. 2011; see Table 1 for a summary of their compositional characteristics). The B1 suite is a basaltic andesite similar to modern boninites or Archean siliceous high-magnesian basalts. The B2 and B3 rocks resemble tholeiitic arc basalts in that they are depleted in HFSE and enriched in LILE (Barnes et al. 2010). In addition to fine-grained noritic sills, there are medium-grained peridotite sills that appear to represent mixtures between B1 magmas and cumulus olivine, orthopyroxene and chromite (Sharpe and Hulbert 1985; Davies and Tredoux 1985; Barnes et al. 2010). Field evidence suggests that they intruded after the fine-grained sills (Curl 2001), consistent with a model whereby the peridotite sills are ejections of crystal slurries from the main chamber (Harmer and Sharpe 1985).

The crystallization sequence of the B1 suite has been modeled as ol → opx + cr → opx + plag → cpx + opx + plag (Harmer and Sharpe 1985; Barnes et al. 2010), consistent with the petrography of the LZ and LCZ. Using thermodynamic modeling software (e.g. PELE; Boudreau 1999), it can be shown that the average B1 magma would crystallize olivine and orthopyroxene with compositions of Fo/Mg# ~87–90 (at low pressure and fO_2 at QFM), broadly consistent with the compositions of the Union Section cumulates. Slightly more magnesian olivines (up to Fo_{92}) occur in the LZ of the northern limb (Hulbert and von Gruenewaldt 1982) and the eastern limb (Wilson and

Chunnett 2010; Wilson 2012), requiring more magnesian parental magmas than the average B1, possibly reaching komatiitic compositions. The coeval Uitkomst Complex also contains rocks that have olivine with compositions up to Fo_{91} (Gauert et al. 1995; Li et al. 2002).

In the B2 and B3 suites, the modeled low-P crystallization sequence is plag + ol → plag + cpx + opx (Barnes et al. 2010). Troctolitic rocks have been reported from the MZ of the northern lobe (Ashwal et al. 2005), but the crystallization order of most UCZ and MZ rocks in the western and eastern lobes is opx + cr → plag + opx → plag + opx + cpx, and troctolites are rare, inconsistent with the crystallization order of the B2 and B3 sills. A possible explanation for the discrepancy could be that the UCZ and MZ cumulates crystallized from mixed B1 and B2/3 magma.

All Bushveld magmas contain a relatively large crustal component, as indicated by relatively high contents in SiO_2 (particularly in the case of B1), LILE (Harmer and Sharpe 1985; Barnes et al. 2010), high $^{87}Sr/^{86}Sr_i$ (0.703–0.708; Harmer and Sharpe 1985; Curl 2001), negative εNd (−4.6 to −6.7; Curl 2001) and, for B1, the crystallization of orthopyroxene before clinopyroxene. Two contrasting interpretations have been offered to account for these features: (1) plume-derived komatiitic or picritic magma assimilated crust during magma ascent and emplacement (Barnes 1989; Maier et al. 2000; Harris et al. 2004). The B1 magma partially melted the upper crust, whereas the B2 and B3 magmas assimilated the crustal residues from the initial melting. (2) The Bushveld magmas formed, at least in part, from metasomatized SCLM (Harmer and Sharpe 1985; Richardson and Shirey 2008). These models are evaluated in more detail in the following section.

Magma derivation

Potential sources for the generation of primitive magmas include the convecting mantle and the lithospheric mantle. In general, most high-Mg magmas are interpreted to be derived from the convecting mantle via adiabatic partial melting of mantle plumes (e.g. Herzberg et al. 2007). In contrast, few primitive magmas are generally accepted to be derived from the SCLM, notable exceptions being Group II kimberlites (Gurney et al. 2005) and lamproites (Lambert et al. 1995). Some continental flood basalts that are highly enriched in crustal components, e.g. the Ventersdorp lavas (Marsh et al. 1992), have also been proposed to be derived from SCLM, as have some alkali basalts (Francis and Ludden 1995). The location of most large PGE deposits in the centre of cratons suggests that a SCLM derivation of their parental magmas is a possibility. For the Bushveld Complex and other PGE-bearing layered intrusions, the model was first proposed by Harmer and Sharpe (1985). Hamlyn and Keays (1986) argued that a mantle source that had undergone a previous, small-degree melting event would be PGE-rich due to residual enrichment in PGE and that second-stage melting of such mantle could liberate the PGE, thereby producing PGE-rich magma. The SCLM has subsequently been shown to be relatively PGE-depleted (e.g. Pearson et al. 2004; Maier et al. 2012a, b; for an exception, see McInnes et al. 1999), probably through large-degree Archean and early Proterozoic melting events, and it seems counterintuitive to derive the magmas to the world's largest PGE deposits from the most PGE-depleted mantle known. Furthermore, some studies (Luguet et al. 2007) have shown that Pt in the lithospheric mantle can occur in the form of alloys and PGM that may be refractory during partial melting of the mantle. On the other hand, the presence of an SCLM component in the Bushveld magmas would be consistent with the relative Pt enrichment of many SCLM samples (Pearson et al. 2004; Maier and Barnes 2004; Maier et al. 2012b) that matches the relatively high Pt/Pd ratio of the Bushveld magmas (Barnes et al. 2010), the Main Sulfide Zone of the Great Dyke (Oberthür 2002), most rocks in the Penikat intrusion (Halkoaho 1994; Maier et al. unpublished data) and many of the ultramafic rocks (albeit not the reefs) of the Stillwater Complex (Keays et al. 2011). A significant SCLM component in the Bushveld would also be consistent with the available isotope data: For example, Curl (2001) argued that the combination of negative εNd and near-chondritic γOs in Bushveld marginal rocks requires a component of sub-continental lithospheric mantle (SCLM) in the Bushveld mantle source. A similar conclusion has been reached by Richardson and Shirey (2008). A possible model to reconcile the seemingly contradictory data could include the following elements (Figs. 21 and 22):

1. Relatively high-degree partial melting of the convecting mantle in the Archean (Pearson et al. 2004), resulting in extraction of komatiitic or komatiitic–basaltic melt and formation of SCLM. The bulk of the Pd in the mantle would have been removed during this step. However, in order for the SCLM to contribute some PGE (in particular Pt) to the Bushveld magmas at a later stage, some Pt must have been left behind in the mantle, i.e. Pt cannot be completely incompatible, or it must have been reintroduced at a later, pre-Bushveld, stage. There are few experimental data to constrain the compatibility of the PGE during mantle melting, but the Pt contents of komatiites (mostly ~8–10 ppb Pt at 30–50 % partial melting; Fiorentini et al. 2011) suggest that Pt is not completely incompatible. If the Archaean mantle had 6 ppb Pt (Maier et al. 2012b) and a 50 % komatiitic partial mantle melt has 8 ppb Pt, then the residue must have 4 ppb Pt, broadly consistent with the 4.5 ppb average Pt content of the Kaapvaal and Karelia SCLM (Maier et al. 2012b).

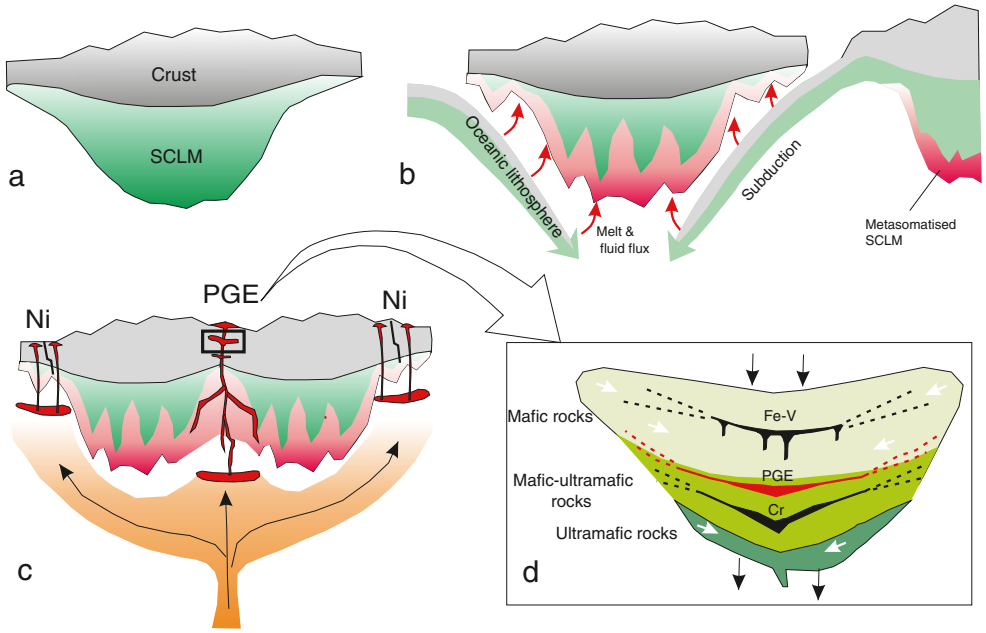

Fig. 21 Schematic diagrams summarizing processes relevant to the formation of PGE and Ni–Cu deposits. **a** Mid-Archean formation of cratonic crust and sub-continental lithospheric mantle. **b** Late-Archean, Proterozoic and Phanerozoic metasomatism of SCLM, predominantly by subduction-derived fluids and melts. **c** Mantle plume impacts on the base of composite craton and undergoes limited adiabatic melting. Melts infiltrate SCLM. Heat of plume and infiltrating plume melts cause melting of metasomatized domains of SCLM. Melts of SCLM and plume mix and ascend along trans-lithospheric suture zones through SCLM and crust to form layered intrusions. **d** *Inset* from **c** showing the formation of PGE, chromite and magnetite reefs in layered intrusion. Crustal loading during magma emplacement causes central subsidence. Incompletely solidified cumulates slump towards the centre of intrusion and disseminated sulfide, chromite and magnetite form massive layers (modified from Maier and Groves (2011))

2. Metasomatism of the refractory mantle residue (Simon et al. 2007), refertilising the SCLM and rendering it once again fusible. Metasomatism and associated introduction of sulfur and volatiles (Lorand and Gregoire 2006) oxidized the SCLM (Yaxley et al. 2011). The Pt mass balance of the mantle and of potential partial melts discussed above suggests that insignificant Pt was reintroduced to the SCLM after initial melting.
3. The arrival of a plume resulting in an increased conductive heat flux into the lithosphere and plume-derived magmas that infiltrate the SCLM together cause partial melting of metasomatised domains of the SCLM. Because the partial melt is relatively oxidized, and Pt solubility is positively correlated with fO_2 (Borisov and Palme 2000), the bulk of the remaining Pt, and any Pd that may have been introduced during metasomatism, can be dissolved. The melting residue would be highly PGE-depleted, consistent with the occurrence of PGE-depleted xenoliths in the Premier kimberlite pipe (Maier et al. 2012b).

Assuming that the Bushveld magmas contained a contribution of between 40 and 75 % SCLM (Richardson and Shirey 2008), the SCLM component must have been highly Pt-enriched because most melts of the convecting mantle contain ~20 % less Pt than Bushveld magmas (Fig. 14). Mass balance suggests that the SCLM magma would have to contain ~20–30 ppb Pt, significantly higher than any known small-degree SCLM-derived partial melts (e.g. kimberlites (McDonald et al. 1995) or MARIDs (Maier et al. 2012b)). Alternatively, the SCLM could have provided all the Bushveld primary melt, in which case the required PGE

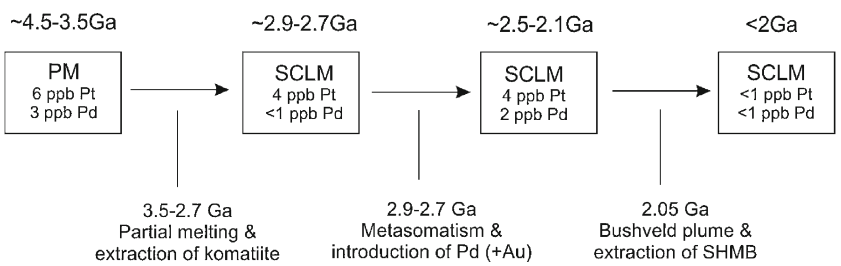

Fig. 22 Flow chart summarizing the PGE contents of mantle reservoirs through time

contents of the SCLM partial melt are somewhat lower (20 ppb Pt, 15 ppb Pd), but the required degree of melting is higher (~20 %). In this model, the unusually low Ti contents of the Bushveld magmas (0.35 % TiO_2) are easier to explain. Neither option seems entirely satisfying, but a model involving the SCLM in the petrogenesis of the PGE reefs would be consistent with the concentration of PGE-mineralized intrusions in the late Archean and early Proterozoic during which the bulk of the SCLM was formed and metasomatised (Griffin et al. 2004; Simon et al. 2007). Subsequent melting of the SCLM clearly did occur, as indicated by the relatively recent ages of Group II kimberlites (Gurney et al. 2005), but the heat flux from mantle plume events likely decreased (Richter 1988), potentially causing a lower degree of subsequent melting of the SCLM and more refractory behaviour of Pt.

The main alternative to the SCLM as a source for the magmas parental to PGE deposits is the convecting mantle. This model may be particularly relevant for intrusions that are located at rifted craton margins and that contain a relatively small crustal component (e.g. Skaergaard, Stewart and De Paolo 1990). If the model was applied to the Bushveld Complex, the high crustal component of the Bushveld magmas would have to be explained via significant (20–40 %) contamination of a primitive primary magma with upper crust, probably in a staging chamber, to produce the observed regional homogeneity of the crustal signature (Maier et al. 2000; Harris and Chaumba 2001; Harris et al. 2004; Barnes et al. 2010). To prevent early S saturation of the magmas, the crust would have to be very S-poor. A problem with the model is that contamination with PGE-poor crust would dilute the PGE in the magma, requiring that the PGE contents of the original magmas were unreasonably high (Barnes et al. 2010). Lesher and Burnham (2001) argued that contamination of magmas with PGE-poor crust may result in an increase in PGE due to the effect of simultaneous fractional crystallization, but in the Bushveld Complex the required amounts of contamination and thus crystallization are so large (30–40 %) that the MgO and Ni contents in the residual magma would become too low. Another problem with the model is that it provides no explanation for the unusually high Pt/Pd of the Bushveld magmas.

A third possibility is to suggest that the Bushveld magmas were derived from an anomalously Pt-enriched convecting mantle source, perhaps resulting from heterogenous mixing-in of Pt-rich late veneer (Pt/Pd, about 1.8; Palme and Jones 2005). However, the data of Maier et al. (2009) suggest that by the time the Bushveld magmas formed, the mantle had largely equilibrated with the late veneer.

A fourth possibility is that the mantle source to the Bushveld magmas contained a component from the Earth's core. If the primitive upper mantle estimates of Becker et al. (2006) are correct (Pt/Pd, about 1.1), then mass balance dictates that the core must have a higher Pt/Pd ratio than the bulk mantle. However, if the PM estimate of Palme and O'Neill (2004) or the Archean mantle estimate of Maier et al. (2012b) was used, the core may not be Pt-enriched. Models involving unusually Pt-rich mantle or core domains are rather speculative, but their attraction lies in their potential to explain why more than 50 % of the world's PGE resources are hosted in a single intrusion that crystallized from magma of unusual PGE distribution patterns.

Magma emplacement

The emplacement depth of the Bushveld Complex was probably relatively shallow. Calc-silicate assemblages in the Marginal Zone indicate equilibration pressures of 0.6–2.4 kbar (<2 to 7 km: Wallmach et al. 1989; shallower still according to Cawthorn and Walraven (1998)), consistent with the fine-grained nature of many of the Bushveld sills. As the xenoliths are now situated at the base of a 6–8-km intrusion, the implication is that much of the complex was built from successive magma influxes that inflated earlier sills. In some cases, magma pulses may have formed sill-like injections into already solidified, or partly solidified, cumulates or formed independant sill-like bodies, consistent with the presence of a screen of quartzite and calc-silicate xenoliths at the contact between the LZ and the UCZ in the northern lobe (Hulbert 1983; Maier et al. 2008a). Significant time intervals between some magma injections were postulated by Holwell et al. (2005) who argued that in the northern lobe the MZ was emplaced on top of solidified CZ.

Further evidence for a relatively shallow emplacement depth of the Bushveld Complex is provided by the inward dip of layering. Based on the morphology of potholes, it is argued that the inward dip formed syn-magmatically due to crustal subsidence, yet the crust would not be able to flex/collapse if it was hot and ductile.

The fine-grained nature of many Bushveld marginal rocks indicates that some of the earliest Bushveld magmas ascended as phenocryst-poor melts, consistent with the occurrence of chilled margins at the base of the LZ (Teigler 1990a; Teigler and Eales 1996; Wilson and Chunnett 2010; Wilson 2012) and the CZ (Grasvalley, Hulbert 1983; Rooipoort, Maier et al. 2008a). However, based on mass balance, Eales (2002) and Eales and Costin (2012) have argued that at least some B1 magma pulses intruded as olivine- and chromite-rich slurries. This model is consistent with the abundance of peridotite sills in the floor of the complex (Sharpe and Hulbert 1985), some of which have harzburgitic chill zones (Eales 2002). Maier and Barnes (1998) and Roelofse (2010) have proposed that the MZ magma intruded as a crystal slurry, based on (1) the paucity of highly differentiated rocks in the MZ, (2) the low incompatible trace element contents of the MZ cumulates, (3) the subdued differentiation trends in many MZ profiles (e.g. in the

northern lobe; Roelofse 2010), (4) the abundant deformation features of plagioclase crystals, (5) the super-cotectic proportions of plagioclase in the MZ, (6) the decoupling of plagioclase and pyroxene differentiation trends (Roelofse 2010), (7) disequilibrium in Sr isotope signatures of mineral pairs (Roelofse 2010) and (8) lack of chilled margins. These studies highlight that the mode of Bushveld magma emplacement remains far from resolved.

The location of the feeder(s) also remains uncertain. Previously proposed feeders include the coeval and cogenetic Uitkomst Complex (Gauert 1998), gravity highs at Union Section and to the northeast of Rustenburg (Eales et al. 1988; Viljoen 1999), the Steelpoort fault (Cawthorn et al. 2002) and the Thabazimbi–Murchison lineament (Silver et al. 2004). The latter proposal is consistent with the occurrence of some of the most primitive LZ rocks in the vicinity of the TML, at Union Section (Eales et al. 1988), Grasvalley (Hulbert 1983) and to the north of Burgersfort (Wilson 2012). Considering the remarkable width (at least 400 km, much more if the Molopo Farms Complex is included and if erosion is accounted for) and thus width/thickness ratio of the Rustenburg Layered Suite, it seems likely that the complex was fed by several feeders (Fig. 8), particularly if bottom flow of intruding magma is envisaged (Naldrett et al. 2009a, b, 2012).

Magma replenishment

In a general sense, the observed magmatic stratigraphy of the Bushveld Complex is consistent with that expected from a magmatic system undergoing progressive fractional crystallization: that is, an olivine-rich LZ is overlain by an orthopyroxene-rich LCZ, a predominantly noritic–gabbronoritic UCZ and MZ, and a ferrodioritic UZ. In detail, the sequence is characterized by numerous lithological and compositional reversals of variable magnitude. Reversals may be expressed by olivine-and chromite-rich rocks on top of plagioclase- or pyroxene-rich rocks (e.g. in the cyclic units of the UCZ or ~1,000 m above the base of the complex where whole-rock Cr contents abruptly double; Fig. 16a), relatively magnesian olivines and pyroxenes on top of relatively more ferric end-members, calcic plagioclase overlying sodic plagioclase or rocks with a low crustal component (relatively low $^{87}Sr/^{86}Sr_i$ and unfractionated LILE) overlying sequences with a more pronounced crustal signature. The most widely accepted explanation for such reversals is that they formed in response to major replenishments to the chamber with relatively primitive magma, either of B-1 (Campbell et al. 1983) and/or B2/3 lineage (Eales et al. 1986). In terms of Mg#, the evidence for magma replenishment is actually rather weak. Compositional reversals are subdued, and in the UCZ the most magnesian compositions tend to be in norites rather than in pyroxenites (Fig. 17). However, a strong argument for frequent magma replenishment in the LZ and CZ is that the entire 2-km sequence is PGE- and Cr-enriched (Fig. 16a, c). Without multiple replenishment of the chamber, the PGE and Cr contents would be expected to decrease rapidly with height in response to Raleigh-type fractionation of sulfide, chromite and orthopyroxene, notwithstanding the fact that some metal-rich sulfides, or chromite and orthopyroxene, may be suspended in the magma for some time. A further argument for magma replenishment is the fact that the UG chromitites show a strong increase in Ru/Ir contents relative to the MG chromitites (Fig. 20). Ruthenium is compatible with regard to chromite (at least in komatiitic liquids; Locmelis et al. 2011; Pagé et al. 2012) and laurite and thus might be expected to progressively decrease with height.

A particularly notable reversal occurs towards the top of the LZ. Using thermodynamic modeling software such as PELE (Boudreau 1999), the bulk of the orthopyroxenites of the LZ and LCZ can be modeled as differentiates of primitive B1 magmas (14.5 % MgO) after about 10–15 % fractionation. In contrast, the ~100-m dunitic–harzburgitic interval at the top of the LZ contains the most primitive rocks of the analysed drill cores with the highest Fo contents (up to Fo_{90}) and whole rock Mg#. This interval also comprises the only rocks that unambiguously crystallized from sulfide-undersaturated magma, as indicated by low PGE contents, mantle-like ratios of PGE to incompatible elements, as well as Cu/Pd~7,000 and Cu/Zr~1 (Figs. 16, 20). These features are consistent with magma replenishment, but in view of the fact that the B1 sills are strongly sulfide-undersaturated, it is remarkable how rare primitive sulfide-undersaturated rocks are in the analysed sequence and that they occur towards the top rather than the base of the Lower Zone. This suggests that the bulk of the most primitive rocks of the Bushveld Complex are contained in its unexposed centre.

Emplacement sequence

The emplacement sequence of the different stratigraphic zones of the RLS has been indirectly constrained by field evidence: Curl (2001) found that the B1 sills were emplaced first, followed by the B2 and B3 sills, and that the fine-grained members of the individual suites predated the coarser-grained sills and the main Bushveld layered suite.

The relative timing of the MZ emplacement has been particularly controversial. Based on stratigraphic relationships, it could be proposed that the MZ was emplaced after the UCZ and before the UZ. In a landmark paper on the Sr isotopic stratigraphy of the Bushveld Complex, Sharpe (1985) proposed that the MZ formed from the final magma influx to the layered suite, emplaced and crystallized between the UCZ crystal pile and residual UZ liquids. Cawthorn et al. (1991) contested the model, arguing that

the relatively cool MZ magma would have mixed with the overlying, hotter UZ liquids.

Maier and Barnes (1998) have shown that the MZ has a broadly similar bulk composition to the B3 sills in terms of compatible elements. They went on to suggest that the MZ solidified from a viscous and relatively cool crystal mush that underwent limited in situ fractionation. It was surmised that mixing of MZ magma with overlying UZ magma would be confined to the interface of the magmas, perhaps producing transition zones of metres to tens of metres in thickness that are characterized by interfingered layers, schlieren and magmatic breccias with highly diverse geochemical characteristics. A weakness of the model is that the samples of B3 studied so far are all relatively fine-grained, but the database remains small and it could be argued that the studied B3 samples represent filter-pressed ejections of crystal-poor liquid into the country rocks.

Maier and Barnes (1998) considered that the MZ slurry could have been emplaced into a largely crystallized cumulate package. In that case, mixing between the MZ magma and the host cumulates would be particularly subdued, consistent with the fact that the MZ stands out as a relatively unlayered, compositionally homogenous, exotic package within a progressively differentiated LZ–CZ–UZ sequence (Fig. 16) and with seismic data of Campbell (1990) showing deformation of the UZ by a dome-like MZ at depth in the Western lobe (in Viljoen (1999); Fig. 15). The model is also consistent with the V-enrichment of the magnetitite seams of the UZ (up to 2.2 % V_2O_5; Cawthorn and Molyneux 1986); Toplis and Corgne (2002) and Balane et al. (2006) showed that the seams crystallized at an oxygen fugacity between NNO and NNO-1 and that the bulk of the V in the magma was in the 3+ state. Under these conditions, V is compatible into clinopyroxene (D 4-10; Toplis and Corgne 2002), and crystallization of 2–3 km of clinopyroxene-rich MZ rocks should have strongly depleted the V content of the residual magmas. Invoking magma replenishment at the Pyroxenite Marker (Cawthorn et al. 1991) does not solve the V mass balance problem: The UZ has a homogenous Sr isotopic signature (Kruger 1994) which suggests that, if there were distinct magmas, they were effectively hybridized, thereby, at least partially, inheriting the V-depleted signature of any MZ residues. In contrast, if the MZ intruded after the bulk of the UZ, the magnetitite seams would have crystallized from residual B1 (CZ) liquids that were likely less V-depleted than residual MZ liquids because clinopyroxene is not a cumulus phase in most of the LZ and CZ.

Cumulate mobilization and deformation

The Bushveld Complex and many other layered intrusions display a distinct pattern of inward-dipping layering that has been explained, in part, by lopolithic subsidence (e.g. in the Lilloise intrusion: Chambers and Brown 1995; Bushveld: Carr et al. 1994). Subsidence may be generated when high intraplate stresses weaken the lower crust to allow viscous flow (Howell and van der Pluijm 1999). This may cause deformation of thin slabs of upper crust. It is possible that the heat flux derived from craton-scale magmatic events related to mantle plume impact at the base of the lithosphere further facilitates the viscous flow of the lower crust.

In the case of the Bushveld Complex, the geometry of the interior of the intrusion remains largely unknown, but it is now widely accepted that the eastern and western limbs are connected at depth (Cawthorn et al. 1998). The dip of the exposed portions of the complex is too steep to be continuous to the centre, and thus the layering either flattens in the centre as has, for example, been documented for the Platreef by Yudovskaya and Kinnaird (2010) and modeled for the Trompsburg intrusion using geophysical data (Maré and Cole 2006) and/or the dip may be locally enhanced by post-emplacement faulting.

Based on field evidence, it is proposed that subsidence resulted in slumping of relatively liquid-rich, semi-consolidated cumulate layers towards the centre of the intrusion. This caused the development of transgressive features such as potholes (Carr et al. 1994), "gaps", pipes, and the many small-scale deformational features summarized earlier. The flow of crystal slurries led to sorting of crystals and unmixing of crystals and liquid in response to buoyancy forces, somewhat analogous to the model proposed by Bédard et al. (2007) for the Ferrar dolerites in Antarctica. Plagioclase was separated from denser pyroxenes and oxides (and sulfides, as discussed below), resulting in an interlayered sequence of ultramafic and leucocratic layers (Fig. 23). Efficient crystal sorting resulted in a distinctly bimodal sequence, with pyroxenites and chromitites on the one hand and leuconorites and anorthosites on the other hand. Melanorites are relatively rare (e.g. Maier and Eales 1997), except for the Merensky Reef.

To be mobile, crystal slurries need to contain a significant liquid component, although debate continues as to how much liquid is required (probably <50 %: Paterson 2009 and references therein). Most of the Bushveld rocks are mesocumulates and thus would seem to have too little trapped liquid to allow mobility, but this likely reflects late-stage compaction and cementation. It is normally accepted that porosities high enough to allow cumulate mobility only occur in the mush zone on top of the crystal pile. However, field evidence suggests that, in places, the cumulates remained unconsolidated for a considerable depth below the top of the pile: (1) In some deep Merensky Reef potholes at Rustenburg platinum mines, the Boulder Bed may slump into the pothole (Fig. 24; Viljoen and Hieber 1986), indicating that for several tens of metres below the Merensky Reef, the footwall rocks were unconsolidated

when the potholes formed; (2) The "gaps" represent kilometre-scale transgressive features, possibly implying that portions of the entire 1–5 km underlying cumulate pile remained incompletely consolidated prior to accumulation of the Upper Zone. Similar large-scale slumping structures occur in the Lilloise intrusion, Greenland (Chambers and Brown 1995); (3) In the Penikat intrusion, potholes of the AP reef transgress for >50 m into their footwall sequence (Halkoaho 1994).

Other evidence suggests that slumping and deformation may affect specific layers within relatively more competent host rocks. For example, the uppermost portion of potholed UG2 chromitite may show flames that inject into the pyroxenitic HW (Fig. 11b: see also Carr et al. 1994). In the Rum intrusion, slumping is concentrated in certain layers that contain fragments of the hanging wall rocks (O'Driscoll et al. 2010). These observations could suggest that relatively dense ultramafic slurries enriched in sulfides may transgressively

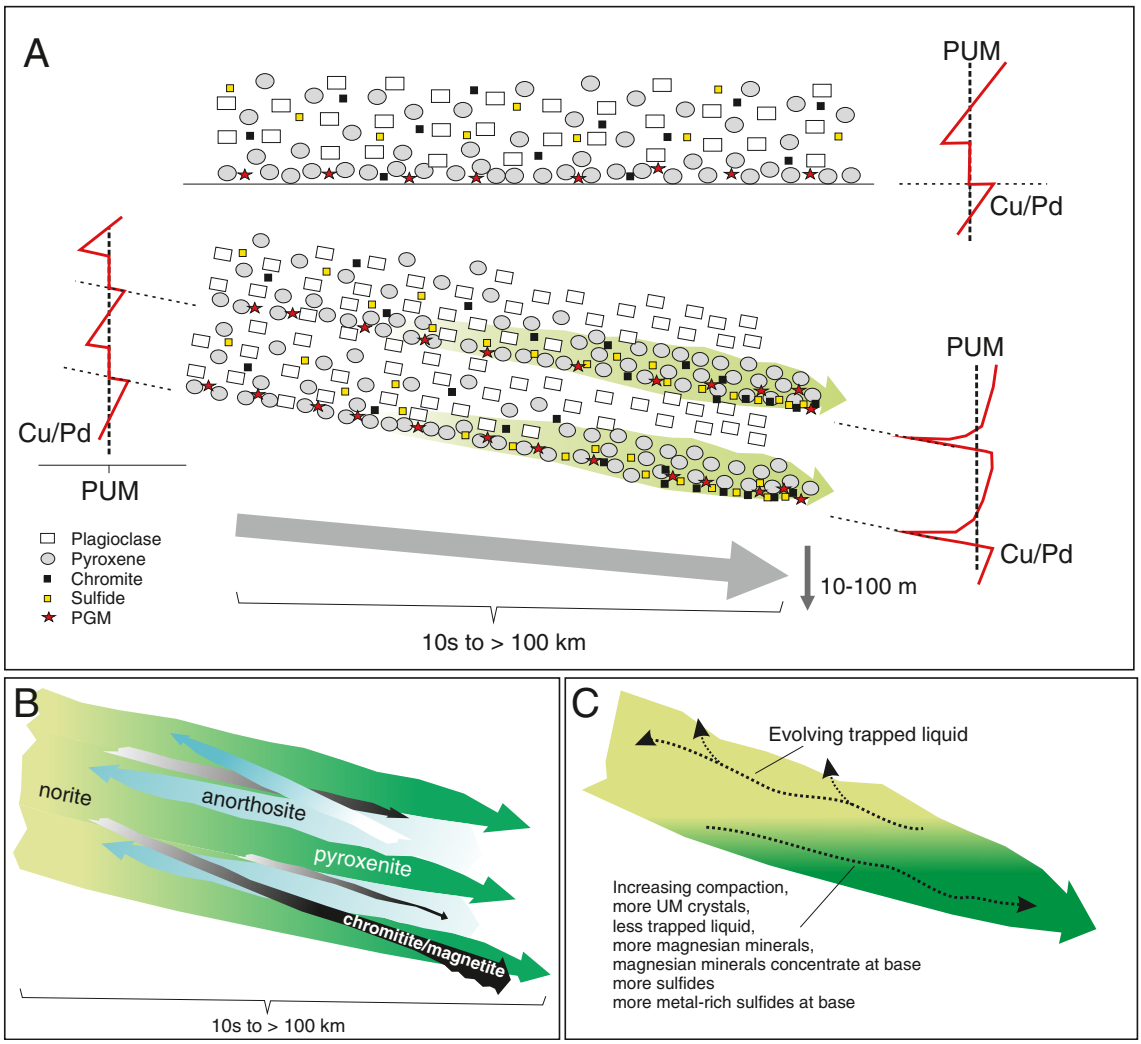

Fig. 23 Schematic diagrams showing **a** cumulate unmixing during subsidence of intrusion, resulting in the formation of sulfide- and chromite-rich pyroxenites, and sulfide- and chromite-poor anorthosites. At the *top* is a semi-consolidated proto cumulate deposited by a fresh influx of sulfide-undersaturated magma prior to the subsidence of the chamber, precipitating first pyroxene, chromite and PGM and later also plagioclase and sulfide. Cu/Pd is initially at mantle level but falls below the mantle once sulfide precipitates and then progressively increases during Raleigh fractionation of sulfide. The *lower part* of panel shows how cumulate layers are progressively sorted during subsidence, resulting in the pronounced layering of pyroxenite, norite and anorthosite in down-dip direction. Sulfides percolate towards the bottom of the ultramafic layer (where they may absorb PGM), thereby also shifting the reversal in Cu/Pd towards the base of the layer and making reversal more pronounced. **b** Relative movement of pyroxenite and oxide vs feldspathic slurries. Note that the oxide slurries may inject downwards into the anorthositic footwall, whereas feldspathic slurries may inject upwards through dense ultramafic cumulates as, e.g., shown in Fig. 7. Also note that the model predicts the significant thickening of oxide layers towards the centre of the intrusion. **c** Compositional evolution of slurries during down-dip slumping, including the relative concentration of mafic minerals and sulfides towards the base of slurry and centre of intrusion and percolation of metal-depleted intercumulus residual liquids upward across the slurries and up-dip towards the margin of intrusion, leading to progressive lowering of metal tenors of intercumulus sulfides

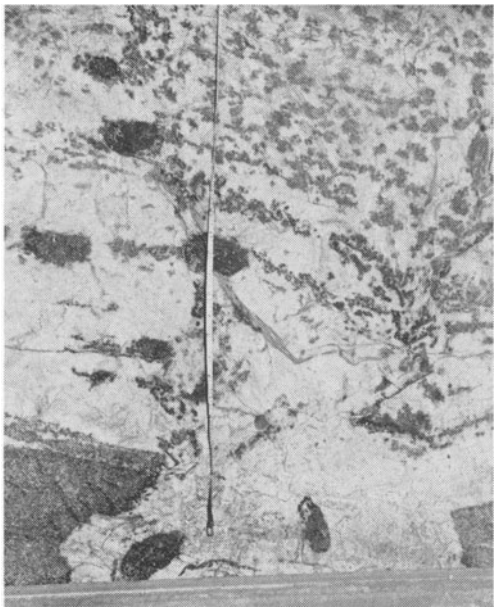

Fig. 24 Slumping of anorthositic Boulder Bed with pyroxenitic boulders into its footwall. Bottom of large complex Merensky and Bastard Reef pothole in Brakspruit area. Base of photograph ~1 m (photograph from Viljoen and Hieber (1986), reproduced with the permission of the Geological Society of South Africa)

inject downwards into less dense, incompletely solidified footwall rocks. Examples of layers that could be interpreted as sills include the Merensky pyroxenite, the UG2 chromitite–pyroxenite, the UG1 chromitite and some magnetite seams based on the knife-sharp bottom and top contacts of the layers (Fig. 5b), their protrusion into the hanging wall (Fig. 5e) and the abundance of autoliths (Fig. 3d). The magnetite plugs of the Bushveld and Duluth complexes may also have formed in response to cumulate mobilization, when semi-consolidated slurries enriched in magnetite and Fe-rich intercumulus melt sagged towards the centre of the intrusions and locally percolated downward through the cumulate pile, possibly exploiting pull-apart structures. Subsequent expulsion of residual liquid led to near-monomineralic magnetite bodies. Transgressive relationships and sill-like injection have also been recorded in anorthosites (Fig. 7). However, as the anorthosites are less dense than their host rocks, it is envisaged that the plagioclase-phyric liquids injected in an up-dip direction, that is, in an opposite sense to the ultramafic sills (Fig. 23b).

Mixing of semi-consolidated crystal slurries within a slumping, metre- to tens-of-metre-wide mush zone during magma chamber subsidence is consistent with the disequilibrium in Sr, Nd and Os isotopic mineral compositions in the LCZ (Eales et al. 1990), the Merensky Reef (Seabrook et al. 2005; Prevec et al. 2005; Hart and Kinloch 1989) and the Pyroxenite Marker (Eales and Cawthorn 1996), the coexistence of laurite and sulfide in the chromitites (Maier et al. 1999) and the intricate compositional variations within the Merensky Reef documented by Arndt et al. (2005). Magma replenishment, associated with renewed tectonism and instability would result in repeated slumping of successively deposited mushes. Injection of slurries would locally prevent residual liquid ejection and may result in high trapped liquid contents of some ultramafic layers (Fig. 18).

Some authors have argued that the model of cumulate sorting proposed here is inconsistent with trace element fractionation trends across individual oxide seams. For example, Naldrett et al. (2012) documented an increase in V content of chromite with height in the UG2 chromitite which they explained by a change in magma composition from which the chromites accumulated on the cumulate pile. The authors argued that the variation is inconsistent with the slurry model because slurries are not expected to sort crystals according to their composition. However, only one seam has been analysed, and thus it is difficult to evaluate how representative the pattern is. There are several alternative possibilities. The specific example cited by Naldrett et al. (2012) could have been caused by the localized equilibration of chromites with residual liquid from below, by superimposition of primitive, relatively V-rich chromite slurry on to a less primitive slurry or by downward transgression of a relatively differentiated, V-poor slurry that injected along the base of an earlier, more primitive slurry. Irvine et al. (1998) have documented localized reversed layering in the Skaergaard intrusion, apparently formed by autolith impact.

Some magnetite layers show a progressive decrease in Cr content with height that has been explained as a result of fractional crystallization (McCarthy et al. 1985). However, the Cr variation in the magnetite layers is highly irregular, with reversals common at various levels in certain layers, whereas other layers lack systematic Cr variation (Klemm et al. 1985; McCarthy et al. 1985). Moreover, the latter authors showed that there is strong lateral variation in Cr content at the base of magnetite layers which they explained by growth nodes. It is argued here that variation in Cr content of magnetite layers (and V content of chromitite layers) may reflect compositional variation in the precursor cumulate sequence. During cumulate sorting and unmixing, the early-formed, large, Cr-rich magnetite grains at the base of the mobilized sequence ended up towards the bottom of the slurry. Unfortunately, due to sintering, original grain size variation is generally not preserved and so this model cannot be tested petrographically.

An important question is whether subsidence was a continuous, gradual process that acted throughout the emplacement of the complex and the building of the cumulate pile or whether it was a more episodic process triggered by particularly large magma replenishment events. The available evidence suggests that layering and ductile deformation is particularly prominent in the UCZ. Geochemical evidence indicates that this interval formed during an episode of major magma replenishment. Enhanced subsidence and

cumulate sorting thus appear to be intrically related to magma replenishment.

Subsidence of the Bushveld Complex and cumulate mobilization could potentially also explain the formation of the IRUPs. They are somewhat reminiscent of the pipes and tubes in syenites as documented by Paterson (2009) who interpreted them to represent siliceous slurries that flowed at crystal contents in excess of 50 %. Scoon and Mitchell (2009) proposed a multi-stage model for the formation of the platiniferous pipes. The first step involved channelized upsurge of dunitic crystal mushes. The slurries caused partial melting of noritic wall rocks, producing Fe-rich partial melts. The Fe-rich melts drained downwards, mainly along the outer margins of the pipes where they metasomatised and replaced the country rocks to form the outermost Fe-rich clinopyroxenite pegmatoid. Reaction of the Fe-rich melts with the magnesian dunite produced Fe-rich wehrlite. Where the Fe-rich liquids percolated through the semi-consolidated centre of the magnesian dunite, hortonolite was produced via reaction replacement. The PGE within the hortonolite dunite are interpreted to be derived from partial melting of the PGE reefs of the UCZ. The early dunitic slurries could have been derived from staging chambers or from slumping LZ and LCZ cumulates dammed up at floor upwarps (Fig. 25). Wagner (1929) described examples of apparent downward movement of chromitite rafts, which could be explained if the upward flow of olivine-rich slurries is locally reversed due to drag from slurries flowing at depth. However, the model would require cumulate mobility far below the top of the crystal pile, which is difficult to reconcile with most numerical studies of cumulate solidification that argue that the mush zone at the top of cumulate piles is relatively thin. Furthermore, if the IRUPs formed during subsidence, they might be expected to intrude at an angle to the layering (Carr et al. 1994). The available information is contradictory; Heckroodt (1959) suggested that the plunge of the pipes is inclined, but recent work by Scoon and Mitchell (2009) suggests that the pipes plunge normal to the layering.

It should be noted that paleomagnetic measurements indicate cooling of the exposed portion of the Bushveld intrusion in the near-horizontal (Letts et al. 2009). However, tilting of the layering prior to solidification is indicated by field evidence in the form of ductile deformation and slumping (Figs. 9–11) and the relatively steep up-dip margins of potholes. At present, these observations cannot be readily reconciled with the paleomagnetic data. Possibly, dip was locally steepened, whereas regional dip was shallow enough to be consistent with the paleomagnetic data (<5°). The Carr et al. (1994) data show localized steepened strike-parallel zones in the western Bushveld. Turbidity currents can occur at slopes as shallow as 1° (Kersey and Hsü 1976). By analogy, it is argued here that cumulate slurries can begin

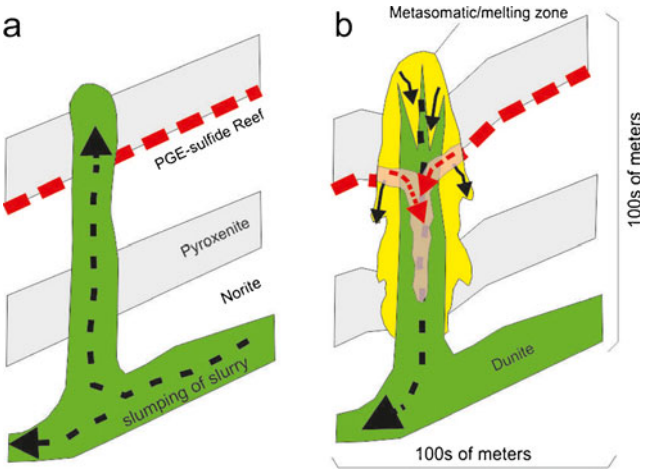

Fig. 25 Schematic diagrams illustrating formation of iron-rich ultramafic pipes. **a** Slumping dunitic slurry is injected upwards into the Upper Critical Zone. **b** Hot dunitic slurry causes partial melting of host rocks (*yellow*), including PGE reefs, leading to the downward percolation of Fe-rich melts (*black arrows*) locally enriched in PGE (*red stippled arrows*)

to slump at very low angles of the chamber floor in the event of, e.g., liquefaction induced by earthquakes.

Formation of PGE reefs

Most authors interpret the PGE reefs in layered intrusions to have formed through magma mixing (e.g. Campbell et al. 1983; Naldrett et al. 2012), but, as discussed in an earlier section, this model is inconsistent with the low S contents of the Bushveld magmas deduced from the composition of the marginal rocks and sills. The formation of the PGE reefs and their location near the ultramafic basal portions of cyclic units (the latter being one of the main arguments for the magma mixing model) thus require an alternative explanation. The spatial association of sulfides with dense silicate and oxide phases, for example in the Merensky, Pseudo and Bastard Reefs, and the UG2 chromitite, is consistent with density sorting during unmixing of semi-consolidated cumulate slurries that slumped towards the centre of the intrusion during subsidence in response to crustal loading. The paucity of sulfides in most chromitite seams can be explained by late- or post-magmatic sulfur loss (Naldrett and Lehmann 1988).

In detail, the following sequence of events is proposed: The basal cumulates of the Bushveld Complex are magnesian olivine-rich rocks (dunites) that crystallized from sulfide-undersaturated B1 magma and are thus PGE-poor. Most of these rocks are located in the unexposed central portions of the complex, but some occur at the top of the LZ exposed in the Union Section profile analysed here. The residual magma became progressively differentiated, resulting in precipitation of first harzburgites and then

orthopyroxenites, but frequent replenishment with primitive magma reversed differentiation temporarily. The magma reached IPGE saturation relatively early, resulting in the crystallization of laurites that were included in chromite phenocrysts. Sulfide saturation was reached after more significant fractionation (15–40 %, depending on the MgO content of the B1 magma) during the crystallization of orthopyroxenites and then norites, resulting in cotectic concentrations (~0.6 %) of PGE-rich disseminated sulfides. Continued frequent magma replenishment led to mafic–ultramafic layering, but this was more diffuse and occurred on a larger scale than the layering now observed. In the largest, most slowly cooling and most frequently replenished intrusions, magma replenishments were accompanied by tectonism and gradual subsidence of the centre of the magma chamber. This resulted in liquefaction and slumping of semi-consolidated cumulates at the top of the mush column and sorting of the slurries, enhancing the phase layering and producing sharper layer contacts. Sulfides were concentrated into reefs, whereas in most of the host rocks to the reefs sulfides were diluted, resulting in sub-cotectic sulfide contents or rocks barren of sulfides.

The increase in PGE grade from the LG chromitites at the base to the UG2 chromitite and the Merensky Reef at the top of the main mineralized sequence may be related to the enhanced intensity of magma replenishment and thus mineral sorting in the UCZ, culminating in the intrusion of the MZ magma pulse that caused the most severe cumulate liquefaction, subsidence and mineral sorting in the underlying rocks. In addition, it is possible that MZ replenishment led to other phenomena that helped to induce sulfide saturation, e.g. a particularly pronounced increase in pressure (Cawthorn 2005).

The residual, sulfide-saturated liquids of the CZ were cooled by the underlying MZ magma, but because the latter was emplaced as a slurry, mixing was limited to a relatively narrow transition interval around the Pyroxenite Marker. Magnetite appeared on the liquidus some 400 m above the Pyroxenite Marker. Continued subsidence of the chamber led to further cumulate sorting and formation of massive magnetite seams, consistent with the observation that (1) the silicate rocks hosting the seams have sub-cotectic proportions of magnetite (~10 %, Von Gruenewaldt 1971) and (2) magnetite contents of the silicate rocks progressively decrease with height above magnetite layers (Harney et al. 1990). As expected within the model, the magnetite seams are relatively enriched in sulfide, but apart from a PGE-rich zone below the main magnetite layer, the sulfides are mostly PGE-poor because the bulk of the PGE were extracted from the magma during the formation of the CZ (Barnes et al. 2004).

The model is consistent with the PGE fractionation within and across individual reefs (Fig. 23a). Slumping and associated sorting of cumulates with no more than cotectic sulfide abundances led to co-concentration of dense sulfides with dense silicates and chromite at the base of cyclic units. This largely preserved original fractionation trends, but reversals in Cu/Pd that originally occurred within the centres of cyclic units, when the sulfide undersaturated magma had reached sulfide saturation, were shifted to the base and compressed significantly (Fig. 23a). At the same time, PGE-depleted residual silicate liquid was filter-pressed towards the top of the slurry where it equilibrated with, and decreased, the PGE content of those sulfides that failed to accumulate at the base of the layer (Fig. 23c).

The model of crystal sorting also explains variation in lithophile elements within cyclic units. It is surmised that, prior to unmixing, most UCZ cumulates formed from mixtures of variable proportions of B1 and B2/3 magmas. Orthopyroxene-rich intervals contained a larger B1 signature than plagioclase-rich cumulates because replenishments with B1 magma spreading out along the floor of the chamber led to precipitation of pyroxenites with a predominantly B1 signature (with higher Mg# and Cr/V and lower $^{87}Sr/^{86}Sr_i$), whereas the overlying norites precipitated from progressively more mixed B1–B3 magmas. Cumulate sorting broadly preserved these trends, but the process locally led to mixing of crystals of different lineage, resulting in isotopic disequilibrium as described by Eales et al. (1990), Seabrook et al. (2005), and Prevec et al. (2005). The enrichment in incompatible trace elements in some pyroxenites, and their pegmatoidal textures, could be explained by injection of slurries into semi-consolidated footwall rocks, preventing escape of residual liquid into the main magma reservoir.

At the margins of intrusions, phase sorting and cumulate unmixing is expected to be less efficient due to faster cooling rates. This would result in less distinct layering and lower metal grades of reefs (Fig. 26a). Notably, bulk PGE grades in the Platreef exceed those of the UCZ (Maier et al. 2008a), and variation in grade can be spectacular, with up to 15 ppm PGE over 20 m at Akanani. The higher bulk PGE contents could be explained by the addition of external sulfide, leading to more efficient PGE extraction from the magma. In addition, the PGE budget of the internal reefs could have been reduced in response to downward slumping of PGE-rich sulfides towards the centre of the intrusion (Fig. 26a). The extreme variation in PGE grade in the Platreef could be explained by enhanced cumulate slumping at tectonically active margins of intrusions leading to local enrichment in sulfides and PGE (Fig. 26b).

The model proposed here shares some similarities with the models of Eales (2002), Eales and Costin (2012) and Irvine et al. (1998) who invoked crystal–liquid suspensions to explain certain features of the Bushveld and Skaergaard complexes. Eales (2002) and Eales and Costin (2012) proposed the intrusion of olivine–chromite slurries from a staging chamber to overcome the olivine and chromite mass

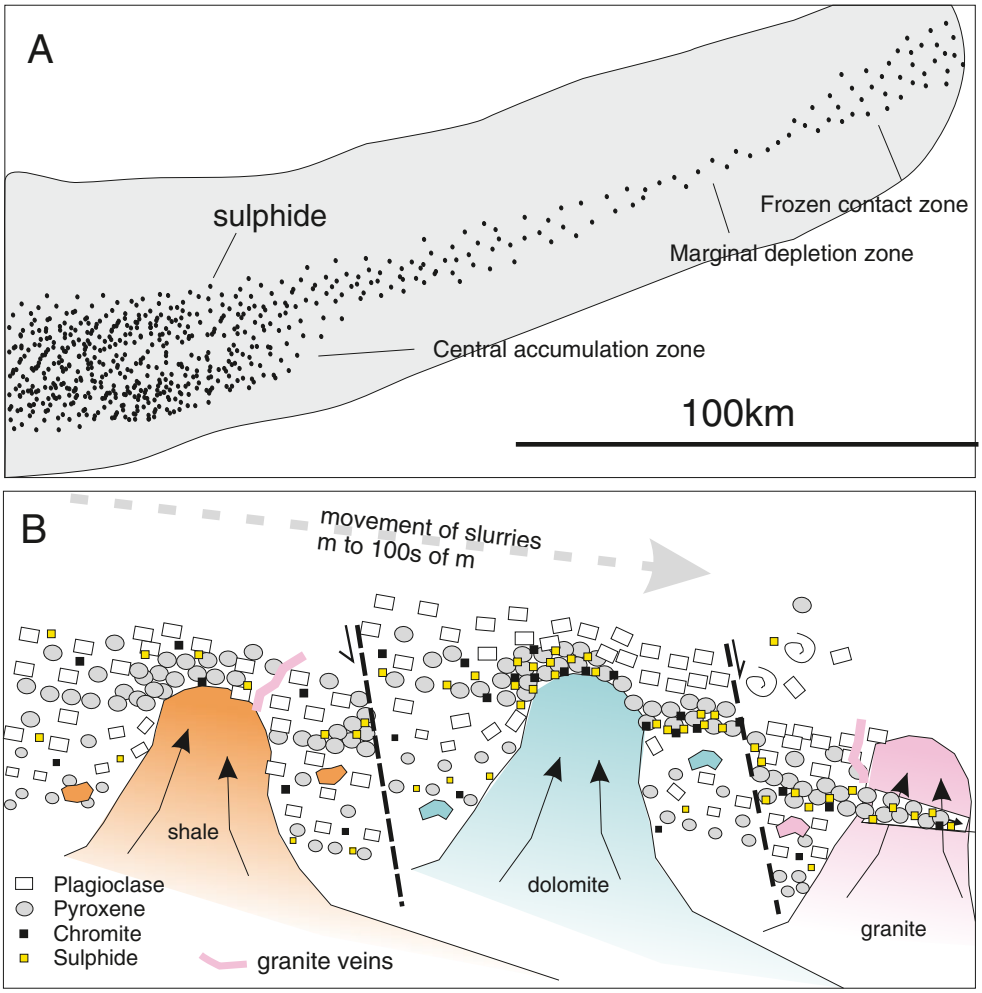

Fig. 26 Schematic diagrams illustrating: **a** variation in sulfide contents between a fast-cooling marginal setting where sulfides form wide, low-grade reefs and central settings where sulfides are concentrated due to slumping of dense slurries. Note the postulated presence of a relatively sulfide- and PGE-depleted zone inboard from the margins resulting from inward slumping of sulfides. **b** Generation of textural and compositional variation in Platreef. Note the gradation from finer-grained rocks to coarser-grained rocks with height and the local juxtaposition of fine-grained and coarse-grained rocks due to faulting, resulting in vari-textured rock packages. Also note the general concentration of pyroxenes, chromite and sulfide in down-dip direction and the localized concentration near floor upwarps and faults

balance problem in the Bushveld Complex. Irvine et al. (1998), perhaps inspired by the pioneering work of Wager and Brown (1964) on the Skaergaard intrusion in which they drew analogies to turbidity currents, proposed that crystal suspensions swept down the wall and the floor of the chamber to deposit graded and autolith-enriched cumulate layers. Both models are consistent with many features of layered intrusions, but they fail to explain the observed Raleigh-type PGE distribution patterns at the base of the Bushveld cyclic units (Fig. 18) because the models predict vigorous mixing of slurries that should have led to homogenization of metal contents. In contrast, the process proposed in the present paper is somewhat analogous to sorting of raisins in a box of corn flakes that is gently shaken. All raisins ultimately accumulate at the bottom of the box, but their position relative to each other is largely preserved.

Implications for PGE prospectivity

1. Intrusions with economic PGE reefs formed during periods of supercontinent amalgamation, possibly because these events were characterized by enhanced plate collision, subduction, mantle metasomatism and refertilization, mantle delamination and thus mantle upwellings, resulting in enhanced partial melting of the convecting and lithospheric mantle.
2. Large layered intrusions containing PGE reefs tend to be located within the central portions of stabilized Archean cratons as this favours the formation and preservation of large, relatively slowly cooling bodies that may undergo mineral sorting during crustal subsidence.
3. The SCLM is relatively Pt-enriched, as are many PGE-rich intrusions. Relative Pt enrichment of mantle-

derived magmas may thus point to an SCLM source and enhanced prospectivity for PGE reefs in associated layered intrusions. However, Pt enrichment of the magma may or may not be preserved in cumulate rocks because of stronger partitioning of Pd relative to Pt into sulfide and higher Pd mobility in fluids.

4. If the generation of PGE-rich magmas requires a melt component from the SCLM, metasomatism of the SCLM is likely a key ore-forming process. This interpretation is consistent with the relatively low-velocity seismic signature of both the Kaapvaal and Zimbabwe cratons (Begg et al. 2009), hosting two of the world's largest PGE deposits. Seismic tomography could thus potentially delinate other relatively metasomatised and thus prospective cratons or portions thereof.
5. High-grade PGE reefs occur predominantly in large intrusions because these are more frequently replenished, cool slower and subside faster than smaller intrusions. Mineral sorting and cumulate unmixing is thus more effective.
6. The thickest oxide layers are expected to occur towards the centre of layered intrusions (Figs. 23b and 27). An example is the Kemi intrusion in Finland where chromitite seams thicken from a few millimetres at the margin to as much as 90 m in the centre (Alapieti et al. 1989). Relations in the Bushveld Complex are less clear due to lack of central exposure, but it is significant that the thickest magnetite layer (layer 21) is located furthest from the margins. Sulfides are also expected to be relatively concentrated in the centre of intrusions, but due to paucity of exposure no clear examples have been identified, with the possible exception of the Great Dyke where bulk PGE contents are highest in the axial portions (Wilson and Tredoux 1990).
7. The central segments of intrusions are expected to contain relatively larger amounts of transgressive oxide and sulfide bodies that may form due to the downward percolation of semi-consolidated oxide–sulfide slurries.
8. It is proposed that the centres of some large layered intrusions may contain chromitite pipes analogous to magnetite pipes.
9. Feeder conduits and areas proximal to feeders may be particularly prospective to form thick concentrations of dense minerals in response to cumulate unmixing because they may show prolonged heat flux, resulting in slower cooling of cumulates. Furthermore, dense slurries may sink back into the feeders when the staging chambers are emptied through other vents. Alapieti and Lahtinen (2002) have described a dyke-like massive chromitite body in the floor of the Kemi intrusion, interpreted as a feeder dyke.
10. The marginal segments of intrusions may undergo reduced cumulate unmixing because they are frozen against the wall and floor (Fig. 26). Layering is thus

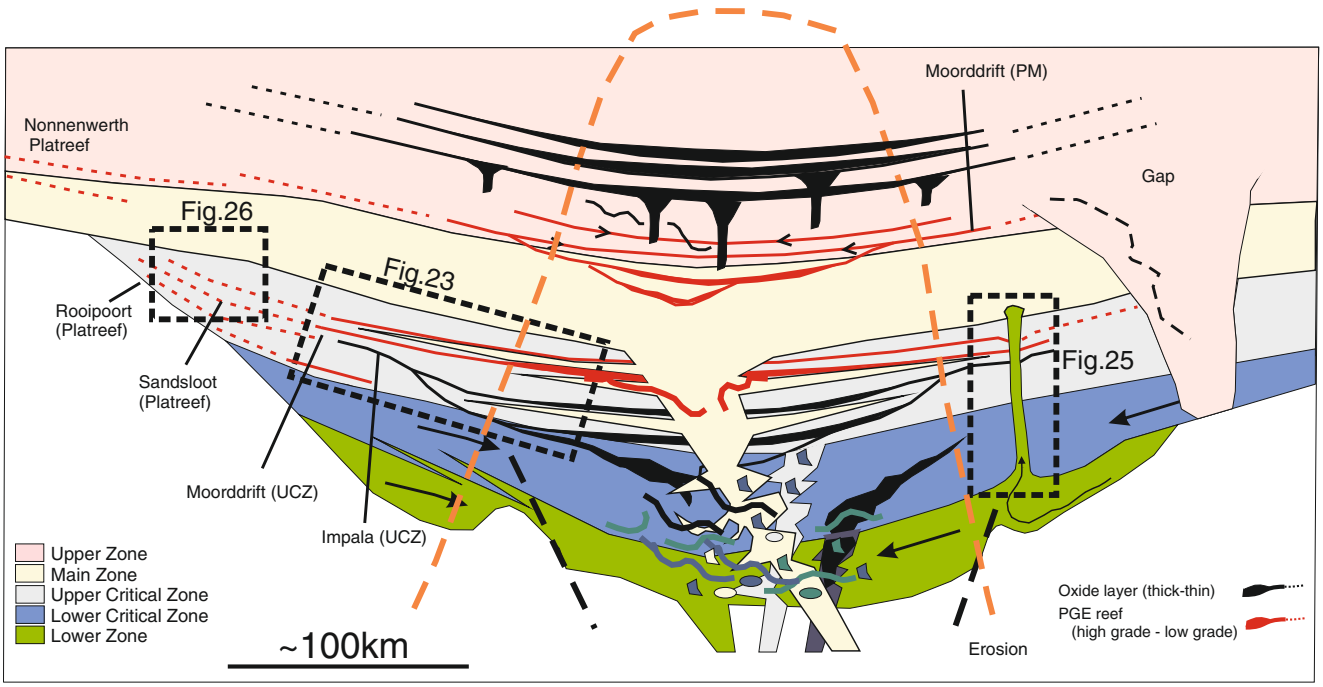

Fig. 27 Schematic diagram illustrating the formation of PGE and oxide reefs in Bushveld Complex. *Arrows* indicate the direction of slumping of cumulates during central subsidence. PGE reefs and oxide layers become increasingly high-grade and thicker towards the centre of the complex. Central feeder zones are speculative. Also shown are geologic environments of localities discussed in the text (see text for further explanation)

expected to be less distinct, and the proportion of norites and gabbronorites relative to anorthosites, chromitites and pyroxenites is larger. Furthermore, layering may be disturbed by interaction of cumulates with floor and wall rocks. Sulfides (and oxides) are mostly less concentrated than in internal reefs, but the bulk amount of sulfides can be higher, possibly because transfer of sulfides to the centres of the intrusions was prevented by relatively fast cooling.

11. Cumulate slurries may locally inject downwards (e.g. chromitites) or upwards (e.g. anorthosites) into their host cumulates, giving rise to locally mineralized sills.
12. The olivine-rich lower portions of many layered intrusions tend to crystallize from sulfide-undersaturated magma and are thus less likely to host PGE reefs than the pyroxene and plagioclase-rich segments. Contamination may drive the magma to sulfide saturation at an early stage, but this tends to result in low R factors and low PGE contents of the sulfides, likely rendering the deposits sub-economic, at least in terms of PGE as a main product.
13. Intrusions formed from komatiitic magma are less likely to contain economic PGE reefs in their ultramafic segments than basaltic intrusions because komatiites are more likely to be sulfide-undersaturated than basalts. In addition, komatiites are less Pt- and Pd-enriched than basalts.
14. Prospective intrusions are characterized by pronounced interlayering of ultramafic and mafic rocks, the presence of slumping and other deformational structures, abundant autoliths and pegmatoids that may form through injection of slurries.
15. Chromitite seams are positive indicators for PGE prospectivity because they require particularly effective cumulate sorting. They may also reflect a Cr-rich parental magma derived from a pyroxene-rich source in the SCLM.
16. Anorthosite layers may form through mineral sorting and cumulate unmixing and could thus also be positive indicators for PGE prospectivity.
17. The presence or absence of a crustal component in the magmas is not discriminative of PGE prospectivity. Prospective SCLM-derived magmas are enriched in crustal components, but so are many magmas from the convecting mantle that are contaminated during ascent through the lithosphere, which could lower their PGE potential. Furthermore, some PGE-mineralized intrusions show no significant crustal component (e.g. Skaergaard).

Summary

Large layered intrusions hosting PGE deposits are located within the central portions of cratons because thick, stable and relatively light cratonic crust favours the formation of intrusions through ponding and differentiation of mantle-derived magma. Buoyant cratons also result in enhanced preservation of the intrusions. The parental magmas are derived from multiple mantle sources. Partial melts of asthenospheric mantle plumes interact with thick SCLM during magma ascent, generating siliceous high-magnesian, high-LILE, low-S basalt characteristic of most of the mineralized intrusions. The presence of an SCLM component in the magmas is consistent with their elevated Pt/Pd ratios. Whether such interaction is critical in leading to economic PGE deposits remains uncertain, but the model provides an explanation for the occurrence of PGE-mineralized intrusions predominantly in the early Proterozoic; this era may have provided the unique combination of favourable conditions, including the presence of thick metasomatised SCLM amenable to fusion and thereby providing extra PGE and high mantle-derived heat flux. In the Archean, the SCLM may have been too refractory to melt, whereas in the Phanerozoic mantle heat flux may have decreased to such a degree that widespread, relatively high degree of melting of the SCLM could no longer occur.

Pathways for magma ascent were provided by extension of the crust and lithosphere, probably along sutures along which the protocratonic nucleii were originally assembled. In the case of Bushveld, the Thabazimbi-Murchison lineament is important, representing a transpressional rift that formed due to collision between the Zimbabwe and Kaapvaal cratons. Equally important may have been the N–S lineament that separates the eastern and western limbs of the complex and along which the Scheel carbonatite and the world-class Vergenoeg fluorite-bearing magnetite-fayalite pipe are located. The clustering of PGE-mineralized intrusions during periods of supercontinent amalgamation may be related to enhanced subduction and mantle metsomatism during such events, causing delamination, plume ascent and melting of fertilized SCLM.

Due to their low sulfur contents (100–450 ppm), the injected magmas were strongly undersaturated in sulfide. Consequently, mechanisms including mixing between replenishing and resident magmas, or pressure changes, are unlikely to have caused sulfide saturation on their own. A model of sulfide saturation via in situ contamination is inconsistent with the laterally continuous grade of the reefs. For all the above models, the question also remains open as to whether small sulfide droplets can settle efficiently through a thick, convecting magma column to produce the narrow reefs.

In the present paper, it is proposed that the Bushveld magmas reached sulfide saturation due to fractionation. Magma replenishment of the chamber must have occurred periodically as indicated, for example, by the lack in Cr or PGE depletion with height in the Critical Zone. Each new magma pulse precipitated initially sulfide-poor ultramafic rocks,

followed by norites in which silicate minerals and sulfide liquid co-precipitated in broadly cotectic proportions. Crustal loading led to progressive subsidence of the central portion of the complex. Semi-consolidated cumulate slurries slumped towards the centre of the intrusion and underwent gravity-driven phase sorting. Dense olivine and pyroxene concentrated at the base of slurries, whereas relatively light plagioclase concentrated in the upper portions of slurries. Sulfides and chromite were concentrated with the ferro-magnesian silicates, causing supercotectic proportions of these phases in the reefs and sub-cotectic proportions in all other lithologies. The dense slurries transgressively eroded their footwall rocks and, in places, injected downwards. In contrast, more buoyant plagioclase-rich slurries moved up-dip and locally injected into overlying denser, more mafic cumulates, until downward draining of dense residual liquid arrested their ascent.

Acknowledgments The present ideas developed over the course of more than two decades, due in large part to discussions with numerous collegues and friends, beginning with WDM's Ph.D. supervisor Hugh Eales at Rhodes University, Ph.D. co-students Billy de Klerk and Bernd Teigler, and later our collegues Sybrand de Waal, Chusi Li, Steve Barnes, Rodger Scoon, Tony Naldrett, Martin Sharpe, Thomas Oberthür, Eero Hanski, Tapio Halkoaho, Ed Ripley, Belinda Godel, "Budgie" Carr, Iain McDonald, Nick Arndt, Hazel Prichard, Jim Mungall, Alan Wilson, Grant Cawthorn, Mike Lesher and Ed Mathez. Many of them do not share the present interpretations but were always willing to engage in, sometimes animated, debate. We are also grateful to the mining companies who provided access to their properties and data (notably JCI, Impala Platinum, Anglo Platinum, Lonmin, Rand Mines, Anglovaal, Caledonia Mining, Pan Palladium, Anooraq Resources) and to the funding agencies that provided research funding over the years, namely, the Foundation for Research Development of South Africa, the National Research Foundation of South Africa, the National Science and Engineering Research Council of Canada, and the Australian Research Council. Thorough reviews of J Scoates, AJ Naldrett and M Lesher led to significant improvement of the manuscript and are greatly appreciated.

References

Alapieti TT, Lahtinen JJ (2002) Platinum-group element mineralization in layered intrusions of northern Finland and the Kola Peninsula, Russia. In: Cabri LJ (ed) The geology, geochemistry, mineralogy and mineral beneficiation of platinum-group elements. Can Inst Min Metall Spec Vol. 54:507–546

Alapieti TT, Kujanpää J, Lahtinen JJ, Papunen H (1989) The Kemi stratiform chromitite deposit, northern Finland. Econ Geol 84:1057–1077

Andersen JCØ, Thalhammer OAR (2006) Platinum-group element and Re–Os isotope variations of the high-grade Kilvenjärvi platinum-group element deposit, Portimo Layered Igneous Complex, Finland. Econ Geol 101:159–177

Andersen JCØ, Rasmussen H, Nielsen TFD, Ronsbo JG (1998) The triple group and the platinova Au and Pd reefs in the Skaergaard intrusion: stratigraphic and petrographic relations. Econ Geol 93:485–509

Armitage PEB, McDonald I, Edwards SJ, Manby GM (2002) Platinum-group element mineralization in the Platreef and calc-silicate footwall at Sandsloot, Potgietersrus District, South Africa. Trans Inst Min Metall B 111:36–45

Arndt NT (2005) The conduits of magmatic ore deposits. In: Mungall JE (ed) Exploration for platinum-group element deposits. Min Assoc Can., Short Course Series 35: 181-201

Arndt N, Jenner G, Ohnenstetter M, Deloule E, Wilson AH (2005) Trace elements in the Merensky Reef and adjacent norites Bushveld Complex South Africa. Mineralium Deposita 40:550–575

Ashwal LD (1990) Anorthosites. Springer, Berlin, p 422

Ashwal LD, Webb SJ, Knoper MW (2005) Magmatic stratigraphy in the Bushveld northern lobe: continous geophysical and mineralogical data from the 2950 m Bellevue drillcore. S Afr J Geol 108:199–232

Balane E, De Villiers JPR, Eeckhout SG, Glatzel P, Toplis MJ, Allard T, Fritsche, Galoisy L, Calas G (2006) The oxidation state of vanadium in titanomagnetite from layered basic intrusions. Am Mineral 91:953–956

Ballhaus CG (1988) Potholes of the Merensky Reef at Brakspruit shaft, Rustenburg platinum mines: primary disturbances in the magmatic stratigraphy. Econ Geol 83:1140–1158

Ballhaus CG, Stumpfl EF (1986) Sulphide and platinum mineralization in the Merensky Reef: evidence from hydrous silicates and fluid inclusions. Contrib Mineral Petrol 94:193–204

Ballhaus CG, Sylvester P (2000) Noble metal enrichment processes in the Merensky Reef, Bushveld Complex. J Petrol 41:545–561

Barnes SJ (1989) Are Bushveld U-type parent magmas boninites or contaminated komatiites? Contrib Min Petrol 101:447–457

Barnes SJ (1993) Partitioning of the PGE and gold between silicate and sulphide magmas in the Munni Munni Complex, Western Australia. Geochim Cosmochim Acta 57:1277–1290

Barnes S-J (1998a) Why are Pd/Pt, Rh/Pt, Pd/Ir and Pd/Os ratios higher in sulfide ores than in mafic and ultramafic magmas? EOS 78:F799

Barnes SJ (1998b) Chromites in komatiites, 1: magmatic controls on crystallization and composition. J Petrol 39:1689–1720

Barnes SJ, Fiorentini ML (2008) Iridium, ruthenium and rhodium in komatiites: evidence for iridium alloy saturation. Chem Geol 257:44–58

Barnes SJ, Naldrett AJ (1985) Geochemistry of the J-M (Howland) reef of the stillwater complex, Minneapolis adit area; I, sulfide chemistry and sulfide-olivine equilibrium. Econ Geol 80:627–645

Barnes SJ, Naldrett AJ (1986) Geochemistry of the J-M reef of the Stillwater Complex, Minneapolis Adit area II: silicate mineral chemistry and petrogenesis. J Petrol 27:791–825

Barnes SJ, Osborne G, Cook D, Barnes L, Maier WD, Godel B (2011) The Santa Rita Ni sulfide deposit in the Fazenda Mirabela intrusion, Bahia, Brazil: geology, sulfide geochemistry and genesis. Econ Geol 106:1083–1110

Barnes S-J, Picard CP (1993) The behaviour of platinum-group elements during partial melting, crystal fractionation, and sulphide segregation: an example from the Cape Smith Fold Belt, northern Quebec. Geochim Cosmochim Acta 57:79–87

Barnes S-J, Maier WD (2002a) Platinum-group elements and microstructures of normal Merensky Reef from Impala Platinum Mines, Bushveld Complex. J Petrol 43:103–128

Barnes S-J, Maier WD (2002b) Platinum-group element distributions in the Rustenburg layered suite of the Bushveld Complex, South Africa. In: Cabri LJ (ed) The geology, geochemistry, mineralogy and mineral beneficiation of platinum-group elements. Can Inst Min Metall Spec Vol 54:431–458

Barnes S-J, Naldrett AJ, Gorton MP (1985) The origin of the fractionation of platinum-group elements in terrestrial magmas. Chem Geol 53:303–323

Barnes S-J, Maier WD, Ashwal LD (2004) Platinum-group elements in the Upper Zone of the Bushveld Complex. Chem Geol 208:293–317

Barnes S-J, Savard D, Bédard LP, Maier WD (2009) Selenium and sulfur concentrations in the Bushveld Complex of South Africa and implications for formation of the platinum-group element deposits. Mineralium Deposita 44:647–663

Barnes S-J, Maier WD, Curl E (2010) Composition of the marginal rocks and sills of the Rustenburg layered suite, Bushveld Complex, South Africa: implications for the formation of the PGE deposits. Econ Geol 105:1491–1511

Barry JA (1964) Pothole and koppie investigation at Rustenburg Platinum Mines. Internal report, Johannesburg Consolidated Industries, 5 pp

Barton JM, Cawthorn RG, White JA (1986) The role of contamination in the evolution of the Platreef of the Bushveld Complex. Econ Geol 81:1096–1108

Becker H, Horan MF, Walker RJ, Gao S, Lorand J-P, Rudnick RL (2006) Highly siderophile element composition of the Earth's primitive mantle: constraints from new data on peridotite massifs and xenoliths. Geochim Cosmochim Acta 70:4528–4550

Bédard JH (1994) A procedure for calculating the equilibrium distribution of trace elements among the minerals of cumulate rocks, and the concentration of trace elements in the coexisting liquids. Chem Geol 118:143–153

Bédard JP, Sparks RSJ, Renner R, Cheadle MJ, Hallworth MA (1988) Peridotite sills and metasomatic gabbros in the eastern layered series of the Rhum complex. J Geol Soc Lond 145:207–224

Bédard JHJ, Marsh BD, Hersum TG, Naslund HR, Mukasa SB (2007) Large-scale mechanical redistribution of orthopyroxene and plagioclase in the basement sill, ferrar dolerites, McMurdo Dry Valleys, Antarctica: petrological, mineral–chemical and field evidence for channelized movement of crystals and melt. J Pet 48:2289–2326

Begg GC, Griffin WL, Natapov LM, O'Reilly SY, Grand SP, O'Neill CJ, Hronsky JMA (2009) The lithospheric architecture of Africa: seismic tomography, mantle petrology, and tectonic evolution. Geosphere 5:23–50

Borisov A, Palme H (2000) Solubilities of noble metals in Fe containing silicate melt as derived from experiments in Fe-free systems. Amer Mineral 85:1665–1673

Boudreau AE (1988) Investigations of the Stillwater Complex: 4. The role of volatiles in the petrogenesis of the J-M Reef, Minneapolis adit section. Can Min 26:193–208

Boudreau AE (1994) Mineral segregation during crystal ageing in two-crystal, two-component systems. S Afr J Geol 97:473–485

Boudreau AE (1999) PELE—a version of the MELTS software program for the PC platform. Computers Geosci 25:201–203

Boudreau AE (2008) Modelling the Merensky Reef, Bushveld Complex, Republic of South Africa. Contrib Min Petrol 156:431–437

Boudreau AE, McCallum IS (1992) Concentration of platinum-group elements by magmatic fluids in layered intrusions. Econ Geol 87:1830–1848

Boudreau AE, Meurer WP (1999a) Concentration of platinum-group elements by magmatic fluids in layered intrusions. Econ Geol 94:1830–1848

Boudreau AE, Meurer WP (1999b) Chromatographic separation of the platinum-group elements, gold, base metals and sulfur during degassing of a compacting and solidifying igneous crystal pile. Contr Mineral Petrol 134:174–185

Brenan JM, Andrews D (2001) High-temperature stability of laurite and Ru–Os–Ir alloy and their role in PGE fractionation in mafic magmas. Can Mineral 39:341–360

Bristow DG, Cawthorn RG, Harmer J, Lee CA, Tegner C, Viljoen MJ, Walraven F, Wislson JR (1993) Excursion guide—symposium on layering in igneous complexes. Wager and Brown 25th Anniversary Commemorative Meeting, Johannesburg, 59 pp

Brown GM (1956) The layered ultrabasic rocks of Rhum, inner Hebrides. Phil Trans Roy Soc Lond B240:1–53

Buchanan DL (1975) The petrography of the Bushveld Complex intersected by boreholes in the Bethal area. Trans Geol Soc S Afr 78:335–348

Buchanan DL, Nolan J, Suddaby P, Rouse JE, Viljoen MJ, Davenport JWJ (1981) The genesis of sulfide mineralization in a portion of the Potgietersrus limb of the Bushveld Complex. Econ Geol 76:568–579

Buick IS, Maas R, Gibson R (2001) Precise U–Pb titanite age constraints on the emplacement of the Bushveld Complex, South Africa. J Geol Soc Lond 158:3–6

Buntin TJ, Granstaff DE, Ulmer GC, Gold DP (1985) A pilot study of geochemical and redox relationships between potholes and adjacent Merensky Reef on the Bushveld Complex. Econ Geol 80:975–987

Bursztyn NE, Olivo GR (2010) PGE rich Ni–Cu sulfide mineralization in the Flin Flon greenstone belt, Manitoba, Canada: implications for hydrothermal remobilization of platinum-group elements in basic–ultrabasic sequences. Econ Geol 105:1469–1490

Button A (1976) Stratigraphy and relations of the Bushveld floor in the eastern Transvaal. Trans Geol Soc S Afr 79:3–12

Cameron EN (1963) Structure and rock sequence of the critical zone of the Eastern Bushveld Complex. Min Soc Am Spec Pap 1:93–107

Cameron EN (1978) The lower zone of the eastern Bushveld Complex in the Olifants River trough. J Petrol 19:437–462

Cameron EN (1980) Evolution of the lower critical zone, central sector, eastern Bushveld Complex. Econ Geol 75:845–871

Cameron EN (1982) The upper critical zone of the eastern Bushveld Complex—precursor of the Merensky Reef. Econ Geol 77:1307–1327

Campbell G (1990) The seismic revolution in gold and platinum prospecting. S Afr Geophys Assoc Yb BPI Geophys Univ Witwatersrand Johannesburg, S Afr:37–45.

Campbell IH (1978) Some problems with the cumulus theory. Lithos 11:311–323

Campbell IH (1986a) Distribution of orthocumulate textures in the Jimberlana intrusion. J Geol 95:35–54

Campbell IH (1986b) A fluid-dynamic model for the potholes of the Merensky Reef. Econ Geol 81:1118–1125

Campbell IH, Naldrett AJ (1979) The influence of silicate:sulfide ratios on the geochemistry of magmatic sulfides. Econ Geol 74:1503–1505

Campbell IH, Naldrett AJ, Barnes SJ (1983) A model for the origin of the platinum-rich sulfide horizons in the Bushveld and Stillwater Complexes. J Petrol 24:133–165

Carr HW, Groves DI, Cawthorn RG (1994) The importance of synmagmatic deformation in the formation of Merensky Reef potholes in the Bushveld Complex. Econ Geol 89:1398–1410

Cawthorn RG (1999a) The platinum and palladium resources of the Bushveld Complex. S Afr J Sci 95:481–489

Cawthorn RG (1999b) The discovery of the platiniferous Marensky Reef in 1924. S Afr J Geol 102:178–183

Cawthorn RG (2002) Magma mixing models for Merensky-style mineralization: the fallacy of binary diagrams. Econ Geol 97:663–665

Cawthorn RG (2005) Pressure fluctuations and the formation of the PGE rich Merensky and chromitite reefs, Bushveld Complex. Mineralium Deposita 40:231–235

Cawthorn RG, Ashwal LD (2009) Origin of anorthosite and magnetite layers in the Bushveld Complex, constrained by major element compositions of plagioclase. J Petrol 50:1607–1637

Cawthorn RG, Boerst K (2006) Origin of pegmatitic pyroxenite in the Merensky Unit, Bushveld Complex, South Africa. J Petrol 47:1509–1530

Cawthorn RG, McCarthy TS (1980) Variations in Cr content of magnetite from the Upper Zone of the Bushveld Complex—evidence for heterogeneity and convection currents in magma chambers. Earth Planet Sci Lett 46:335–343

Cawthorn RG, Molyneux T (1986) Vanadiferous magnetite deposits of the Bushveld Complex. In: Anhaeusser, CR Maske, S (eds) Mineral deposits of Southern Africa. Geol Soc S Afr Johannesburg: 1251–1266

Cawthorn RG, Walraven F (1998) Emplacement and crystallization time for the Bushveld Complex. J Petrol 39:1669–1687

Cawthorn RG, Davies G, Clubley-Armstrong A, McCarthy TS (1981) Sills associated with the Bushveld Complex, South Africa. Lithos 14:1–15

Cawthorn RG, Barton JR, Viljoen MJ (1985) Interaction of floor rocks with the Platreef on Overysel, Potgietersrus, northern Transvaal. Econ Geol 80:988–1006

Cawthorn RG, Meyer PS, Kruger J (1991) Major addition of magma at the Pyroxenite Marker in the western Bushveld Complex, South Africa. J Petrol 32:739–763

Cawthorn RG, Cooper GRJ, Webb SJ (1998) Connectivity between the western and eastern limbs of the Bushveld Complex. S Afr J Geol 101:291–298

Cawthorn RG, Merkle RKW, Viljoen MJ (2002) Platinum-group element deposits in the Bushveld Complex, South Africa. In: Cabri LJ (ed) The geology, geochemistry, mineralogy and mineral beneficiation of platinum-group elements. Can Inst Min Metall Spec 54:389–429

Chambers AD, Brown PE (1995) Lilloise Intrusion, East Greenland: fractionation of a hydrous alkali picritic magma. J Petrol 36:933–963

Charlier B, Namur O, Toplis MJ, Schiano P, Cluzel N, Higgins MD, Vander Auwera J (2011) Large-scale silicate liquid immiscibility during differentiation of tholeiitic basalt to granite and the origin of the Daly gap. Geology 39:907–910

Chung H-Y, Mungall JE (2009) Physical constraints on the migration of immiscible fluids through partially molten silicates, with special reference to magmatic sulfide ores. Earth Planet Sci Lett 286:14–22

Clarke B, Uken R, Reinhardt J (2009) Structural and compositional constraints on the emplacement of the Bushveld Complex, South Africa. Lithos 111:21–36

Coertze FJ (1958) Intrusive relationship and ore deposits in the western part of the Bushveld igneous Complex. Trans Geol Soc S Afr 61:387–392

Coertze FJ, Burger AJ, Walraven F, Marlow AG, McCaskie DR (1978) Field relations and age determinations in the Bushveld Complex. Trans Geol Soc S Afr 81:1–11

Cousins CA (1959) The structure of the mafic portion of the Bushveld igneous complex. Trans Geol Soc S Afr 62:179–189

Cousins CA (1964) The platinum deposits of the Merensky Reef. In: Haughton SH (ed) The geology of some ore deposits in southern Africa, vol 2. Geol Soc S Afr Johannesburg: 225–237

Cousins CA, Feringa G (1964) The chromite deposits of the western belt of the Bushveld Complex. In: Haughton, SH (ed) The geology of some ore deposits in Southern Africa, vol. 2. Geol Soc S Afr, Johannesburg:183–202

Crowson P (2001) Mineral handbook 2000–2001. Mining Journal Books, Edenbridge, p 486

Curl EA (2001) Parental magmas of the Bushveld Complex, South Africa. Ph.D. thesis, Monash University, Australia, p 140

Czamanske GK, Zientek ML (1985) The Stillwater Complex, Montana: geology and guide. Montana Bureau of Mines and Geology. Spec Pub 92:396

Davies G, Tredoux M (1985) The platinum-group element and gold contents of the marginal rocks and sills of the Bushveld Complex. Econ Geol 80:838–848

Davies G, Cawthorn RG, Barton JM, Morton M (1980) Parental magma to the Bushveld Complex. Nature 287:33–35

De Klerk WJ (1992) Petrogenesis of the Upper Critical Zone of the Western Bushveld Complex with emphasis on the UG1 footwall and Bastard Units. Ph.D. thesis, Rhodes University, Grahamstown: 294 pp

De Waal SA (1975) The mineralogy, chemistry, and certain aspects of reactivity of chromitite from the Bushveld Complex. National Institute for Metallurgy Report 1709, Johannesburg

De Waal SA, Armstrong RA (2000) The age of the Marble Hall diorite, its relationship to the Uitkomst Complex, and evidence for a new magma type associated with the Bushveld igneous event. S Afr J Geol 103:128–140

Eales HV (2002) Caveats in defining the magmas parental to the mafic rocks of the Bushveld Complex, and the manner of their emplacement: review and commentary. Mineralog Mag 66:815–832

Eales HV, Cawthorn RG (1996) The Bushveld Complex. In: Cawthorn RG (ed) Layered intrusions. Elsevier, Amsterdam, pp 181–229

Eales HV, Costin G (2012) Crustally contaminated komatiite: primary source of the chromitites and Marginal, Lower, and Critical Zone magmas in a staging chamber beneath the Bushveld Complex. Econ Geol 107:645–665

Eales HV, Marsh JS, Mitchell AA, De Klerk WJ, Kruger FJ, Field M (1986) Some geochemical constraints upon models for the crystallization of the Upper Critical Zone–Main Zone interval, northwestern Bushveld Complex. Mineralog Mag 50:567–582

Eales HV, Field M, de Klerk WJ, Scoon RN (1988) Regional trends of chemical variation and thermal erosion in the Upper Critical Zone, western Bushveld Complex. Mineralog Mag 52:63–79

Eales HV, De Klerk WJ, Teigler B (1990) Evidence for magma mixing processes within the critical and lower zones of the northwestern Bushveld Complex, South Africa. Chem Geol 88:261–278

Edou-Minko A, Grandin G, Campiglio C (2002) Petrologie et geomorphologie dans la region de Kango, Gabon: un grand dyke ultramafique-mafique Archeen. J Afr Earth Sci 32:899–918

Emeleus CH (1986) The Rhum layered complex, inner Hebrides, Scotland. In: Parsons I (ed) Origins of igneous layering. D Reidel, Dordrecht, pp 263–286

Emerman SH (1991) Correlation of a dyke swarn in southeastern Botswana with the Pilanesberg dyke swarm, South Africa. J Afr Earth Sci 12:525–531

Emslie RF (1965) The Michikamau anorthositic intrusion, Labrador. Can J Earth Sci 2:385–399

Fiorentini ML, Barnes SJ, Maier WD, Heggie GJ (2011) Global variability in the PGE contents of komatiites. J Petrol 52:82–112

Francis D, Ludden J (1995) The signature of amphibole in mafic alkaline lavas, a study in the northern Canadian Cordillera. J Petrol 36:1171–1191

Freestone IC (1978) Liquid immiscibility in alkali-rich magmas. Chem Geol 23:116–123

Gain SB (1985) The geologic setting of the platiniferous UG2 chromitite layer on Maandagshoek, eastern Bushveld Complex. Econ Geol 80:925–943

Gain SB, Mostert AB (1982) The geologic setting of the platinoid and base metal sulfide mineralization in the Platreef of the Bushveld Complex on Drenthe, north of Potgietersrus. Econ Geol 77:1395–1404

Gauert CDK (1998) The petrogenesis of the Uitkomst Complex, Mpumalanga Province, South Africa. Ph.D. thesis, Univ Pretoria: 315pp

Gauert CDK, de Waal SA, Wallmach T (1995) Geology of the ultrabasic to basic Uitkomst Complex, estarn Transvaal, South Africa: an overview. J Afr Earth Sci 21:553–570

Godel B, Barnes S-J, Maier WD (2006) 3-D distribution of sulphide minerals in the Merensky Reef (Bushveld Complex, South Africa)

and the J-M reef (Stillwater Complex, USA) and their relationship to microstructures using X-ray computed tomography. J Petrol 47:1853–1872

Godel B, Barnes S-J, Maier WD (2007) The Merensky Reef of the Bushveld Complex, South Africa: a mass balance of platinum group elements in sulfide minerals, platinum group minerals and the whole rock. J Petrol 48:1569–1604

Godel B, Barnes S-J, Maier WD (2011) Parental magma composition inferred from in situ trace elements in cumulus and intercumulus silicate minerals: example from the lower and lower critical zones of the Bushveld Complex (South-Africa). Lithos 125:537–552

Griffin WL, Graham S, O'Reilly SY, Pearson NJ (2004) Lithosphere evolution beneath the Kaapvaal Craton: Re–Os systematics of sulfides in mantle-derived peridotites. Chem Geol 208:89–118

Groves DI, Ho SE, Rock NMS, Barley ME, Muggeridge MT (1987) Archean cratons, diamond and platinum: evidence for coupled long-lived crust–mantle systems. Geology 15:801–805

Groves DI, Vielreicher RM, Goldfarb RJ, Condie KC (2005) Controls on the heterogenous distribution of mineral deposits through time. Geol Soc Lond Spec Pub 248:71–101

Gurney JJ, Helmstaedt HH, LeRoex AP, Nowicki TE, Richardson SH, Westerlund KJ (2005). Diamonds: crustal distribution and formation processes in time and space and an integrated deposit model. Econ Geol 100th Anniv Vol: 143–177

Hahn UF, Ovendale B (1994) UG2 chromitite layer potholes at Wildebeestfontein North Mine, Impala Platinum Limited, XVth CMMI Congress, Johannesburg. S Afr Inst Min Metall 3:195–200

Halkoaho TAA (1994) The Sompujärvi and Ala-Penikka PGE reefs in the Penikat layered intrusion, northern Finland. Acta Universitatis Ouluensis Ser A 249:122

Halkoaho TAA, Alapieti TT, Lahtinen JJ (1990a) The Sompujärvi PGE reef in the Penikat layered intrusion, northern Finland. Mineral Petrol 42:39–55

Halkoaho TAA, Alapieti TT, Lahtinen JJ (1990b) The Ala-Penikka PGE reefs in the Penikat layered intrusion, northern Finland. Mineral Petrol 42:23–38

Hall AL (1932) The Bushveld igneous complex in the central Transvaal. Geol Soc S Afr Mem 28:544

Hamilton PJ (1977) Sr isotope and trace element studies of the Great Dyke and Bushveld mafic phase and their relation to early Proterozoic magma genesis in southern Africa. J Petrol 18:24–52

Hamlyn PR, Keays RR (1986) Sulfur saturation and second stage melts: application to the Bushveld platinum metal deposits. Econ Geol 81:1431–1445

Harmer RE (2004) The Volspruit PGE-Ni reef: platinum mineralization in the Lower Zone south of Mokopane (Potgietersrus), South Africa. Geoscience Africa, Johannesburg, Abstracts:256–257

Harmer RE, Armstrong RA (2000) Duration of Bushveld (sensu lato) magmatism: constraints from new SHRIMP zircon chronology. Abstract, Workshop on the Bushveld Complex, Gethlane Lodge, Burgersfort

Harmer RE, Sharpe MR (1985) Field relation and strontium isotope systematics of the marginal rocks of the eastern Bushveld Complex. Econ Geol 80:813–837

Harmer RE, Auret JM, Eglington BM (1995) Lead isotope variations within the Bushveld complex, South Africa: a reconnaissance study. J Afr Earth Sci 21:595–606

Harney DMW, Merkle RKW, von Gruenewaldt G (1990) Platinum-group element behaviour in the lower part of the Upper Zone, eastern Bushveld Complex—implications for the formation of the Main Magnetite Layer. Econ Geol 85:1777–1789

Harper MP (2004) Platinum group element mineralization in "Ballrooms" of the J-M reef of the Stillwater Complex, Montana. MSc thesis, Brigham Young University: 54pp

Harris C, Chaumba JB (2001) Crustal contamination and fluid–rock interaction during the formation of the Platreef, northern limb of the Bushveld Complex, South Africa. J Petrol 42:1321–1347

Harris C, Pronost JJM, Ashwal LD, Cawthorn RG (2004) Oxygen and hydrogen isotope stratigraphy of the Rustenburg layered suite, Bushveld Complex: constraints on crustal contamination. J Petrol 46:579–601

Hart SR, Kinloch ED (1989) Os isotope systematics in Witwatersrand and Bushveld ore deposits. Econ Geol 84:1651–1655

Hatton CJ, Schweitzer JK (1995) Evidence for synchronous extrusive and intrusive Bushvekld magmatism. J Afr Earth Sci 21:579–594

Hatton CJ, von Gruenewaldt G (1990) Early Precambrian layered intrusions: a review. Inst Geol Res Bushveld Complex Research Rep 83:53

He B, Xu Y-B, Huang X-L, Luo Z-Y, Shi Y-R, Yang Q-J, Yu S-Y (2007) Age and duration of the Emeishan flood volcanism, SW China: geochemistry and SHRIMP zircon U–Pb dating of silicic ignimbrites, post-volcanic Xuanwei Formation and clay tuff at the Chaotian section. Earth Planet Sci Lett 255:306–323

Heckroodt RO (1959) The geology around the dunite pipe on Driekop (Eastern Transvaal). Trans Geol Soc S Afr 62:59–73

Helz RT (1985) Compositions of fine grained mafic rocks from sills and dykes associated with the Stillwater Complex. In: Czamanske GK, Zientek ML (eds) The Stillwater Complex, Montana: geology and guide. Montana Bur Mines Geol Spec Pub 92:396pp

Herzberg C, Asimov PD, Arndt NT, Niu Y, Lesher CM, Fitton JG, Cheadle MJ, Saunders AD (2007) Temperatures in ambient mantle and plumes: constraints from basalts, picrites, and komatiites. Geochemistry, Geophysics, Geosystems 8, Q02006, doi:10.1029/2006GC001390

Hiemstra SA (1986) The distribution of chalcophile and platinum-group elements in the UG2 chromitite layer of the Bushveld Complex. Econ Geol 81:1080–1086

Hirschmann MM, Renne PR, McBirney AR (1997) $^{40}Ar/^{39}Ar$ dating of the Skaergaard intrusion. Earth Planet Sci Lett 146:645–658

Holness MB, Stripp G, Humphreys CS, Veksler IV, Nielsen TFD, Tegner C (2011) Silicate liquid immiscibility within the crystal mush: late stage magmatic microstructures in the Skaergaard Intrusion, East Greenland. J Petrol 52:175–222

Holwell DA, McDonald I (2006) Petrology, geochemistry, and the mechanisms determining the distribution of platinum-group element and base metal sulfide mineralization in the Platreef at Overysel, northern Bushveld Complex, South Africa. Min Dep 41:575–598

Holwell DA, Armitage PEB, McDonald I (2005) Observations on the relationship between the Platreef and its hangingwall. Trans Instit Min Metal 114:199–207

Holwell DA, Boyce AJ, McDonald I (2007) Sulfur isotope variations within the Platreef Ni-Cu-PGE deposit: genetic implications for the origin of sulfide mineralization. Econ Geol 102:1091–1110

Holzer L, Barton JR, Paya BK, Kramers JD (1999) Tectonothermal history in the western part of the Limpopo Belt: test of the tectonic models and new perspectives. J Afr Earth Sci 28:383–402

Howell PD, van der Pluijm BA (1999) Structural sequences and style of subsidence in the Michigan basin. Geol Soc Am Bull 111:974–991

Hulbert LJ (1983) A petrological investigation of the Rustenburg layered suite and associated mineralization south of Potgietersrus. Ph.D. thesis, University of Pretoria, 501 pp

Hulbert LJ, von Gruenewaldt G (1982) Nickel, copper, and platinum mineralization in the Lower Zone of the Bushveld Complex, south of Potgietersrus. Econ Geol 77:1296–1306

Iljina MJ, Lee CA (2005) PGE deposits in the marginal series of layered intrusions. In: Mungall JE (ed) Exploration for platinum

group element deposits. Mineralog Assoc Can Short Course Series 35: 75–96
Ireland KL (1986) The Winterveld Chrome Mine Limited, eastern Bushveld Complex, In: Anhaeusser CR, Maske S (eds) Mineral deposits of Southern Africa. Geol Soc S Afr Johannesburg 1183–1188
Irvine TN (1970) Crystallization sequences in the Muskox intrusion and other layered intrusions. 1. Olivine–pyroxene–plagioclase relations. 441–476. In: Visser DJL, von Gruenewaldt G (eds) Symposium on the Bushveld igneous complex and other layered intrusions. Geol Soc S Afr Spec Pub, 1
Irvine TN (1975) Crystallization sequences in the Muskox intrusion and other layered intrusions—II. Origin of chromitite layers and similar deposits of other magmatic ores. Geochim Cosmochim Acta 39:991–1020
Irvine TN (1980) Infiltration metasomatism, adcumulus growth, and double diffusive fractional crystallization in the Muskox intrusion and other layered intrusions. In: Hargaves RB (ed) Physics of magmatic processes. Princeton University Press, Princeton, pp 325–383
Irvine TN (1986) Layering and related structures in the Duke Island and Skaergaard intrusions: similarities, differences and origins. In: Parson I (ed) Origins of igneous layering. D Reidel, Dordrecht, pp 185–246
Irvine TN, Keith DW, Todd SG (1983) The J-M platinum–palladium reef of the Stillwater Complex, Montana II: origin by double-diffusive convective magma mixing and implications for the Bushveld Complex. Econ Geol 78:1287–1334
Irvine TN, Andersen JCO, Brooks CK (1998) Included blocks (and blocks within blocks) in the Skaergaard intrusion: geological relations and the origins of rhythmic modally graded layers. Geol Soc Amer Bull 110:1398–1447
Jackson ED (1961) Primary textures and mineral associations in the ultramafic zone of the Stillwater Complex, Montana. US Geol Surv Prof Pap 358:1–106
Jakobsen JK, Veksler IV, Tegner C, Brooks CK (2005) Immiscible iron- and silica-rich melts in basalt petrogenesis documented in the Skaergaard intrusion. Geology 33:885–888
Kazanov OV, Kalinin A (2008) The structure and PGE mineralization of the east Pansky layered Massif. Strategic mineral resources of Lapland-base for the sustainable development of the North. Interreg-Tacis Project, Apatity, Russia, 57–68
Keays RR, Lightfoot PC, Hamlyn PR (2010) Sulphide saturation history of the Stillwater Complex, Montana: chemostratigraphic variation in platinum group elements. Abstr 11th Platinum Symposium, Sudbury, Canada
Keays RR, Lightfoot PC, Hamlyn PR (2011) Sulfide saturation history of the Stillwater Complex, Montana: chemostratigraphic variation in platinum group elements. Miner Deposita. doi:10.1007/s00126-011-0346-7
Kersey DG, Hsü KJ (1976) Energy relations and density current flows: an experimental investigation. Sedimentology 23:761–790
Kinloch ED (1982) Regional trends in the platinum-group mineralogy of the critical zone of the Bushveld Complex, South Africa. Econ Geol 77:1328–1347
Kinnaird JA, Hutchinson D, Schurmann L, Nex PAM, De Lange R (2005) Petrology and mineralization of the southern Platreef: northern limb of the Bushveld Complex, South Africa. Mineralium Deposita 40:576–597
Klemm DD, Henckel J, Dehm R, von Gruenewaldt G (1985) The geochemistry of titanomagnetite in magnetite layers and their host rocks of the eastern Bushveld Complex. Econ Geol 80:1075–1088
Kruger FJ (1990) The stratigraphy of the Bushveld Complex: a reappraisal and relocation of the Main Zone boundaries. S Afr J Geol 93:376–381
Kruger FJ (1992) The origin of the Merensky cyclic unit: Sr isotopic and mineralogical evidence for an alternative orthomagmatic model. Austr J Earth Sci 39:255–261
Kruger FJ (1994) The Sr-isotopic stratigraphy of the western Bushveld Complex. S Afr J Geol 97:393–398
Kruger FJ, Marsh JS (1985) The mineralogy, petrology and origin of the Merensky cyclic unit in the western Bushveld Complex. Econ Geol 80:958–974
Lambert DD, Simmons EC (1987) Magma evolution in the Stillwater Complex, Montana: I. Rare earth element evidence for the formation of the ultramafic series. American J Sci 287:1–32
Lambert DD, Simmons EC (1988) Magma evolution in the Stillwater Complex, Montana: II. Rare earth element evidence for the formation of the J-M reef. Econ Geol 83:1109–1126
Lambert DD, Walker RJ, Morgan JW, Shirey SB, Carlson RW, Zientek ML, Lipin BR, Koski MS, Cooper RL (1994) Re–Os and Sm–Nd isotope geochemistry of the Stillwater Complex, Montana: implications for the petrogenesis of the J-M reef. J Petrol 35:1717–1753
Lambert DD, Shirey SB, Bergman SC (1995) Proterozoic lithospheric mantle source for the Prairie Creek lamproites: Re–Os and Sm–Nd isotopic evidence. Geology 23:273–276
Latypov RM (2003) The origin of marginal compositional reversals in basic–ultrabasic sills and layered intrusions by Soret fractionation. J Petrol 44:1579–1618
Lee CA (1981) Post depositional structures in the Bushveld Complex mafic sequence. J Geol Soc 138:327–341
Lee CA (1983) Trace and platinum-group element geochemistry and the development of the Merensky Unit of the western Bushveld Complex. Min Deposita 18:173–190
Lee CA (1996) A review of mineralization in the Bushveld Complex and some other layered intrusions. In: Cawthorn RG (ed) Layered intrusions. Elsevier, Amsterdam, pp 103–145
Lee CA, Butcher AR (1990) Cyclicity in the Sr isotope stratigraphy through the Merensky and Bastard Reefs, Atok Section, eastern Bushveld Complex. Econ Geol 85:877–883
Lee CA, Parry SJ (1988) Platinum-group element geochemistry of the lower and middle group chromitites of the eastern Bushveld Complex. Econ Geol 83:1127–1139
Lee CA, Tredoux M (1986) Platinum-group element abundances in the lower and the lower critical zones of the eastern Bushveld Complex. Econ Geol 81:1087–1095
Leeb-du Toit A (1986) The Impala Platinum Mines. In: Anhaeusser CR, Maske S (eds) Mineral deposits of Southern Africa. Geol Soc S Afr Johannesburg, 1091–1106.
Lesher CM, Burnham OM (2001) Multicomponent elemental and isotopic mixing in Ni–Cu–(PGE) ores at Kambalda, Western Australia. Can Mineralogist 39:421–446
Letts S, Torsvik TH, Webb S, Ashwal LD (2009) Palaeomagnetism of the 2054 Ga Bushveld Complex (South Africa): implications for emplacement and cooling. Geophys J Int 179:850–872
Li C, Ripley EM (2005) Empirical equations to predict the sulfide content of mafic magmas at sulfide saturation and applications to magmatic sulfide deposits. Mineralium Deposita 40:218–230
Li C, Ripley EM, Maier WD, Gomwe TE (2002) Olivine and sulfur isotopic compositions of the Uitkomst sulfide-bearing intrusion, South Africa: evidence for sulfur contamination and multiple magma emplacements. Chem Geol 188:149–159
Li C, Ripley EM, Oberthür T, Miller JD Jr, Joslin GD (2008) Textural, mineralogical and stable isotope studies of hydrothermal alteration in the main sulfide zone of the Great Dyke, Zimbabwe and the precious metals zone of the Sonju Lake Intrusion, Minnesota, USA. Mineral Dep 43:97–110
Liebenberg L (1970) The sulfides in the layered sequence of the Bushveld igneous complex. Geol Soc S Afr Spec Pub 1:108–208

Lipin BR (1993) Pressure increases, the formation of chromite seams, and the development of the ultramafic series in the Stillwater Complex, Montana. J Petrol 34:955–976

Locmelis M, Pearson NJ, Barnes SJ, Fiorentini ML (2011) Ruthenium in komatiitic chromite. Geochim Cosmochim Acta 75:3645–3661

London (2008) Pegmatites. Can Min Spec Pub 10:374

Lorand J-P, Gregoire M (2006) Petrogenesis of base metal sulphide assemblages of some peridotites from the Kaapvaal craton (South Africa). Contrib Mineral Petrol 151:521–538

Luguet A, Shirey SB, Lorand J-P, Horan MF, Carlson RW (2007) Residual platinum-group minerals from highly depleted harzburgites of the Lherz massif (France) and their role in HSE fractionation of the mantle. Geochim Cosmochim Acta 71:3082–3097

Mahoney JJ, Coffin MF (eds) (1997) Large igneous provinces: continental, oceanic and, planetary flood volcanism. AGU Geophysical Monograph, 100

Maier WD (2002) Concentrations of the PGE in the Platreef on the farm Townlands, northern Bushveld Complex. Abstr, 9th International Platinum Symposium, Billings, USA

Maier WD (2005) Platinum-group element (PGE) deposits and occurrences: mineralization styles, genetic concepts, and exploration criteria. J Afr Earth Sci 41:165–191

Maier WD, Barnes S-J (1998) Concentrations of rare earth elements in silicate rocks of the Lower, Critical and Main zones of the Bushveld Complex. Chem Geol 150:85–103

Maier WD, Barnes S-J (1999) Platinum-group elements in silicate rocks of the Lower, Critical, and Main zones at Union Section, western Bushveld Complex. J Petrol 40:1647–1671

Maier WD, Barnes S-J (2003) Platinum-group elements in the Boulder Bed, western Bushveld Complex, South Africa. Mineral Deposita 38:370–380

Maier WD, Barnes S-J (2004) Pt/Pd and Pd/Ir ratios in mantle-derived magmas: a possible role for mantle metasomatism. S Afr J Geol 107:333–340

Maier WD, Barnes S-J (2008) Platinum-group elements in the UG1 and UG2 chromitites and the Bastard reef at Impala platinum mine, western Bushveld Complex. S Afr J Geol 111:159–176

Maier WD, Barnes S-J (2010) The petrogenesis of PGE reefs in the Upper Main Zone of the northern lobe of the Bushveld Complex on the farm Moorddrift, South Africa. Econ Geol 105:841–854

Maier WD, Eales HV (1997) Correlation within the UG2–Merensky Reef interval of the Western Bushveld Complex, based on geochemical, mineralogical and petrological data. Geol Surv S Afr Bull 120:56

Maier WD, Groves DI (2011) Temporal and spatial controls on the formation of magmatic PGE and Ni–Cu deposits. Min Deposita 46:841–857

Maier WD, Teigler B (1995) A facies model for the Western Bushveld Complex. Econ Geol 90:2343–2349

Maier WD, Prichard HM, Barnes S-J, Fisher PC (1999) Compositional variation of laurite at Union Section in the western Bushveld Complex. S Afr J Geol 102:286–292

Maier WD, Arndt NT, Curl EA (2000) Progressive crustal contamination of the Bushveld Complex: evidence from Nd isotopic analyses of the cumulate rocks. Contrib Mineral Petrol 140:316–327

Maier WD, Barnes S-J, van der Merwe MJ (2001) The concentrations of PGE in the Pyroxenite Marker, Bushveld Complex: implications for the formation of the Main Zone. S Afr J Geol 104:335–342

Maier WD, Barnes S-J, Gartz V, Andrews G (2003) Pt–Pd reefs in magnetitites of the Stella layered intrusion, South Africa: a world of new exploration opportunities for platinum-group elements. Geology 31:885–888

Maier WD, de Klerk L, Blaine J, Manyeruke T, Barnes S-J, Stevens MVA, Mavrogenes JA (2008a) Petrogenesis of contact-style PGE mineralization in the northern lobe of the Bushveld Complex: comparison of data from the farms Rooipoort, Townlands, Drenthe and Nonnenwerth. Mineral Deposita 43:255–280

Maier WD, Teigler B, Miller R (2008b) The Kunene anorthosite complex and its satellite intrusions. In: RMcG Miller (ed) The geology of Namibia. Geol Surv Namibia, 9–1 to 9–18

Maier WD, Barnes SJ, Campbell IH, Fiorentini ML, Peltonen P, Barnes S-J, Smithies RH (2009) Progressive mixing of meteoritic veneer into the early Earth's deep mantle. Nature 460:620–623

Maier WD, Peltonen P, McDonald I, Barnes SJ, Barnes S-J, Hatton C, Viljoen F (2012a) The platinum-group element budget of the Kaapvaal and Karelian sub-continental lithospheric mantle: implications for mantle evolution. Chem Geol 302–303:119–135

Maier WD, Rasmussen B, Fletcher I, Yang S (2012b) Direct precipitation of Pt alloys from basaltic magma in the 2.77 Ga Monts de Cristal Complex, Gabon. Abstr, 12th Int Ni–Cu–PGE symposium, Guiyang

Manyeruke T, Maier WD, Barnes S-J (2005) Major and trace element geochemistry of the Platreef on the farm Townlands, northern Bushveld Complex. S Afr J Geol 108:379–394

Maré LP, Cole J (2006) The Trompsburg Complex, South Africa: a preliminary three dimensional model. J Afr Earth Sci 44:314–330

Marsh JS, Bowen MP, Rogers NW, Bowen TB (1992) Petrogenesis of Late Archean flood-type basic lavas from the Klipriviersberg group, Ventersdorp Supergroup, South Africa. J Petrol 33:817–847

Mathez EA, Mey JL (2005) Character of the UG2 chromitite and host rocks and petrogenesis of its pegmatoidal footwall, northeastern Bushveld Complex. Econ Geol 100:1617–1630

Mathez EA, Waight TE (2003) Lead isotopic disequilibrium between sulfide and plagioclase in the Bushveld Complex and the chemical evolution of large layered intrusions. Geochim Cosmochim Acta 67:1875–1888

McBirney A (1975) Differentiation of the skaergaard intrusion. Nature 253:691–694

McBirney AR, Hunter RH (1995) The cumulate paradigm reconsidered. J Geol 103:114–122

McBirney AR, Noyes RM (1979) Crystallization and layering of the Skaergaard intrusion. J Petrol 20:487–554

McCandless TE, Ruiz J (1991) Osmium isotopes and crustal sources for platinum-group mineralization in the Bushveld Complex, South Africa. Geology 19:1225–1228

McCarthy TS, Cawthorn RG, Wright CJ, McIver JR (1985) Mineral layering in the Bushveld Complex: implications of Cr abundances in magnetite from closely spaced magnetite and intervening silicate rich layers. Econ Geol 80:1062–1074

McDonald I, Holwell DA (2011) Geology of the northern Bushveld Complex and the setting and genesis of the Platreef Ni–Cu–PGE deposit. In Li C, Ripley EM (eds) Magmatic Ni–Cu and PGE deposits: geology, geochemistry, and genesis. Rev Econ Geol 17:297–327

McDonald I, De Wit MJ, Smith CB, Bizzi LA, Viljoen KS (1995) The geochemistry of the platinum-group elements in Brazilian and southern African kimberlites. Geochim Cosmochim Acta 59:2883–2903

McDonald I, Ohnenstetter D, Rowe JP, Tredoux M, Pattrick RAD, Vaughan DJ (1999) Platinum precipitation in the Waterberg deposit, Naboomspruit, South Africa. S Afr J Geol 102:184–191

McDonald I, Holwell DA, Armitage PEB (2005) Geochemistry and mineralogy of the Platreef and critical zone of the northern lobe of the Bushveld Complex, South Africa: implications for Bushveld

stratigraphy and the development of PGE mineralization. Miner Deposita 40:526–549
McInnes BIA, McBride JS, Evans NJ, Lambert DD, Andrew AS (1999) Osmium isotope constraints on metal recycling in subduction zones. Science 286:512–516
Merensky H (1926) Die neuentdeckten Platinfelder im mittleren Transvaal, und ihre wissenschaftliche Bedeutung. Berliner Zeitschr Deut Geol Gesell 78:298–314
Miller JD Jr, Andersen JCO (2002) Attributes of Skaergaard-type reefs. In: Boudreau A (ed) Extended abstracts. 9th Int Platinum Symposium, Billings, Montana, 305–308
Miller JD, Green JC, Severson MJ, Chandler VW, Hauck SA, Peterson DM, Wahl TE (2002) Geology and mineral potential of the Duluth Complex and related rocks of northeastern Minnesota. Minnesota Geol Surv Report 58:207 p
Mitchell AA (1986) The petrology, mineralogy and geochemistry of the Main Zone of the Bushveld Complex at Rustenburg Platinum Mine, Union Section. Ph.D. thesis, Rhodes University, Grahamstown, 157pp
Mitchell AA (1996) Compositional cyclicity in a pyroxenitic layer from the Main Zone of the western Bushveld Complex: evidence for repeated magma influx. Min Mag 60:149–161
Mitchell AA, Scoon RN (2007) The Merensky Reef at Winnaarshoek, eastern Bushveld Complex: a primary magmatic hypothesis based on a wide reef facies. Econ Geol 102:971–1009
Molyneux TG (1970) A geological investigation of the Bushveld Complex in Sekhukhuneland and part of the Steelpoort Valley, eastern Transvaal, with particular reference to the oxide minerals. D.Sc. thesis, University of Pretoria, Pretoria.
Molyneux TG (1974) A geological investigation of the Bushveld Complex in Sekhukuneland and part of the Steelpoort valley. Trans Geol Soc S Afr 77:329–338
Mondal SK, Mathez EA (2007) Origin of the UG2 chromitite layer, Bushveld Complex. J Petrol 48:495–510
Morse SA (1988) Motion of crystals, solute and heat in layered intrusions. Can Mineralogist 26:209–224
Mossom RJ (1986) The Atok Platinum Mine. In: Anhaeusser, C.R., Maske, S (eds) Mineral deposits of Southern Africa Geol Soc S Afr, Johannesburg 1143–1154
Mutanen T (1997) Geology and petrology of the Akanvaara and Koitelainen mafic layered intrusions and Keivitsa–Satovaara layered complex, northern Finland. Geol Surv Finl Bull 395:233
Mutanen T, Huhma H (2001) U–Pb geochronology of the Koitelainen, Akanvaara and Kevitsa layered intrusions and related rocks. In: Vaasjoki M (ed) Radiometric age determinations from Finnish Lapland and their bearing on the timing of Precambrian volcano-sedimentary sequences. Geol Surv Fin Spec Pap 33:229–246
Nabil H (2003) Genèse des depots de Fe–Ti–P associés aux intrusions litées (exemples: l'intrusion mafique de Sept-Iles, au Québec; Complexe de Duluth aux Etats Unis. Ph.D. thesis, Univ Quebec at Chicoutimi, 441 p
Naldrett AJ (2004) Our friend platinum. Geol Soc S Afr Bull 47–2:4–12
Naldrett AJ (2009) Fundamentals of magmatic sulfide deposits. In: Li C, Ripley EM (eds) New developments in magmatic Ni–Cu and PGE deposits. Geol Publ House, 1–26
Naldrett AJ (2010) Secular variation of magmatic sulfide deposits and their source magmas. Econ Geol 105:669–688
Naldrett AJ, Lehmann J (1988) Spinel non-stoichiometry as the explanation for Ni-, Cu-, and PGE-enriched sulphides in chromitites. In: Pritchard HM, Potts PJ, Bowles JFW, Cribb SJ (eds) Geo-Platinum 87. Elsevier Applied Science, London, pp 113–143
Naldrett AJ, von Gruenewaldt G (1989) Association of platinum-group elements with chromitite in layered intrusions and ophiolite complexes. Econ Geol 84:180–187
Naldrett AJ, Gasparrini EC, Barnes SJ, Von Gruenewaldt G, Sharpe MR (1986) The upper critical zone of the Bushveld Complex and the origin of Merensky-type ores. Econ Geol 81:1105–1117
Naldrett AJ, Kinnaird J, Wilson A, Yudovskaya M, McQuade S, Chunnett G, Stanley C (2009a) Chromite composition and PGE content of Bushveld chromitites: part 1—the lower and middle groups. Trans Inst Min Metall B118:131–161
Naldrett AJ, Wilson A, Kinnaird J, Chunnett G (2009b) PGE tenor and metal ratios within and below the Merensky Reef, Bushveld Complex: implications for its genesis. J Petrol 50:625–659
Naldrett AJ, Wilson A, Kinnaird J, Yudovskaya M, Chunnett G (2012) The origin of chromitites and related PGE mineralization in the Bushveld Complex: new mineralogical and petrological constraints. Min Deposita 47:209–232
Naslund HR (1983) The effect of oxygen fugacity on liquid immiscibility in iron-bearing silicate melts. Am J Sci 283:1034–1059
Naslund HR, McBirney AR (1996) Mechanisms of formation of igneous layering. In: Cawthorn RG (ed) Layered intrusions. Elsevier, Amsterdam, pp 1–43
Nex PAM (2004) Formation of bifurcating chromitite layers of the UG1 in the Bushveld Igneous Complex, an analogy with sand volcanoes. J Geol Soc Lond 161:903–909
Nicholson DM, Mathez EA (1991) Petrogenesis of the Merensky Reef in the Rustenburg section of the Bushveld Complex. Contrib Mineral Petrol 107:293–309
O'Driscoll B, Emeleus CH, Donaldson CH, Daly JS (2010) Cr-spinel seam petrogenesis in the Rhum layered suite, NW Scotland: cumulate assimilation and in situ crystallization in a deforming crystal mush. J Petrol 51:1171–1201
Oberthür T (2002) Platinum-group element mineralization of the Great Dyke, Zimbabwe. In: Cabri LJ (ed) The geology, geochemistry, mineralogy and mineral beneficiation of platinum-group elements. Can Inst Min Metall Spec Vol 54:483–506
Olsson JR, Söderlund U, Hamilton MA, Klausen MB, Helffrich GR (2011) A late Archaean radiating dyke swarm as possible clue to the origin of the Bushveld Complex. Nat Geosci 4:865–869
Oosterhuis WR (1998) Andalusite, sillimanite and kyanite, 53–58. In: Wilson MGC, Anhaeusser CR (eds) The mineral resources of South Africa, handbook. Council for Geoscience, 740pp
Page NJ, von Gruenewaldt G, Haffty J, Aruscavage PJ (1982) Comparison of platinum, palladium, and rhodium distributions in some layered intrusions with special reference to the late differentiates (Upper Zone) of the Bushveld Complex, South Africa. Econ Geol 91:439–450
Pagé P, Barnes S-J, Bédard JH, Zientek ML (2012) In situ determination of Os, Ir, and Ru in chromites formed from komatiite, tholeiite and boninite magmas: implications for chromite control of Os, Ir and Ru during partial melting and crystal fractionation. Chemical Geology 302–303:3–15
Palme H, Jones A (2005) Solar system abundances of the elements. In: Holland HD, Turekian KK (eds) Meteorites, comets and planets. Treatise on geochemistry, vol 1. Elsevier, Amsterdam, pp 41–62
Palme H, O'Neill HStC (2004) Cosmochemical estimates of mantle composition. In: Carlson RW (ed) The mantle and core. In: Holland HD, Turekian KK (eds) Treatise on geochemistry, vol. 2. Elsevier, Oxford, pp 1–38
Paterson SR (2009) Magmatic tubes, pipes, troughs, diapirs, and plumes: late-stage convective instabilities resulting in compositional diversity and permeable networks in crystal-rich magmas of the Tuolumne batholith, Sierra Nevada, California. Geosphere 5:496–527
Pearson DG, Irvine GJ, Ionov DA, Boyd FR, Dreibus GE (2004) Re–Os isotope systematics and platinum-group element fractionation during mantle melt extraction: a study of massif and xenolith peridotite suites. Chem Geol 208:29–59

Penniston-Dorland SC, Wing BA, Nex PAM, Kinnaird JA, Farquhar J, Brown M, Sharman ER (2007) Multiple sulfur isotopes reveal a magmatic origin for the Platreef platinum group element deposit, Bushveld Complex, South Africa. Geology 36:979–982

Penniston-Dorland SC, Farquhar J, Polley GJ, Mathez EA, Kinnaird EA (2011) Can multiple S isotopes be used as a tracer for subcontinental lithospheric mantle in the Bushveld? Abstr. Goldschmidt Conference, Prague.

Philpotts AR (1967) Origin of certain iron–titanium oxide and apatite rocks. Econ Geol 62:303–315

Prendergast M, Wilson AH (1989) The Great Dyke of Zimbabwe II: mineralization and mineral deposits. In: Prendergast MD, Jones MJ (eds) Magmatic sulfides—the Zimbabwe volume. The Institution of Mining and Metallurgy, London, pp 21–42

Prendergast M (1988) An investigation of the stratigraphy and petrology of the pyroxenite no 1 layer in the Wedza Subchamber of the Great Dyke, Zimbabwe, with special reference to the characteristic features and origin of the PGE bearing Main Sulfide Zone. Ph.D. thesis, University of Zimbabwe

Prendergast M (1991) The Wedza–Mimosa platinum deposit, Great Dyke, Zimbabwe: layering and stratiform PGE mineralization in a narrow mafic magma chamber. Geol Mag 128:235–249

Prendergast M, Keays RR (1989) Controls of platinum-group element mineralization and the origin of the PGE-rich main sulfide zone of the Great Dyke, Zimbabwe: implications for the genesis of, and the exploration for stratiform PGE mineralization in layered intrusions. In: Prendergast MD, Jones MJ (eds) Magmatic sulfides—the Zimbabwe volume. The Institution of Mining and Metallurgy, London, pp 43–69

Prendergast M, Bennett M, Henicke G (1998) Platinum exploration in the Rincon del Tigre Complex, eastern Bolivia. Trans Inst Min Metall 107:B39–47

Prevec SA, Ashwal LD, Mkaza MS (2005) Mineral disequilibrium in the Merensky Reef, western Bushveld Complex, South Africa: new Sm–Nd isotope evidence. Contrib Mineral Petrol 149:306–315

Pronost JJM, Harris C, Pin C (2008) Relationship between footwall contamination, crustal contamination, and fluid–rock interaction in the Platreef, Bushveld Complex, South Africa. Mineral Deposita 43:825–848

Quadling K, Cawthorn RG (1994) The layered gabbronorite sequence, Main Zone, eastern Bushveld Complex. S Afr J Geol 97:442–454

Raedeke LD, Vian RW (1986) A three-dimensional view of mineralization in the Stillwater J-M reef. Econ Geol 81:1187–1195

Reid DL, Basson IJ (2002) Iron-rich ultramafic pegmatite replacement bodies within the Upper Critical Zone, Rustenburg Layered Suite, Northam Platinum mine, South Africa. Mineral Mag:895–914

Reisberg L, Tredoux M, Harris C, Coftier A, Chaumba J (2011) Re and Os distribution and Os isotope composition of the Platreef at the Sandsloot mine, Bushveld Complex, South Africa. Chem Geol 281:352–363

Reischmann T (1995) Precise U/Pb age determination with baddeleyite (ZrO_2), a case study from the Phalaborwa igneous complex, South Africa. S Afr J Geol 98:1–4

Reynolds IM (1985) The nature and origin of titaniferous magnetite-rich layers in the Upper Zone of the Bushveld Complex: a review and synthesis. Econ Geol 80:1089–1108

Reynolds IM (1986) The mineralogy and ore petrology of the Bushveld titaniferous magnetite-rich layers. In: Anhaeusser CR, Maske S (eds) Mineral deposits of southern Africa. Geol Soc S Afr Johannesburg 2:1267–1286.

Richardson SH, Shirey SB (2008) Continental mantle signature of Bushveld magmas and coeval diamonds. Nature 453:910–913

Richter FM (1988) A major change in the thermal state of the Earth at the Archean–Proterozoic boundary: consequences for the nature and preservation of continental lithosphere. J Petrol Spec Lithosphere issue: 39–52

Robins B (1982) Finger structures in the Lille Kufjord layered intrusion, Finnmark, Northern Norway. Cont Min Petrol 81:290–295

Roedder E (1978) Silicate liquid immiscibility in magmas and in the system K_2O-FeO-AI_2O_3-SiO_2: an example of serendipity. Geochim Cosmochim Acta 42:1597–1617

Roelofse F (2010) Constraints on the magmatic evolution of the Lower Main Zone and Platreef on the northern limb of the Bushveld Complex as inferred from the Moordkopje drill core. Ph.D. thesis, University of the Witwatersrand, 155pp

Sá HS, Barnes S-J, Prichard HM, Fisher PC (2005) The distribution of base metals and platinum-group elements in magnetitites and their host rocks in the Rio Jacaré intrusion, Northeastern Brazil. Econ Geol 100:333–348

SACS (South African Committee for Stratigraphy) (1980) Kent LE (compiler) Stratigraphy of South Africa. Geol Surv S Afr Pretoria, Handbook, 8, 690pp

Sattari P, Brennan JM, Horn I, McDonough WF (2002) Experimental constraints on the sulfide- and chromite–silicate melt partitioning behavior of rhenium and the platinum-group elements. Econ Geol 97:385–398

Savard D, Barnes S-J, Meisel T (2010) Comparison between nickel–sulfur fire assay Te co-precipitation and isotope dilution with high-pressure asher acid digestion for the determination of PGE Re and gold. Geostandards and Geoanalytical Res 34:281–291

Schiffries CM (1982) The petrogenesis of a platiniferous dunite pipe in the Bushveld Complex: infiltration metasomatism by a chloride solution. Econ Geol 77:1439–1453

Schiffries CM, Rye DM (1989) Stable isotope systematics of the Bushveld Complex: I. Constraints on hydrothermal processes in layered intrusions. Am J Sci 289:841–873

Schmidt ER (1952) The structure and composition of the Merensky Reef and associated rocks in the Rustenburg platinum mine. Trans Geol Soc S Afr 55:234–279

Schmitz MD, Bowring SA, de Wit MJ, Gartz V (2004) Subduction and terrane collision stabilize the western Kaapvaal craton tectosphere 2.9 billion years ago. Earth Planet Sci Let 222:363–376

Schönberg R, Kruger FJ, Nägler TF, Meisel T, Kramers JD (1999) PGE enrichment in chromitite layers and the Merensky Reef of the western Bushveld Complex; a Re–Os and Rb–Sr isotope study. Earth Planet Sci Lett 172:49–64

Schönberg R, Nägler TF, Gnos E, Kramers JD, Kamber BS (2003) The source of the Great Dyke, Zimbabwe, and its tectonic significance: evidence from Re–Os isotopes. J Geol 111:565–578

Schwellnus CM (1935) The nickel–copper occurrences in the Bushveld Igneous Complex, west of the Pilanesberg. Geol Surv S Afr Bull 5:36p

Scoates JS (2000) The plagioclase–magma density paradox re-examined and the crystallization of Proterozoic anorthosites. J Petrol 41:627–649

Scoates JS, Friedman RM (2008) Precise age of the platiniferous Merensky Reef, Bushveld Complex, South Africa, by the U–Pb zircon chemical abrasion ID-TIMS technique. Econ Geol 103:465–471

Scoates JS, Lindsley DH, Frost BR (2010) Magmatic and structural evolution of an anorthositic magma chamber: the Poe Mountain intrusion, Laramie Anorthosite Complex, Wyoming. Can Min 48:851–885

Scoates JS, Wall CJ, Friedman RM, Chamberlain KR (2011) Revisiting the age of the Merensky Reef, Bushveld Complex. Abstr, Goldschmidt Conference 2011

Scoates JS, Wall CJ, Friedman RM, Vantongeren JA, Mathez EA (2012) The age of the Bushveld Complex. Abstr, Goldschmidt Conference, Montreal, Canada

Scoon RN, Mitchell AA (1994) Discordant iron-rich ultramafic pegmatites in the Bushveld Complex and their relationship to iron-rich intercumulus and residual liquids. J Petrol 35:881–917

Scoon RN, Mitchell AA (2004) The platiniferous dunite pipes in the eastern limb of the Bushveld Complex: review and comparison with unmineralized discordant ultramafic bodies. S Afr J Geol 107:505–520

Scoon RN, Mitchell AA (2009) A multi-stage orthomagmatic and partial melting hypothesis for the Driekop Platiniferous Dunite Pipe, eastern limb of the Bushveld Complex, South Africa. S Afr J Geol 112:163–186

Scoon RN, Teigler B (1994) Platinum-group element mineralization in the critical zone of the Western Bushveld Complex: I sulfide-poor chromitites below the UG2. Econ Geol 89:1094–1121

Seabrook CL, Cawthorn RG, Kruger FJ (2005) The Merensky reef, Bushveld Complex: mixing of minerals not mixing of magmas. Econ Geol 100:1191–1206

Sharpe MR (1978) "Cone-type" diabases from the eastern Transvaal—representatives of a quenched magma. Trans Geol Soc S Afr 81:373–378

Sharpe MR (1981) The chronology of magma influxes to the eastern compartment of the Bushveld Complex, as exemplified by its marginal border group. J Geol Soc Lond 138:307–326

Sharpe MR (1985) Strontium isotope evidence for preserved density stratification in the main zone of the Bushveld Complex. Nature 316:119–126

Sharpe MR, Hulbert LJ (1985) Ultramafic sills beneath the eastern Bushveld Complex: mobilized suspensions of early lower zone cumulates in a parental magma with boninitic affinities. Econ Geol 80:849–871

Sharpe MR, Irvine TN (1983) Mixing relations of two Bushveld chilled margin rocks and implications for the origin of chromitite. Carnegie Inst Geophys Lab Yearbook 82:295–300

Silver PG, Fouch MJ, Gao SS, Schmitz M, Kaapvaal Seismic Group (2004) Seismic anisotropy, mantle fabric, and the magmatic evolution of Precambrian southern Africa. S Afr J Geol 107:45–58

Simon NSC, Carlson RW, Pearson DG, Davies GR (2007) The origin and evolution of the Kaapvaal cratonic lithospheric mantle. J Petrol 48:589–625

Smith D (2007) Challenges of mining PGMs at depth. Geoforum, Johannesburg

Sparks RSJ, Huppert HE, Kerr RC, McKenzie DP, Tait SR (1985) Postcumulus processes in layered intrusions. Geol Mag 122:555–568

Stewart AD (1966) On certain slump structures in the Torridonian sandstones of Applecross. Geol Mag 100:205–218

Stewart BW, DePaolo DJ (1990) Isotopic studies of processes in mafic magma chambers: II. The Skaergaard intrusion, East Greenland. Contrib Mineral Petrol 104:125–141

Stone WE, Crocket JH, Fleet ME (1990) Partitioning of palladium, iridium, platinum and gold between sulfide liquid and basalt melt at 1200 °C. Geochim et Cosmochim Acta 54:2341–2344

Stumpfl EF, Rucklidge JC (1982) The platiniferous dunite pipes of the eastern Bushveld. Econ Geol 77:1419–1431

Tegner C, Wilson JR, Brooks CK (1993) Intraplutonic quench zones in the Kap Edvard Holm layered gabbro Complex, east Greenland. J Petrol 34:681–710

Tegner C, Cawthorn RG, Kruger FJ (2006) Cyclicity in the main and upper zones of the Bushveld complex, South Africa: crystallization from a zoned magma sheet. J Petrol 47:2257–2279

Tegner C, Thy P, Holness MB, Jakobsen JK, Lesher CE (2009) Differentiation and compaction in the Skaergaard intrusion. J Petrol 50:813–840

Teigler B (1990a) Mineralogy, petrology and geochemistry of the Lower and Lower Critical Zones, northwestern Bushveld Complex. Ph.D. thesis, Rhodes University, Grahamstown

Teigler B (1990b) Platinum-group element distribution in the lower and middle group chromitites in the Western Bushveld Complex. Mineral Petrol 42:165–179

Teigler B, Eales HV (1996) The lower and critical zones of the western limb of the Bushveld Complex, as indicated by the Nooitgedacht boreholes. Geol Surv S Afr Bull 111:126

Teigler B, Eales HV, Scoon RN (1992) The cumulate succession in the critical zone of the Rustenburg layered suite at Brits, western Bushveld Complex. S Afr J Geol 95:17–28

Tollari N, Toplis MJ, Barnes S-J (2006) Predicting phosphate saturation in silicate magmas: an experimental study of the effects of melt composition and temperature. Geochim Cosmochim Acta 70:1518–1536

Tollari N, Baker D, Barnes S-J (2008a) Experimental effects of pressure and fluorine on apatite saturation in mafic magmas, with reference to layered intrusions and massif anorthosites. Contrib Mineral Petrol 156:161–175

Tollari N, Barnes S-J, Nabil H, Cox RA (2008b) Trace elements concentrations in apatites from the intrusive suite of Sept-Îles, Canada—implications for the genesis of nelsonites. Chem Geol 252:180–190

Toplis MJ, Carroll MR (1995) An experimental-study of the influence of oxygen fugacity on Fe–Ti oxide stability, phase-relations, and mineral–melt equilibria in ferro-basaltic systems. J Petrol 36:1137–1170

Toplis MJ, Carroll MR (1996) Differentiation of ferro-basaltic magmas under conditions open and closed to oxygen: implications for the Skaergaard intrusion and other natural systems. J Petrol 37:837–858

Toplis MJ, Corgne A (2002) An experimental study of element partitioning between magnetite, clinopyroxene and iron-bearing silicate liquids with particular emphasis on vanadium. Cont Min Petrol 144:22–37

Ulmer GC (1969) Experimental investigation of chromite spinels. Econ Geol Monogr 4:114–131

Van der Merwe J, Cawthorn RG (2005) Structures at the base of the upper group 2 chromitite layer, Bushveld Complex, South Africa, on Karee Mine (Lonmin Platinum). Lithos 83:214–228

Van Deventer JL, Eriksson PG, Snyman CP (1986) The Thabazimbi iron ore deposits, northwestern Transvaal. In: Anhaeusser CR, Maske S (eds) Mineral deposits of Southern Africa Geol Soc S Afr, Johannesburg 923–930

Vermaak CF (1976a) The Ni pipes of Vlakfontein and vicinity, western Transvaal. Econ Geol 71:261–286

Vermaak CF (1976b) The Merensky Reef—thoughts on its environment and genesis. Econ Geol 71:1270–1298

Vermaak CF, von Gruenewaldt G (1986) Introduction to the Bushveld Complex. In: Anhaeusser CR, Maske S (eds) Mineral deposits of Southern Africa. Geol Soc S Afr, Johannesburg 1021–1029

Viljoen MJ (1999) The nature and origin of the Merensky Reef of the western Bushveld Complex based on geological facies and geophysical data. S Afr J Geol 102:221–239

Viljoen MJ, Hieber R (1986) The Rustenburg section of Rustenburg Platinum Mines Limited, with reference to the Merensky Reef. In: Anhaeusser CR, Maske S (eds) Mineral deposits of Southern Africa. Geol Soc S Afr, Johannesburg 1117–1134

Viljoen MJ, Schürmann LW (1998) Platinum group metals. In: Wilson MGC, Anhaeusser CR (eds) The mineral resources of South Africa. Council for Geoscience, Pretoria, pp 532–568

Viljoen MJ, Scoon RN (1985) The distribution and main geologic features of discordant bodies of Fe rich ultramafic pegmatite in the Bushveld Complex. Econ Geol 80:1109–1128

Viljoen MJ, de Klerk WJ, Coetzer PM, Hatch NP, Kinloch E, Peyerl W (1986a) The Union section of Rustenburg Platinum Mines Ltd with reference to the Merensky Reef. In: Anhaeusser CR, Maske S (eds) Mineral deposits of Southern Africa. Geol Soc S Afr, Johannesburg 1061–1090.

Viljoen MJ, Theron J, Underwood B, Walters BM, Weaver J, Peyerl W (1986b) The Amandelbult section of Rustenburg Platinum Mines Limited, with reference to the Merensky Reef. In: Anhaeusser CR, Maske S (eds) Mineral deposits of Southern Africa. Geol Soc S Afr, Johannesburg 1041–1060

Viring RG, Cowell MW (1999) The Merensky Reef on Northam Platinum Limited. S Afr J Geol 102:192–208

Von Gruenewaldt G (1971) A petrographical and mineralogical investigation of the rocks of the Bushveld igneous complex in the Tauteshoogte–Roossenekal area of the eastern Transvaal. Ph.D. thesis, University of Pretoria, 228pp

Von Gruenewaldt G (1973) The main and upper zones of the Bushveld Complex in the Roossenekal area, eastern Transvaal. Trans Geol Soc S Afr 76:207–227

Von Gruenewaldt G (1976) Sulfides in the upper zone of the eastern Bushveld Complex. Econ Geol 71:1324–1336

Von Gruenewaldt G (1979) A review of some recent concepts of the Bushveld Complex, with particular reference to sulfide mineralization. Can Mineralogist 17:233–256

Von Gruenewaldt G, Klemm DD, Henckel J, Dehm RM (1985) Exsolution features in titanomagnetites from massive magnetite layers and their host rocks in the Upper Zone, eastern Bushveld Complex. Econ Geol 80:1049–1061

Von Gruenewaldt G, Hatton CJ, Merkle RKW, Gain SB (1986) Platinum-group element–chromitite associations in the Bushveld Complex. Econ Geol 81:1067–1079

Voordouw R, Gutzmer J, Beukes NJ (2009a) Intrusive origin for upper group (UG1, UG2) stratiform chromitite seams in the Dwars River area, Bushveld Complex, South Africa. Mineral Petrol 97:75–94

Voordouw R, Gutzmer J, Beukes NJ (2009b) Zoning of platinum-group mineral assemblages in the UG2 chromitite determined through in situ SEM-EDS based image analysis. Mineral Dep 45:147–159

Vuollo J, Huhma H (2005) Proterozoic mafic dykes in NE Finland. In: Lehtinen M, Nurmi PA, Rämö OT (eds) Precambrian geology of Finland, key to the evolution of the Fennoscandian Shield. Elsevier, Amsterdam, pp 195–236

Wager LR (1963) The mechanism of adcumulus growth in the layered series of the Skaergard intrusion. Min Soc Amer Spec Pap 1:1–9

Wager LR, Brown GM (1964) Layered igneous rocks. Oliver and Boyd, Edinburgh, p 588

Wagner PA (1929) The platinum deposits of the Bushveld Complex. Oliver and Boyd, Edinburgh, p 588

Wallmach T, Hatton CJ, Droop GTR (1989) Extreme facies of contact metamorphism developed in calc-silicate xenoliths in the eastern Bushveld Complex. Can Mineral 27:509–523

Walraven F (1997) Geochronology of the Rooiberg Group, Transvaal Supergroup, South Africa. University of Witwatersrand. Econ Geol Res Unit Info Circular 316:21

Walraven F, Hattingh E (1993) Geochronology of the Nebo granite, Bushveld Complex. S Afr J Geol 96:31–41

Walraven F, Frick C, Lubala RT (1992) Pb-isotope geochronology of the Schiel Complex, Northern Transvaal, South Africa. J Afr E Sci 15:103–110

Webb SJ, Cawthorn RG, Nguuri T, James D (2003) Gravity modeling of Bushveld Complex connectivity supported by Southern African Seismic experiment results. S Afr J Geol 107:207–218

Webb SJ, Ashwal LD, Cawthorn RG (2011) Continuity between eastern and western Bushveld Complex, confirmed by xenoliths from kimberlite. Contrib Mineral Petrol 162:101–107

White JA (1994) The Potgietersrus project geology and exploration history. Proceedings of the 15th CMMI Congress. S Afr Inst Min Metall 173–182

Willemse J (1969) The vanadiferous magnetic iron ore of the Bushveld Igneous Complex. Econ Geol Monogr 4:137–208

Willmore CG, Boudreau AE, Kruger FJ (2000) The halogen geochemistry of the Bushveld Complex, Republic of South Africa: implications for chalcophile element distribution in the lower and critical zones. J Petrol 41:1517–1539

Wilson AH (2012) A chill sequence to the Bushveld Complex: insight into the first stage of emplacement and implications for the parental magmas. J Petrol 53:1123–1168

Wilson MGC, Anhaeusser CR (1998) The mineral resources of South Africa. Council for Geoscience, Handbook 16, 740pp

Wilson AH, Chunnett G (2006) Trace element and platinum group element distributions and the genesis of the Merensky Reef, Western Bushveld Complex, South Africa. J Petrol 47:2369–2403

Wilson AH, Chunnett G (2010) New insight into the stratigraphy, emplacement and evolution of the basal ultramafic succession in the eastern Bushveld Complex, South Africa, Abstr. 11th Plat Symposium, Sudbury

Wilson AH, Tredoux M (1990) Lateral and vertical distribution of platinum-group elements and petrogenetic controls on the sulfide mineralization in the P1 pyroxenite layer of the Darwendale subchamber of the Great Dyke, Zimbabwe. Econ Geol 85: 556–584

Wilson JR, Sorensen HS (1996) The Fongen–Hyllingen layered intrusive complex, Norway. In: Cawthorn RG (ed) Layered intrusions. Elsevier, Amsterdam, pp 303–330

Wilson JR, Cawthorn RG, Kruger FJ, Grundvig S (1994) Intrusive origin for the uncomformable upper zone in the northern gap, western Bushveld Complex. S Afr J Geol 97:462–472

www.petmin.co.za (2010) Petmin annual review. Director's review of operations—Veremo

Yaxley GM, Berry AJ, Kamenetsky VS, Woodland AB, Paterson D, De Jong MD, Howard DL (2011) Redox profile through the Siberian craton: Fe K-edge XANES determination of Fe^{3+}/Fe^{2+} in garnet from peridotite xenoliths of the Udachnaya kimberlite. Abstr. Goldschmidt Conference, Prague

Yudovskaya M, Kinnaird JA (2010) Chromite in the Platreef (Bushveld Complex, South Africa): occurrence and evolution of its chemical composition. Mineral Deposita 45:369–391

Yudovskaya M, Kinnaird JA, Naldrett AJ, Mokhov A, Kuznetsova M, McDonald I (2010) Facies variability of PGE mineralization in Platreef chromitites (abstract). Ontario Geological Survey Miscellaneous Release Data-269

Yudovskaya M, Kinnaird JA, Sobolev A, Kuzmin D, Wilson A (2012) Petrogenesis of the Lower Zone cumulates beneath the Platreef and their correlation with recognised occurrences in the Bushveld Complex. Ext Abstr, 12th Int Ni–Cu–PGE symposium. Guiyang

Zhou M-F, Robinson PT, Lesher CM, Keays RR, Zhang C-J, Malpas J (2005) Geochemistry, petrogenesis and metallogenesis of the Panzhihua gabbroic layered intrusion and associated Fe–Ti–V oxide deposits, Sichuan Province, SW China. J Petrol 46:2253–2280

Zientek ML, Foose MP, Mei L (1986) Palladium, platinum and rhodium contents of rocks near the lower margin of the Stillwater Complex, Montana. Econ Geol 81:1169–1178

Zientek ML, Cooper RW, Corson SR, Geraghty EP (2002) Platinum-group element mineralization in the Stillwater Complex, Montana. In Cabri LJ (ed) The geology, geochemistry, mineralogy and mineral beneficiation of platinum-group elements. Can Inst Min Metall Spec Vol 54:459–481